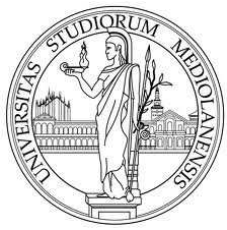

Università degli Studi di Milano

Scuola di dottorato
Fisica, Astrofisica e Fisica applicata

Dipartimento di Fisica

Corso di dottorato di ricerca in
Fisica, Astrofisica e Fisica applicata
Ciclo XXIII

High Energy Resummation in Perturbative QCD

Settore Scientifico disciplinare FIS/02

Tesi di Dottorato di:
Giovanni Diana

Supervisore: Prof. Stefano Forte
Coordinatore: Prof. Marco Bersanelli

A.A. 2009-2010

Contents

[...] Mentre il sole inebriava l'orizzonte,
sull'opaco oltremare ondeggiava
l'albero maestro della Costante Umanitaria.
- Spalma.. spalma l'uovo! - urlò ad un tratto
Domenico Bullara disteso sul ponte. [...]

Chapter 1

Introduction

Hadron collider such as Tevatron at Fermilab and LHC at Cern provide essential data from the TeV region in order to explore the electroweak symmetry breaking (EWSM) scale.

Hadron colliders probe fundamental interactions in a wide energy range, which is an important requirement in order to discover new physics signals that will emerge at the EWSB scale. However, in hadronic processes, high p_T events are seen in association with multiparticle emissions and low energy radiation which makes hadronic final states more complex to describe. Thus a key ingredient in the quest for physics beyond the Standard Model is the precise understanding of hadron processes.

Quantum Chromo-Dynamics (QCD) provides the modern description of strong interactions in terms of more fundamental particles, quarks and gluons; its remarkable success is due to the notion of asymptotic freedom of non Abelian gauge theories.

QCD is a non Abelian gauge theory with gauge group $SU(3)$. The QCD Lagrangian reads

$$\mathcal{L} = -\frac{1}{4} F_a^{\mu\nu} F^a_{\mu\nu} + \sum_f \bar{\psi}_i^{(f)} ((i \not{\partial} - m_f)\delta_{ij} - g_S t^a_{ij} \not{A}_a) \psi_j^{(f)} \tag{1.0.1}$$

$$F^a_{\mu\nu} = \partial_\mu A^a_\nu - \partial_\nu A^a_\mu - g_S \sum_{b,c} f_{abc} A^b_\mu A^c_\nu, \tag{1.0.2}$$

where f is the flavour index, the 3×3 traceless matrices t^a are the $SU(3)$ generators and f_{abc} are the structure constant of the $SU(3)$ algebra

$$[t^a, t^b] = i f_{abc} t^c. \tag{1.0.3}$$

The non Abelian character of QCD is manifest by looking at the field strength $F^a_{\mu\nu}$, indeed the last term in eq. (1.0.2) is responsible for the three and four point gluon vertices.

Analogously to the case of QED, we can introduce the coupling constant

$$\alpha_S = \frac{g_S^2}{4\pi}. \tag{1.0.4}$$

At leading order the scale dependence of the running coupling is given by

$$\alpha_S(p_T^2) = \frac{1}{b_0 \log \frac{p_T^2}{\Lambda_{QCD}^2}}, \qquad b_0 = \frac{11C_A - 4T_F n_f}{12\pi} \tag{1.0.5}$$

where $T_F = 1/2$, $C_A = 3$ When the tipical scale p_T^2 of the hadron process becomes large compared to Λ_{QCD}, the coupling α_S becomes small and quarks and gluons behave like free particles.

The perturbative expansion is the ordinary tool which allows us to make predictions from field theories. Hadronic observables however cannot be calculated from perturbative QCD only because the strong interaction forces quarks and gluons to be confined in colorless bound states after a complex fragmentation process where long distances effect, not described by perturbative QCD, dominate. One of the most important results is that non perturbative effects which determine how quarks and gluons are bounded in hadrons can be factorized out in the cross section and their contribution can be expressed in terms of universal parton distribution functions (PDFs) which contain all the informations on how fundamental particles are stored inside bound states. We can extract the PDFs from one experiment and use them as an input to make predictions on other cross sections. Therefore, the predictivity of perturbative QCD is guaranted by the factorization theorem, which allows us to determine hadronic observables in terms of hard (short distances) cross sections which can be calculated in perturbation theory and universal quantities (PDFs) which encode all the non perturbative effects.

Quantitatively reliable QCD predictions require next-to-leading order (NLO) calculations. For very precise measurements as for the vector bosons production, or for processes which are very sensitive to radiative corrections like Higgs boson production, the next-to-next-to-leading order results is required to obtain theoretical uncertainties less then 10%.

However, large radiative corrections can invalidate the perturbative expansion especially in particular kinematic configurations like in presence of thresholds in the phase space or when some characteristic scale becomes large. The presence of large logarithms, tipically, is the signal that the coupling constant is not the suitable parameter for perturbation theory since contributions of the form

$$\left(\alpha_S(p_T^2) \log \frac{\mu^2}{p_T^2}\right)^n \tag{1.0.6}$$

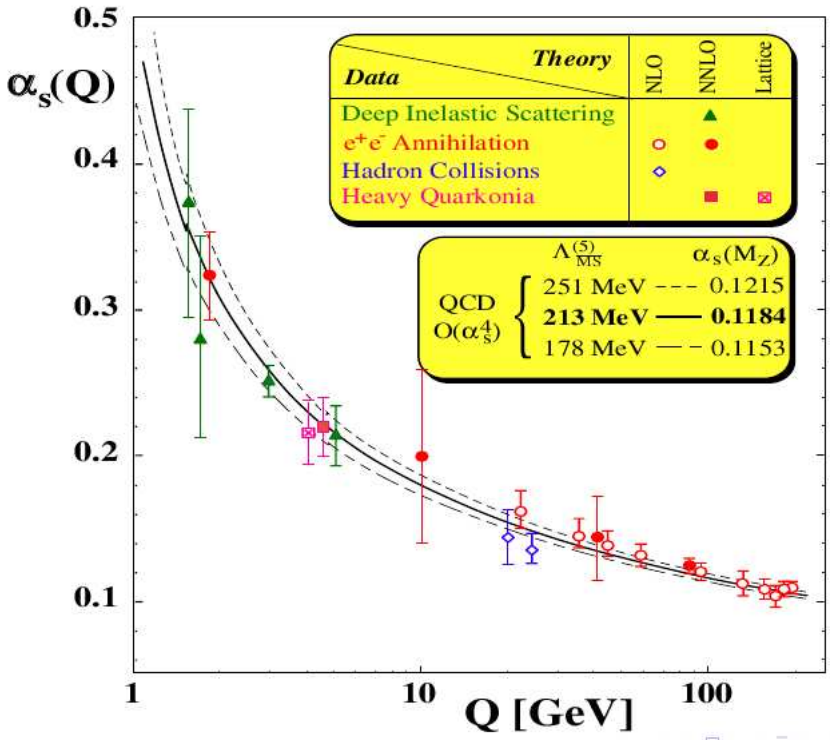

Figure 1.1: Running coupling evolution. Comparison between data and theoretical prediction up to next-to-next-to leading calculation.

are always of the same order when $\mu^2 \gg p_T^2$ even though the coupling is small. This is the tipical problem when there is a hierarchy between the various scales of the process. All these cases require a different treatment which involve an all-order resummation procedure to recover the accuracy of NLO calculations.

When the center-of-mass energy S is large compared with the tipical scale p_T^2, the ratio

$$x = \frac{4p_T^2}{S} \tag{1.0.7}$$

is small and the hard cross section is affected by large corrections characterized by powers of $\alpha_S \log x$ to all order tipically of order 1. The resummation of such tower of terms, in principle, could predict a huge deviation from the leading order results. However, once all pieces are properly added, the impact of the resummation is tiny and in the most of the cases negligible even at the LHC energy range. In this thesis we review the resummation procedure at high energy and discuss the application of the technique to the case of the prompt photon production and discuss the phenomenological impact of the

resummation at Tevatron and LHC.

As was pointed out from the beginning of the hadronic collider hera, electromagnetic probe such as the production of direct photons in hadron collisions are important processes in order to understand the strong interactions. In particular, the prompt photon production process represents the most important reducible background for the $H \to \gamma\gamma$ signal in the light Higgs scenario. Moreover, prompt photon data would provide a constraint to the gluon structure function which can be used in a global fit of parton distribution functions, however the inclusion of such data in a global fit is a long-standing problem due to discrepancies between theoretical results and a particular class of these data.

As we shall discuss in the following chapter, the inclusion of high energy enhanced higher order terms do not change significantly the NLO QCD result. The impact of the resummation is les than 1% thus it is negligible compared to the theoretical uncertainties of parton distributions and unphysical scales. However, even though the resummation has no impact on the NLO result, it will be necessary when the theoretical accuracy will reach the NNLO level in order to stabilize the logarithmic growth of the cross section in the high energy limit.

The content of this thesis is organized as follows:
in Chapter 2 we give a brief overview of general aspects of QCD, in particular we will focus on the factorization properties of the cross section and the DGLAP evolution equations, which are both essential ingredients of the theory.

Chapter 3 is devoted to the prompt photon production process. We will discuss the motivations which make this process particularly interesting from a phenomenological point of view. Moreover, the prompt photon production involves several theoretical and experimental issues which nowdays are only partially solved. In particular, discrepancies between fixed target data sets and NLO QCD are not yet fully understood. As we shall see, the photon must be considered as a hadronic final state. As a consequence, the factorization theorem for this process contain two separate pieces, the direct component and the fragmentation component. The separation of the two contributions to the cross section is not trivial and it is responsible for the presence of collinear singularities of the final state.

In Chapter 4 we review resummation techniques which allow precise predictions in high energy (small-x) region. This region is now of high interest since LHC will probe hadronic processes at very low values of the scaling variable x (up to 10^{-4} in the case of prompt photon). We will show how resummed coefficient functions can be obtained for inclusive quantities as well as for rapidity distributions in terms of simple recipes.

In Chapter 5 we will discuss how to apply the high energy resummation to the case of direct component of the prompt photon production. Resummed analitical results for the coefficient function will be derived.

In Chapter 6 the resummation of the direct photon production will be discussed from a phenomenological point of view in comparison with CDF Tevatron data.

In Chapter 7 we summarize our conclusions and discuss future works and prospects.

Chapter 2

Perturbative Quantum Chromo-dynamics

In this chapter we briefly review fundamental aspects of perturbative QCD, from asymptotic freedom to the DLGLAP evolution equations. One of the most remarkable properties of QCD is that non perturbative effects can be factorized in terms of universal quantities. We will show how this factorization property arises for the deep inelastic scattering (DIS) cross section in the framework of the operator product expansion (OPE).

The factorization of collinear singularities arising from initial state radiation yield to the DGLAP evolution equations which describe the scale dependence of parton distributions. As we shall see, the renormalization group invariance of the cross section will provide a procedure for the resummation of large logarithms of the hard scale of the process.

2.1 Renormalization group invariance

2.1.1 Large logarithms

The renormalization group was first discussed by Gell-Mann & Low (1954) in order to extend perturbation theory at high energy. The n-loop contribution for a matrix element contains powers of $\log q_i/m$, hence at high momentum, a rearrangement of the perturbative expansion is needed, because the smallness of the coupling no longer guarantees the smallness of higher order corrections, indeed, if $\alpha \log \frac{q_i}{m} \approx 1$, all terms of the form $\left(\alpha \frac{q_i}{m}\right)$ are of the same size.

The problem is solved by imposing the independence of the parameters (cut-off, dimensional scales, large masses) which we introduced in the theory in order to regularize cross sections and physical observables: clearly all these quantities do not depends on the choice we make to extract the

physical content of the theory. Imposing such an invariance correspond to write renormalization group equation, from which we can resum all large logarithms and resum them. As a result, the coupling "constant" becomes a function of the scale.

Since the logarithmic enhancement of physical quantities is a common feature in quantum field theory, some general consideration can be made. Consider a physical amplitude $\Gamma(E, \Lambda, x, g_\Lambda, m)$ that depends on an over-all energy scale E, a set of angles x, various dimensionless constants g and the masses m. The additional scale Λ is a regularization parameter. By naive dimensional analysis, at fixed Λ, it follows that:

$$\Gamma(E, \Lambda, x, g_\Lambda, m) = E^D \, \Gamma(1, \frac{\Lambda}{E}, x, g_\Lambda, \frac{m}{E}) \tag{2.1.1}$$

where D is the mass dimension of Γ. From this observation, we could expect that at very high energy $E \gg m$, Γ behaves according to the power law given by its dimension, but this is not the case since logarithmic corrections arise in perturbative expansion. At this level, two obserbation can be made: first, since Λ is an arbitrary parameter, we can choose $E = \Lambda$ obtaining:

$$\Gamma(E, \Lambda, x, g_\Lambda, m) = E^D \, \Gamma(1, 1, x, g_E, \frac{m}{E}) \tag{2.1.2}$$

this is the reason because we need a running coupling constant in order to get rid of the regularization scale. Second, since at high energy E, Γ depends only on the ratio $\frac{m}{E}$ the large logs structure is related to the massless limit.

2.1.2 Asymptotic freedom and confinement

In this section we introduce the concept of asymptotic freedom of the running coupling in QCD. One of the main properties of strong interactions is that asymptotic states are not given by quarks and gluons, instead, non perturbative effects which dominate at long distances produce a mass gap. This is the reason why final states in hadronic collisions are showers of heavy colorless hadrons. For this phenomenological reason in the past it was hard to believe that a quantum field theory could describe such processes. The discovery of asymptotic freedom in non Abelian gauge theory changed drastically the situation and QCD became early the best candidate as a model of strong interactions.

In order to describe asymptotic freedom, let us consider a dimensionless observable R in the limit where the only relevant scale is Q^2, *i.e.* where Q^2 is much larger than any other physical mass scale. In this limit we could expect a constant behaviour (scaling), however, in quantum field theories the

renormalization procedure introduces a mass scale μ, due to the subtraction of ultraviolet singularities, as the fixed energy value where physical input of the theory (physical masses and couplings) are evaluated.

The presence of the renormalization scale μ introduce a non trivial scale dependence tipically characterized by logarithms of the ratio Q^2/μ^2. However, the physical predictions of a field theory should not depend on μ as a free parameter. This independence is known as renormalization group invariance and for our quantity R can be expressed by

$$\mu^2 \frac{d}{d\mu^2} R(Q^2/\mu^2, \alpha_s) = \left[\mu^2 \frac{\partial}{\partial \mu^2} + \mu^2 \frac{\alpha_s}{\partial \mu^2} \frac{\partial}{\partial \alpha_s} \right] R = 0 \tag{2.1.3}$$

by using the standard notation $t = \log Q^2/\mu^2$ and $\beta(\alpha_s) = \mu^2 \frac{\partial \alpha_s}{\partial \mu^2}$ we have

$$\left[-\frac{\partial}{\partial t} + \beta(\alpha_s) \frac{\partial}{\partial \alpha_s} \right] R(e^t, \alpha_s) = 0 \tag{2.1.4}$$

which can be solved in terms of a new function $\alpha(Q^2)$ known as running coupling which satisfy the equation

$$\frac{\partial \alpha(Q^2)}{\partial t} = \beta(\alpha(Q^2)). \tag{2.1.5}$$

Therefore $R(1, \alpha(Q^2)$ is the solution where the independence on μ is explicit.

2.1.3 Dimensional transmutation

So far, we have seen how the coupling constant acquires a dependence on the energy scale through logarithmic quantum corrections. In a classical theory, without mass scales (for example massive terms in the Lagrangian), there is a conformal symmetry in the Lagrangian. When we introduce quantum correction, the simmetry is broken (conformal anomaly), this is the reason why after the renormalization procedure, a change in the coupling constant corresponds to a change in the energy scale. This phenomenon is called dimensional transmutation.

Consider a renormalizable massless theory [1] with a dimensionless coupling constant g and μ the energy scale given in the renormalization procedure. Let Λ be a physical observable of dimension of a mass (the mass of a particle, for example). Physical quantities must be independent of the renormalization parameter μ, thus:

$$\mu \frac{d\Lambda(g, \mu)}{d\mu} = \mu \frac{\partial \Lambda}{\partial \mu} + \beta(g) \frac{\partial \Lambda}{\partial g} = 0. \tag{2.1.6}$$

Since μ is the only scale of the theory Λ must be a product of μ times a function of g only, thus we have:

$$\Lambda + \beta(g)\frac{\partial \Lambda}{\partial g} = 0, \tag{2.1.7}$$

where we have used the expansion $\beta(g) = -\beta_0 g^2 - \beta_1 g^3 - \ldots$.

The solution is given by:

$$\begin{aligned} \Lambda &= \mu\, C\, \exp\left\{-\int_{g_0}^{g} \frac{dg'}{\beta(g')}\right\} = \\ &= \mu C \exp\left\{-\frac{1}{\beta_0 g} - \frac{\beta_1}{\beta_0}\log g + \mathcal{O}(g^2)\right\} \end{aligned} \tag{2.1.8}$$

where C is a constant fixed by the value of g mesured at an energy μ_0. This calculation implies that non-zero particle masses cannot be computed in ordinary perturbation theory (in a theory with no mass in the Lagrangian). Moreover, if the theory is asymptotically free ($\beta_0 > 0$) we have $\mu \gg \Lambda$ whenever $g(\mu)$ is small, than perturbation theory is very useful only when all momenta are much bigger of Λ. We have seen that in a theory without energy scales, renormalization group imposes strong limits on the validity of perturbation theory, which show up when we try to calculate massive observables.

Solving the renormalization group equation, the coupling constant becomes scale-dependent. A meaningful scale in QCD is given by Λ_{QCD}: the energy at which colour confinement occurs. This scale separates the perturbative spectrum of the theory from the region where the coupling becomes effectively strong.

In the next section I briefly discuss the main application of this formalism in the case of deep-inelastic scattering. Renormalization group solves the problem of (divergent) collinear gluon radiation and allow us to prove (in DIS) factorization of the non-perturbative contributions in physical processes.

2.2 Deep inelastic scattering

2.2.1 The DIS cross section

Consider the process in fig. (2.1) where a high energy electron scatters from a proton beam. The relevant variables are

$$Q^2 = -q^2, \qquad x = \frac{Q^2}{2q \cdot p} \tag{2.2.1}$$

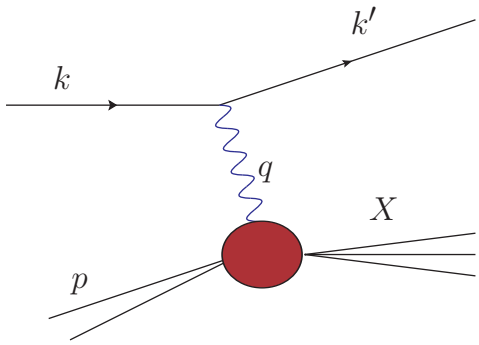

Figure 2.1: Deep inelastic scattering.

The full inclusive cross section for the DIS process can be written as

$$Q^4 \frac{d\sigma}{dxdQ^2} = \mathcal{L}_{\mu\nu} W^{\mu\nu}, \tag{2.2.2}$$

where $\mathcal{L}_{\mu\nu} = 4e^2(k_\mu k'_\nu + k_\nu k'_\mu - g_{\mu\nu} k \cdot k')$ and the hadronic tensor $W^{\mu\nu}$can be parametrized as

$$W_{\mu\nu} = \left(-g_{\mu\nu} + \frac{q_\mu q_\nu}{q^2}\right) F_1 + \left(p_\mu - q_\mu \frac{p \cdot q}{q^2}\right)\left(p_\nu - q_\nu \frac{p \cdot q}{q^2}\right) \frac{F_2}{p \cdot q} \tag{2.2.3}$$

in terms of structure functions F_1 and F_2 which contain all the information about the proton wave function.

From the optical theorem we know that

$$2\mathrm{Im}\mathcal{A}(\gamma P \to \gamma P) = \sum_{X=\text{final states}} \int d\mathrm{LIPS}(X) \cdot |\mathcal{A}(\gamma P \to X)|^2 \tag{2.2.4}$$

therefore the hadronic tensor can be written as the time product of two electromagnetic currents

$$W_{\mu\nu} = \frac{1}{2\pi}\,\mathrm{Im} \int d^4x e^{iq\cdot x} \langle P|T(J_\mu(0)J_\nu(x))|P\rangle. \tag{2.2.5}$$

where $|P\rangle$ represents the proton state.

2.2.2 The Operator product expansion

When q is much larger than any external momentum, the operator product in eq. (2.2.5), can be expressed as a sum of operators of definite spin

$$T_{\mu\nu}(q) \equiv \int e^{iq\cdot x} T(J_\mu(0)J_\nu(x)) \sim \sum_s C_{\mu\nu}^{\mu_1\cdots\mu_s}(q)\mathcal{O}_{\mu_1\cdots\mu_s}. \tag{2.2.6}$$

In order to separe the contributions to F_1 and F_2 in eq. (2.2.3) we parametrize the coefficients of eq. (2.2.6) as

$$\sum_s C_{\mu\nu}^{\mu_1\cdots\mu_s}(q)\mathcal{O}_{\mu_1\cdots\mu_s} = \sum_s \left(\frac{2}{Q^2}\right)^s \left[\left(-g_{\mu\nu}+\frac{q_\mu q_\nu}{q^2}\right) C_s^{(1)}(q) q_{\mu_1} q_{\mu_2} + \right.$$
$$\left. + \left(g_{\mu\mu_1}g_{\nu\mu_2} - g_{\nu\mu_1}\frac{q_\mu q_{\mu_2}}{q^2} - g_{\mu\mu_1}\frac{q_\nu q_{\mu_2}}{q^2} + q_\mu q_\nu \frac{q_{\mu_1}q_{\mu_2}}{q^4}\right) Q^2 C_s^{(2)}(q)_s \right] q_{\mu_3}\cdots q_{\mu_s}\mathcal{O}^{\mu_1\cdots\mu_s} \tag{2.2.7}$$

where we have factorized a Q^{-s} in the sum in order to compensate the $p^{\mu_1}\cdots p^{\mu_s}$. Since operators of definite spin are traceless, the matrix element of such operators between the proton state can be expressed simply as

$$\langle P|\mathcal{O}_{\mu_1\cdots\mu_s}|P\rangle = 2A_s(p^2)p_{\mu_1}\cdots p_{\mu_s} \tag{2.2.8}$$

because we have only p as a Lorentz vector. Thus by using eq. (2.2.8) we obtain

$$\langle P|T^{\mu\nu}|P\rangle = \sum_s \left[\left(-g_{\mu\nu}+\frac{q_\mu q_\nu}{q^2}\right) x^{-s} C_s^{(1)}(q) + \right.$$
$$\left. + \left(p_\mu - q_\mu\frac{p\cdot q}{q^2}\right)\left(p_\nu - q_\nu\frac{p\cdot q}{q^2}\right)\frac{2x^{-s+1}}{p\cdot q}C_s^{(2)}(q)\right] 2A_s(p^2) \tag{2.2.9}$$

In the high Q^2 limit only a subset of operators give the leading contribution to the Wilson expansion. Let us consider an operator of dimension d and spin s. From eq. (2.2.8) the dimension of the scalar coefficients A is $d-s-2$ and since $\langle P|T^{\mu\nu}|P\rangle$ is dimensionless, we have $[C] = -d+s+2$. Since the functions C_s and A_s depend respectevely on p^2 and q^2, the contribution of the operator $\mathcal{O}$ is of orders

$$\left(\frac{1}{x}\right)^s \left(\frac{m_P}{Q}\right)^{d-s-2}. \tag{2.2.10}$$

The quantity $t = d-s$ is the "twist" of the operator, higher twist operator are power suppressed in the Wilson expansion.

Let us concentrate on the second tensor structure in eq. (2.2.9), which will allow us to express F_2 in terms of Wilson coefficients. We define

$$T_2 \equiv \sum_s \lambda^{s-1} 4A_s C_s^{(2)}(\lambda, Q^2), \tag{2.2.11}$$

where we used $\lambda = 1/x$. By looking at eq. (2.2.5), we see that the hadronic tensor must be invariant under the transformation $(q,\mu)\to(-q,\lambda)$, therefore also the structure function F_2 must satisfies the parity relation $F_2(\lambda) =$

$F_2(-\lambda)$. This means that in eq. (2.2.11) operators of odd spin do not contribute. The convergence radius of the series in eq. (2.2.11) is 1, thus we can perform an analytic continuation of T_2 as a function of the complex variable λ. $T_2(\lambda)$ has two branch cuts in the regions $|\mathrm{Re}\lambda|^2 > 1$.

By dividing eq. (2.2.11) by λ^k and integrating around a circle centered in the origin, we can obtain $4A_kC_k$ as the residue of the pole $1/\lambda$ via the Cauchy theorem, thus we have

$$4(2\pi i)A_kC_k = \oint \frac{d\lambda}{\lambda}\lambda^{-k+1}T_2. \tag{2.2.12}$$

By modifying the contour integral on the right hand side of eq. (2.2.12) and using the parity of T_2 we obtain

$$\begin{aligned} A_kC_k &= \frac{1}{4(2\pi i)}2\int_1^\infty \frac{d\lambda}{\lambda}\lambda^{-k+1}(2i)\mathrm{Im}T_2 = \\ &= \int_0^1 \frac{dx}{x}x^{k-1}F_2 = \mathcal{M}\left[\frac{F_2}{x}\right] \end{aligned} \tag{2.2.13}$$

where we defined the Mellin transform

$$\mathcal{M}\left[f\right](N) \equiv f(N) = \int_0^1 \frac{dx}{x}f(x)x^N. \tag{2.2.14}$$

which satisfies the following convolution theorem

$$\mathcal{M}\left[f\otimes g\right] = f(N)g(N), \qquad f\otimes g \equiv \mathcal{M}\left[\int_x^1 \frac{dy}{y}f(x)g(y/x)\right]. \tag{2.2.15}$$

If we rewrite A_k and C_k as Mellin transforms

$$A_k = \int_0^1 \frac{dx}{x}x^k q(x) \tag{2.2.16}$$

$$C_k = \int_0^1 \frac{dx}{x}x^k C(x) \tag{2.2.17}$$

we can obtain F_2 using eq. (2.2.15)

$$F_2(x,Q^2) = x[C\otimes q]. \tag{2.2.18}$$

In general, with n_f flavours we can separate the contribution of quarks and gluon to obtain the factorization theorem in DIS

$$F_2(x,Q^2) = x\sum_{f=1}^{n_f} C_f\otimes(q_f+\bar{q}_f) + C_g\otimes G. \tag{2.2.19}$$

in terms of parton distribution functions (PDFs) q_f and G which can be interpreted as the probability of finding partons of momentum xp inside a proton of momentum p. In particular PDFs do not depend on the particular process we choose to describe. The coefficient functions C_f do depend on the process but can be calculated in perturbative QCD by using quarks and gluons as external states. At leading order, we have

$$C_f(x) = e_f^2 \delta(1-x), \quad C_g(x) = 0 \tag{2.2.20}$$

where e_f is the quark electric charge. Thus, using the simple leading order result in eq. (2.2.20) we obtain

$$F_2(x, Q^2) = x \sum_{f=1}^{n_f} e_f^2 (q_f + \bar{q}_f). \tag{2.2.21}$$

2.2.3 Collinear logarithms and factorization

Since the hadronic tensor and $W^{\mu\nu}$ must be independent of our arbitrary scale μ as well, we can write the Callan Symanzik equations for coefficient functions:

$$\frac{\mathrm{d}}{\mathrm{d}\log\mu^2}\left[C_k\left(\frac{Q^2}{\mu^2},\ \alpha_{\mu^2}\right) A_k(\mu^2,\ \alpha_{\mu^2})\right] = 0 \tag{2.2.22}$$

by defining the anomalous dimension $\gamma_k(\alpha) = \frac{\mathrm{d}\log A_k(\mu^2,\ \alpha)}{\log\mu^2}$ and using the chain rule it follows:

$$\left(\mu^2\frac{\partial}{\partial\mu^2} + \beta(\alpha_{\mu^2})\frac{\partial}{\partial\alpha_{\mu^2}}\right) C_k = -\gamma_k C_k, \tag{2.2.23}$$

Since $\mu^2\frac{\partial}{\partial\mu^2} = -Q^2\frac{\partial}{\partial Q^2}$, we obtain the following Callan Symanzik equation:

$$\left(Q^2\frac{\partial}{\partial Q^2} - \beta(\alpha_{\mu^2})\frac{\partial}{\partial\alpha_{\mu^2}}\right) C_k\left(\frac{Q^2}{\mu^2},\ \alpha_{\mu^2}\right) = \gamma_k(\alpha_{\mu^2}) C_k\left(\frac{Q^2}{\mu^2},\ \alpha_{\mu^2}\right) \tag{2.2.24}$$

It is easy to find the solution of Eq. (2.2.24) using the method of characteristics. We introduce the running coupling $\alpha(Q^2)$:

$$\begin{cases} Q^2\frac{\partial}{\partial Q^2}\alpha(Q^2) = \beta(\alpha(Q^2)) \\ \alpha(\mu^2) = \alpha_{\mu^2} \end{cases}, \tag{2.2.25}$$

Let us now introduce the running of the coupling $\alpha(Q^2)$ in the product of coefficient function and the matrix element:

$$C_k\left(\frac{Q^2}{\mu^2},\ \alpha(Q^2)\right) A_k(\mu^2,\ \alpha(Q^2)). \tag{2.2.26}$$

With a straightforward computation, after substituting in Eq. (2.2.24) the two terms in l.h.s. become (omitting the arguments):

$$\begin{aligned} Q^2\frac{\partial}{\partial Q^2}\, C_k &= Q^2\frac{\partial}{\partial Q^2}\, C_k\Big|_{\alpha(Q^2)\ \text{fixed}} + \beta(\alpha(Q^2))\frac{\partial}{\partial \alpha(Q^2)}\, C_k \\ \beta(\alpha_{\mu^2})\frac{\partial}{\partial \alpha_{\mu^2}}\, C_k &= \beta(\alpha_{\mu^2})\frac{\beta(\alpha(Q^2))}{\beta(\alpha(Q^2))}\frac{\partial}{\partial \alpha_{\mu^2}}\, C_k = \beta(\alpha(Q^2))\frac{\partial}{\partial \alpha(Q^2)}\, C_k. \end{aligned} \tag{2.2.27}$$

All terms in β cancel and the equation for the coefficients C_ks becomes

$$Q^2\frac{\partial}{\partial Q^2}\, C_k\Big|_{\alpha(Q^2)\ \text{fixed}} = \gamma_k(\alpha(Q^2))\, C_k. \tag{2.2.28}$$

Notice that the argument of γ_k now has changed since in Eq. (2.2.26) we have rearranged the Q^2 dependence. The Callan Symanzik equation integrates to

$$C_k\left(\frac{Q^2}{\mu^2},\ \alpha(Q^2)\right) = C_k\left(1,\ \alpha(Q^2)\right)\cdot \exp\left\{\int_{\mu^2}^{Q^2}\frac{\mathrm{d}k^2}{k^2}\ \gamma_k(\alpha(k^2))\right\}. \tag{2.2.29}$$

By expanding in α both γ_k and β:

$$\begin{aligned} \beta(\alpha) &= -\alpha^2\beta_0 + \mathcal{O}(\alpha^3) \\ \gamma_k(\alpha) &= \alpha\gamma_0 + \mathcal{O}(\alpha^2). \end{aligned} \tag{2.2.30}$$

We obtain:

$$-\int_{\mu^2}^{Q^2}\frac{\mathrm{d}k^2}{k^2}\ \gamma(\alpha) = -\int_{\alpha_{\mu^2}}^{\alpha(Q^2)}\mathrm{d}\alpha'\ \frac{\gamma_0}{\beta_0}\cdot\frac{1}{\alpha'} = -\frac{\gamma_0}{\beta_0}\log\frac{\alpha(Q^2)}{\alpha_{\mu^2}} \tag{2.2.31}$$

while from the definition of $\alpha(Q^2)$ Eq. (2.2.25) at *leading log* it follows:

$$\alpha(Q^2) = \frac{\alpha_{\mu^2}}{1+\beta_0\alpha_{\mu^2}\log\frac{Q^2}{\mu^2}} + \mathcal{O}\left(\alpha_{\mu^2}^{n+2}\log^n\frac{Q^2}{\mu^2}\right). \tag{2.2.32}$$

Finally we obtain the expression at leading order for the coefficient functions

$$\begin{aligned} C_k\left(\frac{Q^2}{\mu^2},\ \alpha(Q^2)\right) &= C_k\left(1,\ \alpha(Q^2)\right)\cdot\left(\frac{\alpha(Q^2)}{\alpha_{\mu^2}}\right)^{-\frac{\gamma_0}{\beta_0}} = \\ &= C_k\left(1,\ \alpha(Q^2)\right)\cdot\left(1+\gamma_0\alpha_{\mu^2}\log\frac{Q^2}{\mu^2}+\mathcal{O}(\alpha^2)\right). \end{aligned} \tag{2.2.33}$$

The term in eq. (2.2.33) proportional to $\log Q^2$ is the first of the leading log series in powers of $\alpha \log Q^2$. Where do these logs come from? In order to anwer to this question, consider the phase space for two real gluon emissions in the t channel from an initial state quark of momentum p. We parametrize the two gluon momenta as

$$\begin{aligned} k_1 &= (1-z_1)p + \bar{z}_1 n + k_1^T, \quad \bar{z}_1 = \frac{\mathbf{k}_1^2}{2p\cdot n(1-z_1)} \\ k_2 &= (1-z_2)z_1 p + \bar{z}_2 n + k_2^T, \quad \bar{z}_2 = \frac{\mathbf{k}_2^2}{2p\cdot n(1-z_2)z_1} \end{aligned}$$

where n is a light-like fourvector with $2n\cdot p = s > 0$ and k^T are such that $k^T \cdot p = k^T \cdot n = 0$. By following the fermion line of the relative Feynmann graph we have two propagators of virtuality

$$\begin{aligned} (p-k_1)^2 &= -\frac{\mathbf{k}_1^2}{(1-z_1)}, \\ (p-k_1-k_2)^2 &= -\mathbf{k}_1^2\left(1+\frac{z_1 z_2}{1-z_1}\right) - \frac{\mathbf{k}_2^2}{1-z_2} - 2\mathbf{k}_1\cdot\mathbf{k}_2. \end{aligned}$$

Now if we take the limit of $\mathbf{k}_1 \ll \mathbf{k}_2$ we get the factor

$$\int_{\mu^2}^{Q^2} \frac{d\mathbf{k}_1^2}{\mathbf{k}_1^2} \int_{\mu^2}^{\mathbf{k}_1^2} \frac{d\mathbf{k}_2^2}{\mathbf{k}_2^2} = \frac{1}{2}\log^2\frac{Q^2}{\mu^2}. \tag{2.2.34}$$

Therefore, the leading log series in powers of $\log Q^2$ is produced exactly by multiple collinear emission from the initial state with strong ordering of transverse momenta $\mathbf{k}_1 \ll \mathbf{k}_2 \ll \cdots \ll \mathbf{k}_n$.

2.2.4 DGLAP equations

Now let us come back to the product $C_k A_k$ we have started from. In order to guarantee the independence on the arbitrary scale of regularization, the coefficients C_k and the matrix elements A_k must contain the opposite μ^2 dependence, in order to make the resulting product properly independent. Moreover, we can get rid of the scale μ in the coefficient function since we are interested on the Q^2-evolution from a physical scale Q_0^2 which represent our initial condition. We can write explicitly the initial condition by separating the integral in two region: from the arbitrary scale μ to Q_0 and from Q_0 to Q. By using the structure of the result, we can factorize the contribution starting from Q_0 into the coefficient function (which can be used in order to compute the partonic structure function F) and move the remaining integration into

the matrix element which again cancels the μ dependence of the product. So we have:

$$\begin{aligned} & C_k\left(\frac{Q^2}{\mu^2},\ \alpha(Q^2)\right) A_k(\mu^2,\ \alpha(Q^2)) = \\ & = C_k\left(1,\ \alpha(Q^2)\right) \cdot e^{\int_{Q_0^2}^{Q^2} \frac{\mathrm{d}k^2}{k^2}\ \gamma_k(\alpha(k^2))} \cdot e^{\int_{\mu^2}^{Q_0^2} \frac{\mathrm{d}k^2}{k^2}\ \gamma_k(\alpha(k^2))} A_k(\mu^2,\ \alpha(Q^2)) \\ & = C_k\left(1,\ \alpha(Q^2)\right) \cdot e^{\int_{Q_0^2}^{Q^2} \frac{\mathrm{d}k^2}{k^2}\ \gamma_k(\alpha(k^2))} \cdot A_k(Q_0^2,\ \alpha(Q^2)) \end{aligned} \tag{2.2.35}$$

In order to derive the GLAP evolution equations, we only have to focus on the matrix elements A_k.As shown above, the evolution equation of the A_ks is given by:

$$Q^2 \frac{\mathrm{d}}{\mathrm{d}Q^2} A_k = \gamma_k A_k \tag{2.2.36}$$

If we define the parton distribution functions (PDF) $q(x)$ and the splitting functions $P(x)$:

$$A_k = \mathcal{M}[q](k) \tag{2.2.37}$$

$$\gamma_k = \mathcal{M}[P] \tag{2.2.38}$$

using the definition above, Eq. (2.2.36) take the standard form of Altarelli-Parisi equation:

$$Q^2 \frac{\mathrm{d}}{\mathrm{d}Q^2} q(x,\ Q^2) = \int_x^1 \frac{\mathrm{d}z}{z} P(z, \alpha(Q^2))\ q\left(\frac{x}{z},\ Q^2\right) \tag{2.2.39}$$

Finally, since the cross section is proportional to the structure functions, which are obtained by convolution between parton densities and coefficient functions, the general form of cross section in deep-inelastic scattering, according to factorization theorem, can be written as a convolution as well:

$$\sigma(x, Q^2) = \int_z^1 dx\ C(x/z, Q^2/\mu^2, \alpha_{\mu^2}) q(z, \mu^2) \tag{2.2.40}$$

where C are the hard perturbative coefficients and μ is the factorization scale. In Mellin space we have:

$$\begin{aligned} \sigma(N, Q^2) &= C(N, Q^2/\mu^2, \alpha_{\mu^2}) q(N, \mu^2) = \\ &= C(N, 1, \alpha(Q^2)) q(N, Q^2) \end{aligned} \tag{2.2.41}$$

where the last equation gives the standard renormalization group improved form of the factorized cross section.

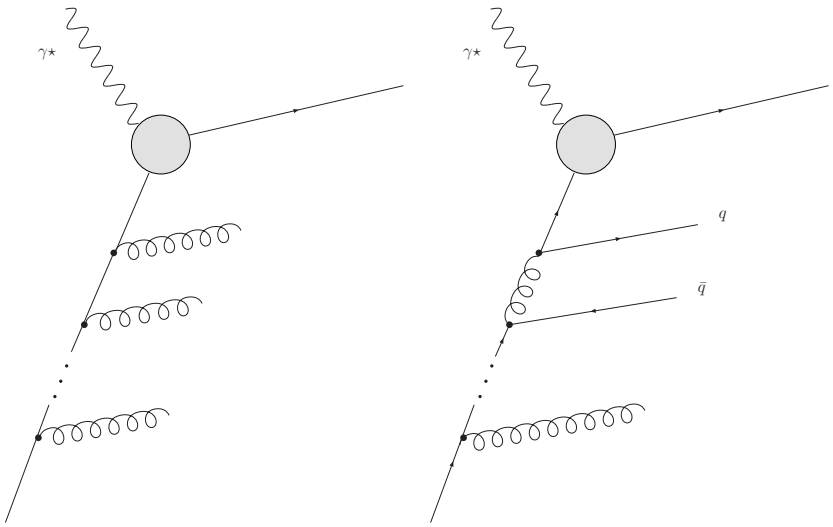

Figure 2.2: Multiple radiation of gluons.

2.2.5 Amplitudes in the collinear limit

As we have seen, powers of $\log Q^2$ are produced by radiation of collinear partons. If we rewrite the left hand side of eq. (2.2.33) in x-space and dropping all the functional dependencies for simplicity we obtain

$$C(Q^2/\mu^2, x) = C(1, x) + \alpha \int_x^1 \frac{dy}{y} P_0(x/y) C(y) \log \frac{Q^2}{\mu^2} + \mathcal{O}(\alpha^2). \quad (2.2.42)$$

We can view the splitting function $P_{ij}(x)$ as the probability that the splitting ij occurs, since they appear as coefficients for the relative collinear logarithm.

In this section we show how the factorization properties of the cross section arise naturally at the amplitude level. To show this, we use the helicity formalism described in Appendix B. Furthermore, the colour decomposition of the amplitude lead us to the study of simpler colour ordered amplitudes. The colour decomposition of the tree-level n-gluon amplitude is [2, 3]

$$A_n = g^{n-2} \sum_{S_n/Z_n} \mathrm{Tr}(T^{d_{\sigma(1)}} \cdots T^{d_{\sigma(n)}}) \mathcal{A}_n(p_{\sigma(1)}, \nu_{\sigma(1)}; \cdots; p_{\sigma(n)}, \nu_{\sigma(n)}) \quad (2.2.43)$$

where $d_1, \cdots, d_n$ and $\sigma_1, \cdots, \sigma_n$ are respectively the colours and the polarizations of the gluons, the T's are the colour matrices in the fundamental rapresentation of $SU(3)$ and the sum is over the non-cyclic permutations S_n/Z_n of the set $\{1, \cdots, n\}$.

First we recall from Appendix B a short hand notation for the two component (Weyl) spinors associated with an n-parton process [4, 5]

$$(\lambda_i)_\alpha \equiv [u_+(k_i)]_\alpha, \qquad (\tilde{\lambda}_i)_{\dot{\alpha}} \equiv [u_-(k_i)]_{\dot{\alpha}}. \quad (2.2.44)$$

It is also convenient to describe the spinors with a 'bra' and 'ket' notation

$$\lambda_i = |i^+\rangle = \langle i^-|, \tag{2.2.45}$$
$$\tilde{\lambda}_i = |i^-\rangle = \langle i^+|. \tag{2.2.46}$$

Lorentz-invariant spinor products can be defined using the antisymmetric tensors $\epsilon^{\alpha\beta}$ and $\epsilon_{\dot{\alpha}\dot{\beta}}$ for the two $SU(2)$ factors in the Lorentz algebra:

$$\langle jl\rangle = \epsilon^{\alpha\beta}(\lambda_j)_\alpha(\lambda_l)_\beta = \bar{u}_-(k_j)u_+(k_l), \tag{2.2.47}$$
$$[jl] = \epsilon^{\dot{\alpha}\dot{\beta}}(\tilde{\lambda}_j)_{\dot{\alpha}}(\tilde{\lambda}_l)_{\dot{\beta}} = \bar{u}_+(k_j)u_-(k_l). \tag{2.2.48}$$

The usual momentum dot products can be constructed from the spinor products using the relation

$$\langle lj\rangle[jl] = 2k_j \cdot k_l \tag{2.2.49}$$

Whith this notation, for the class of partial amplitude known as Maximal Helicity Violating (MHV) where all the helicities are positive (negative) but two of them, a simple analytical expression holds

$$\begin{aligned}\mathcal{A}_n^{\text{tree MHV},(jk)} &\equiv \mathcal{A}_n(1^+,\ldots,j^-,\ldots,k^-,\ldots,n^+) = \\ &= i\frac{\langle jk\rangle}{\langle 12\rangle\langle 23\rangle\cdots\langle n1\rangle}.\end{aligned} \tag{2.2.50}$$

In this expression, only gluons j and k have negative helicity; the remaining $(n-2)$ gluons have positive helicity. The splitting function P_{gg} can be easily calculated taking advantage of the spinor formalism with color ordered Feynman rules. Let us consider the five point amplitude $\mathcal{A}(1^-,2^-,3^+,4^+,5^+)$ shown in fig. (2.3). The explicit form of the amplitude is given by the general form of MHV amplitudes

$$\mathcal{A}(1^-,2^-,3^+,4^+,5^+) = \frac{i\langle 12\rangle^4}{\langle 12\rangle\langle 23\rangle\langle 34\rangle\langle 45\rangle\langle 51\rangle}. \tag{2.2.51}$$

Now if we take the collinear limit where $k_5 = (1-z)k_4$ and $P = k_4+k_5 = zk_4$, we can replace $|5\rangle \to \sqrt{1-z}/\sqrt{z}|P>$ and $|4\rangle \to 1/\sqrt{z}|P\rangle$ in the amplitude, therefore we get

$$\mathcal{A}_5(1^-,2^-,3^+,4^+,5^+) \xrightarrow{4||5} \frac{z}{\sqrt{1-z}}\frac{g_s}{\langle 45\rangle}\mathcal{A}_4(1^-,2^-,3^+,P^+). \tag{2.2.52}$$

In order to compute the P_{gg} splitting function we have to consider all the possible helicity configurations of 4 and 5, sum the squared amplitude and

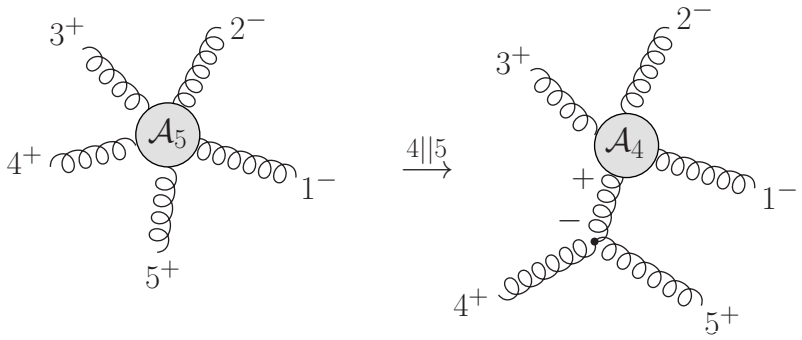

Figure 2.3: Factorization of the five point amplitude in the collinear limit 4||5, the opposite choice of the helicities in the internal line vanishes.

extract the factor of $|\mathcal{A}_4|^2$. By taking the collinear limit in the $(+,-)$, $(-,-)$ and $(-+)$ helicity amplitudes we obtain

$$\begin{aligned}
\mathcal{A}_5(1^-,2^-,3^+,4^+,5^-) &\xrightarrow{4||5} \frac{1}{z\sqrt{1-z}}\frac{g_s}{[45]}\mathcal{A}_4(1^-,2^-,3^+,P^+)\\
\mathcal{A}_5(1^-,2^-,3^+,4^-,5^-) &\xrightarrow{4||5} 0\\
\mathcal{A}_5(1^-,2^-,3^+,4^-,5^+) &\xrightarrow{4||5} \frac{(\sqrt{1-z})^3}{z}\frac{g_s}{[45]}\mathcal{A}_4(1^-,2^-,3^+,P^+).
\end{aligned}$$

By taking the modulus squared and summing over the helicity configurations of 4 and 5 we have

$$\sum|\mathcal{A}_5|^2 = \frac{g_s^2}{(k_4-k_5)^2}\frac{2}{z}P_{gg}(z)|\mathcal{A}_4|^2 \tag{2.2.53}$$

where

$$P_{gg}(z) = P_{gg}(1-z) = \frac{(1-x+x^2)^2}{x(1-x)}. \tag{2.2.54}$$

By using the Sudakov parametrization $k_5 = (1-z)p_4 + \bar{z}n + k_T$ for the phase space integration on k_5 the contribution to the cross section reads

$$\sigma_{\text{collinear}} \sim \frac{1}{2s}\int\frac{dzd^2k_T}{2(1-z)}\frac{1}{(k_4-k_5)^2}\frac{2}{z}P_{gg}(z)\int d\Pi|\mathcal{A}_4|^2 \tag{2.2.55}$$

If we use $(k_4-k_5)^2 = \frac{k_T^2}{(1-z)}$ and the reduced flux factor $2s' \equiv 2zs$ we obtain

$$\sigma_{\text{collinear}} \sim \frac{\alpha_s}{2\pi}\left(\int\frac{dk_T^2}{k_T^2}\right)\int dzP(z)\sigma' \tag{2.2.56}$$

where we factorized out the k_T integration which produces the collinear logarithm and σ' is the cross section of the process with an incoming gluon of momentum zp_4 instead of the two collinear gluons 4 and 5.

Analogously, one can obtain the splitting function related to quark branching

$$P_{qq}(x) = \frac{2}{1-x} - 1 - x \tag{2.2.57}$$

$$P_{qg}(x) = x^2 + (1-x)^2 \tag{2.2.58}$$

$$P_{gq}(x) = \frac{1+(1-x)^2}{x} \tag{2.2.59}$$

Chapter 3

Prompt Photon Production

Prompt photon production [6] is a relevant processes for the study of hard interactions in high-energy collisions. For example, it is the most important reducible background for the $H \to \gamma\gamma$ signal in the light Higgs scenario [7].

In this chapter we will discuss several features of prompt photon production. Compared to hadronic jet production, the study of direct photons at hadron colliders has many advantages, for example no jet reconstruction algorithm is needed. Currently the direct photon cross-section is known up to $\mathcal{O}(\alpha\alpha_s^2)$ [8] and Sudakov resummation effects have been computed up to NLL accuracy [9]. Prompt photon production is especially useful to probe the gluon parton density over a wide range of x [10], since the initial state gluon appears already at leading order. Direct photons data can be used in PDFs fits as a strong constraint for the gluon distribution. However all the data obtained so far are still not completely understood, in particular, some of them show large deviations from the NLO QCD prediction.

The most peculiar aspect of prompt photon process is that we have two different contribution to the cross section: the direct component, where the photon participate to the hard process and the fragmentation component, where the photon is emitted at the hadronization level, thus closely accompained by hadronic activity. The second component involve much more theoretical uncertainty since the fragmentation function of the photon is poorly known. In order to suppress the fragmentation component contribution, tipically isolation cuts are applied on the electromagnetic trigger. At the end of the chapter we will describe the various prescriptions which are adopted in the currently used NLO codes.

3.1 General aspects

3.1.1 Direct photons

The use of direct photon production as an electromagnetic probe of hard scattering processes has a long history. As in the case of DIS, the point-like coupling of the photon to charged particles allows an easier treatment compared to hadronic probes. Furthermore, already at leading order in perturbation theory, the gluon participates to the process of direct photon production via Compton scattering.

Analogously to the deep inelastic process, we can introduce a scaling variable x as

$$x = \frac{4p_T^2}{S} \tag{3.1.1}$$

where p_T is the transverse momentum of the photon and S is the center-of-mass energy of the hadron process. The tipical range of transverse momenta avaiable at hadron collider can reach very low values ($p_T > 20GeV$). Recent measurements at Tevatron from CDF, use a minimum value of $p_T = 32GeV$ which brings the x-range down to 10^{-3}.

From both the experimental and theoretical side, direct photon production is an interesting process, however various complications arise basically because the photon can be produced during the hadronization process. This possibility require a particular treatment of the cross section. Let us clarify this point by looking at the factorization formula for prompt photon production[9] in the hadronic process $pp \to \gamma + X$

$$\begin{aligned} p_T^3 \frac{d\sigma_\gamma(x_\perp, p_T^2)}{dp_T} &= \sum_{a,b} \int_{x_\perp}^1 dx_1 \; f_{a/H_1}(x_1, \mu_F^2) \int_{x_\perp/x_1}^1 dx_2 \; f_{b/H_2}(x_2, \mu_F^2) \times \\ &\times \int_0^1 dx \left\{ \delta\left(x - \frac{x_\perp}{x_1 x_2}\right) \mathcal{C}_{ab}^\gamma(x, \alpha_s(\mu^2); p_T^2, \mu_F^2, \mu_f^2) + \right. \\ &\left. + \sum_c \int dz \; z^2 d_{c/\gamma}(z, \mu_f^2) \delta\left(x - \frac{x_\perp}{z x_1 x_2}\right) \mathcal{C}_{ab}^c(x, \alpha_s(\mu^2); p_T^2, \mu_F^2, \mu_f^2) \right\}. \end{aligned} \tag{3.1.2}$$

The first contribution to the sum in this formula is known as the direct component, f_{a/H_i} are the customary PDFs corresponding to the probability density of finding a parton a with momentum fraction x_i in the hadron H_i and $\mathcal{C}_{ab}^\gamma$ is the short distance cross section related to the hard process $a + b \to \gamma + X$. Here the photon participates at the level of the hard cross section. The second term in eq. (3.1.2) is the fragmentation component.

This contribution involve every subprocess $ab \to c + X$ where a, b, c are all partons. The relative hard cross section given by $\mathcal{C}_{ab}^{c}$ is multiplied by PDFs, which describe the initial state, as well by a fragmentation function of the photon $d_{c/\gamma}(z)$ which gives the probability of finding a photon of momentum fraction z in the hadronization shower produced by the parton c.

In the factorization formula, three arbitrary scales appear: the factorization scale μ_F, the renormalization scale μ_R and the fragmentation scale μ_f. All this scales are defined as the subtraction points of collinear (from initial and final state) and ultraviolet divergencies. The cross section cannot depend on these subtraction scales, indeed one can improve the fixed order results by imposing renormalization group invariance, which is equivalent to resum higher order contributions which cure this unphysical dependence. Therefore, the fixed order scale dependence gives informations about the relevance of higher order terms which can be viewed as a source of theoretical uncertainty. Tipically, an estimate of this uncertainty can be obtained by varying independently μ_F^2, μ^2 and μ_f^2 from p_T^2/k to kp_T^2 [1], however this procedure tipically overestimates the uncertainty, a more suitable choice is to avoid the presence of those large scale ratios which would produce a larger scale dependence.

The inclusion of a fragmentation component is due to the presence of collinear singularities in the final state which do not cancel in the direct component, instead they must be absorbed in the fragmentation function definition. Analogously to the PDFs, the fragmentation function satisfies a DGLAP evolution equation. From a phenomenological point of view, the fragmentation component is an issue because it represents a large source of uncertainty since the fragmentation function which describe the hadronic content of the photon is poorly known.

The procedure to reduce the fragmentation contribution is to impose isolation cuts realized by drawing a cone of fixed aperture in (η, ϕ) space around the photon, restricting the hadronic transverse energy allowed in this cone to a certain small fraction ϵ of the photon transverse energy. In this way, the fragmentation contribution is substantially reduced, However, the cone isolation is not enough to get rid of this contribution, in particular at very low values of the transverse momentum ($p_T \lesssim 20GeV$) the fragmentation term gives the 30% of the cross section$x$[11], thus at small-x is certainly relevant.

An alternative isolation criterion has been proposed by Frixione in Ref. [12]; with this particular choice, the fragmentation component is identically zero, and the direct component aquires a physical meaning. We shall discuss this prescription in the next section.

[1] The tipical choice is $k = 2$.

Collaboration	Reaction	$\sqrt{s}$ [GeV]	$p_{_T}$ range [GeV/c]	$x_{_F}$/rapidity range	$x_{_T}$ range
WA70[13]	$p\ p$	23.0	$p_{_T} > 4.0$	$-.35 < x_{_F} < .45$	$x_{_T} > .35$
UA6[14]	$p\ p$	24.3	$p_{_T} > 4.1$	$-0.1 < \eta < 0.9$	$x_{_T} > .34$
UA6[14]	$\bar{p}\ p$	24.3	$p_{_T} > 4.1$	$-0.1 < \eta < 0.9$	$x_{_T} > .34$
E706[15]	$p\ Be$	31.6	$p_{_T} > 3.5$	$-.75 < \eta < .75$	$x_{_T} > .22$
E706[15]	$p\ Be$	38.8	$p_{_T} > 3.5$	$-1.0 < \eta < 0.5$	$x_{_T} > .18$
R806[16]	$p\ p$	63.	$p_{_T} > 3.5$	$-0.2 < \eta < 0.2$	$x_{_T} > .11$
R110[17]	$p\ p$	63.	$p_{_T} > 4.5$	$-0.8 < \eta < 0.8$	$x_{_T} > .14$
AFS/R807[18]	$p\ p$	63.	$p_{_T} > 4.5$	$-0.7 < \eta < 0.7$	$x_{_T} > .14$
CDF RunII[19]	$\bar{p}p$	1960.	$30 < p_T < 350$	$-1 < \eta < 1$	$x_T > 10^{-3}$

Table 3.1: Summary of the main features of the data sets. The transverse and longitudinal variables $2p_T/\sqrt{s}$ and $2p_{_L}/\sqrt{s}$.

3.1.2 Consistency among data sets

Prompt-photon production at high transverse momentum has been measured in various hadron processes including pp, $p\bar{p}$ and pN. A comparison between data and NLO prediction is shown in Fig. (3.1).

One of the principal experimental complications in this process is that photons can be accompained by hadronic activity, indeed, the tipical background comes from the π_0 decay. This is the reason why one has to introduce the a perturbative fragmentation function.

Despite to many years of experimental efforts, this process is not yet fully understood, since some measurements, in particular the fixed-target ones show large discrepancies from the NLO pQCD prediction. The problem of consistency among fixed target data has been discussed in Ref. [20], however still there is no agreement on how to treat these data in order to include the photon production on a global fit of PDFs. Several attempts have been done in the past to explain the fixed target data. It has been shown that the disagreement between theoretical prediction and data cannot be explained by fine-tuning of unphysical scales and the gluon density. Alternative solutions to this problem take into account intrinsic transverse momentum of the gluon produced by initial state radiation. Such corrections can have various origines, soft and high energy resummation, non perturbative or higher-twist effect, therefore can be included only with *ad hoc* models. This possibility has been investigated using phenomenological models with gaussian k_T smearing for justify the enhancement of the E706 data[15].

These model-dependent contributions are only partially under control and moreover they are not sufficient to recover the consistency of fixed-target and

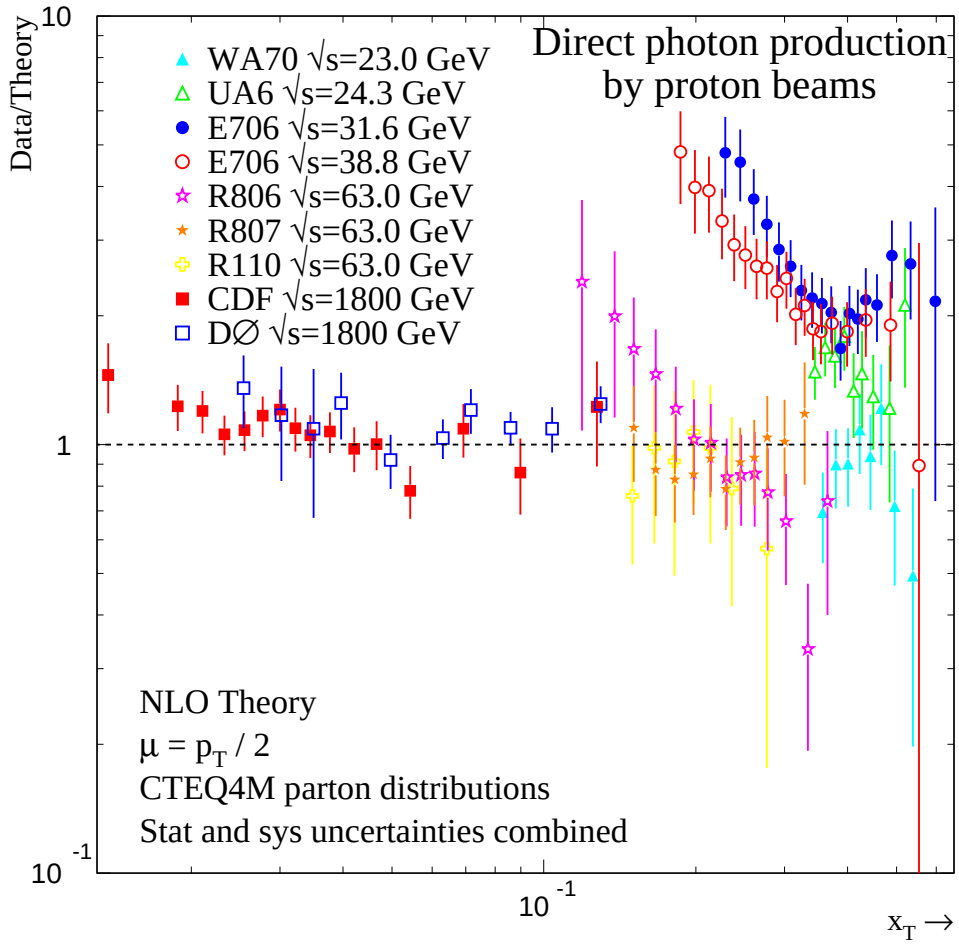

Figure 3.1: Comparison between prompt photon data and NLO prediction for several experiments as a function of $2p_T^2/S$.

collider data, thus it is still an open problem the consistent treatment of these data.

The more recent measurement from CDF shows a good agreement with the NLO prediction (see Fig. (3.2). However, at low values of the transverse momentum the NLO underpredicts the cross section. This discrepancy is partially understood in terms of soft resummation as shown in Ref. [21] in the framework of soft collinear effective theory. The inclusion of higher-order contributions coming from the soft radiation improves the agreement with CDF data. As we shall discuss, this deviation is not related to small-x effects.

3.2 Prompt photons: theoretical results

In this section we review the known perturbative results on prompt photon production. As we already mentioned, according to perturbative factorization, the NLO cross section can be written as shown in eq. (3.1.2), where the coefficient functions are series in the strong coupling

$$\begin{aligned}\mathcal{C}^{\gamma}_{ab}(x,\alpha_s(\mu^2);p_T^2,\mu_F^2,\mu_f^2) &= \alpha\alpha_s(\mu^2)\left[\mathcal{C}^{\gamma(0)}_{ab}(x)+\sum_{n=1}^{\infty}\alpha_s^n(\mu^2)\mathcal{C}^{\gamma(n)}_{ab}(x,\alpha_s(\mu^2);p_T^2,\mu_F^2,\mu_f^2)\right]\\ \mathcal{C}^{c}_{ab}(x,\alpha_s(\mu^2);p_T^2,\mu_F^2,\mu_f^2) &= \alpha_s^2(\mu^2)\left[\mathcal{C}^{c(0)}_{ab}(x)+\sum_{n=1}^{\infty}\alpha_s^n(\mu^2)\mathcal{C}^{c(n)}_{ab}(x,\alpha_s(\mu^2);p_T^2,\mu_F^2,\mu_f^2)\right].\end{aligned} \tag{3.2.1}$$

At leading order in perturbation theory, the direct component receives contribution from the $q\bar{q}$ annihilation and the qg channel (Compton scattering). The corresponding leading-order hard coefficient functions are given by [6, 22]

$$\mathcal{C}^{\gamma,LO}_{q\bar{q}}(x) = \frac{\mathbf{q}^3 d\hat{\sigma}_{q\bar{q}\to\gamma g}}{d\mathbf{q}} = \alpha\alpha_s Q_q^2\pi\frac{C_F}{C_A}\frac{x}{\sqrt{1-x}}(2-x), \tag{3.2.2}$$

$$\mathcal{C}^{\gamma,LO}_{q(\bar{q})g}(x) = \frac{\mathbf{q}^3 d\hat{\sigma}_{q(\bar{q})g\to\gamma q(\bar{q})}}{d\mathbf{q}} = \alpha\alpha_s Q_q^2\pi\frac{1}{2C_A}\frac{x}{\sqrt{1-x}}(1+\frac{x}{4}) \tag{3.2.3}$$

in terms of the partonic variable $x = 4\mathbf{q}^2/\hat{s}$, where $\hat{s}$ is the partonic center-of-mass energy.

3.2.1 The NLO cross section and computer codes

The NLO calculation[23, 24, 25] $\mathcal{O}(\alpha\alpha_s^2)$ receives contributions from the subprocesses $q\bar{q}\to\gamma gg$, $gq(\bar{q})\to\gamma gq(\bar{q})$ and from the virtual corrections to the Born diagrams. In the litterature the following factorization formula can be found

$$\begin{aligned}E_\gamma\frac{d^3\sigma^{AB}}{d^3p_\gamma} &= \frac{1}{\pi p_T^4}\sum_{a,b}\int_{\frac{\sqrt{x}}{2}e^{\eta}}^{1-\frac{\sqrt{x}}{2}e^{-\eta}}dv\int_{\frac{\sqrt{x}}{2v}e^{\eta}}^{1}dw\; x_1 f_a^A(x_1)\; x_2 f_b^B(x_2)\cdot\\ &\qquad\cdot v(1-v)w\hat{s}\frac{d\hat{\sigma}^{ab}}{dvdw}\end{aligned} \tag{3.2.4}$$

in terms of the variables v and w which are related to x_1, x_2 and the rapidity η by the relations

$$x_1 = \frac{\sqrt{x}e^{\eta}}{2vw}, \qquad x_2 = \frac{\sqrt{x}e^{-\eta}}{2(1-v)}, \tag{3.2.5}$$

Analitic expressions for the v and w distribution are avaiable in Ref. [25]. The next-to-leading order prediction for both polarized and unpolarized cross section, including isolation prescriptions, have been implemented in various numerical codes. All the plots shown in this thesis have been produced by the Gordon-Vogelsang's code[25] which is based on the analitic calculation and it is fully inclusive in the hadronic final state.

The advantage of using the inclusive calculation is that the cancellation of soft singularities is performed analitically, which makes the code faster than a MonteCarlo program. The inclusion of isolation criteria is performed by adding suitable "subtraction" terms to the cross section. This procedure is equivalent to imposing cuts in the phase space in the narrow-cone approximation. Since the flexibility of an inclusive code is limited, fully exclusive MonteCarlo codes have been developped like Fixione-Vogelsang[26] and `JETPHOX`[27, 28]. In Fig. (3.3) we show the unisolated NLO cross section normalized to the leading order one. As shown in the plot, the correction increase the LO result of 15-20% in the range between 20GeV and 400GeV.

As we already mentioned, one of the important feature of the prompt photon production is that the gluon participate at leading order by a Compton-like subprocess. This is the reason why this process can provide an important constraint to the gluon density. Let us investigate which is the region x-space which gives the dominant contribution to the cross section. This can be easily achieved by considering the following function

$$R(x_{\min}) = \frac{1}{\sigma}\int_{x_{\min}}^{1} dx_1 G_1(x_1) \int_{x_{\min}/x_1} G_2(x_2)\mathcal{C}^{\gamma}(\hat{x}), \quad \hat{x} = \frac{x_T}{x_1 x_2} \qquad (3.2.6)$$

which schematically is the convolution of a parton density G with the NLO coefficient function $\mathcal{C}^{\gamma}$. The function $R(x_{\text{xmin}})$ is the contribution to the cross section coming from the region $x_{\min} > x_T$ inside the convolution integral normalized to the inclusive cross section. The meaning of this function is to select the contribution to the cross section coming from the region of the phase space where the parton densities are evaluated at $x_1 > x_{\min}$ and $x_1 x_2 > x_{\min}$.

As shown in Fig. (3.4) the function $R(x_{\min}$ at $p_T = 20\text{GeV}$ is close to one up to $5 \cdot 10^{-2}$ at the Tevatron energy and up to $5 \cdot 10^{-3}$ at LHC. In the case of Tevatron, at $p_T = 20\text{GeV}$ we have $x \approx 4 \cdot 1{-}^{-4}$, therefore the convolution integral is dominated by medium-large arguments of the PDFs $x_1, x_2 > 5 \cdot 10^{-2}$ and, correspondly, the coefficient function is evaluated in the range $\hat{x} < 20 x_T \approx 10^{-2}$. Namely, the prompt photon cross section is very sensitive to the parton densities for medium-large values of x_i, thus we expect that the inclusion of prompt photon data in a global PDF fit would provide a constraint in that region.

3.2.2 Isolation prescriptions

From the experimental point of view, it is not difficult to select a data sample where the direct contribution is dominant over the fragmentation mechanism. This can be achieved by imposing a selection cut on those events where the photon is not isolated from hadronic tracks. From the theory side, instead, the problem to isolate a photon from the hadronic activity is more involved. Indeed, the naive procedure to avoid soft radiations of quarks and gluons inside a cone drawn around the photon momentum would spoil the cancellation of infrared divergency, which is a crucial requirement in order to obtain a physical cross section.

Traditional isolation cuts which preserve the infrared safety of the cross section are based on the cone approach[12], where only a small amount of hadronic energy can be found inside the cone as a fraction of photon energy

$$E < \epsilon E_\gamma \tag{3.2.7}$$

where ϵ is a fixed parameter. With such isolation prescription we put a maximum limit on the energy contribution coming from QCD radiation, therefore soft partons can be emitted as well as the collinear radiation. The latter still require a fragmentation component but its contribution to the total cross section is reduced by the isolation cut as shown Fig. (3.5).

Now we will describe a different approach which allows us to define a physical cross section given only by the direct component. The profound reason why we need a fragmentation component is the presence collinear singularities when the photon momentum becomes parallel to the quark inside the cone. These singularities cancel in the sum of the direct and fragmentation parts, therefore such a criterion must involve a suitable constraint on the phase space which avoid purely collinear radiation. Let us define the quantity

$$R_{i\gamma} = \begin{cases} \delta_{i\gamma} & e^+e^- \text{process} \\ \sqrt{(\eta_i - \eta_\gamma)^2 + (\phi_i - \phi_\gamma)^2} & \text{hadronic collisions} \end{cases} \tag{3.2.8}$$

where $\delta_{i\gamma}$ is the angle between the three-momenta of a parton i and the photon while, in the case of hadronic collision, η and ϕ are the pseudorapidity and azimuthal angle. In terms of this angular distance, given a fixed cone drawn around the photon momentum of fixed angle δ_0, the condition which allow to get rid of collinear radiation is

$$\sum_i E_i \theta(\delta - R_{i\gamma}) \leq \mathcal{H}(\delta) \;\; \text{for all } \delta < \delta_0 \tag{3.2.9}$$

where $\mathcal{H}$ is an arbitrary function which satisfies

$$\lim_{\delta \to 0} \mathcal{H}(\delta) = 0. \tag{3.2.10}$$

This constraint forces the hadronic energy due to quark and gluon radiation inside the cone to scale as a function of the opening angle which vanishes when δ approaches to zero, thus the collinear singularity is dampted by the soft quark region. With the condition in eq. (3.2.9) a parton emitted collinearly to the photon must be soft. A suitable function $\mathcal{H}(\delta)$ is given by

$$\mathcal{H}(\delta) = E_\gamma \epsilon_\gamma \left(\frac{1 - \cos\delta}{1 - \cos\delta_0} \right)^n \tag{3.2.11}$$

where E_γ is the photon energy, for e^+e^- process, or p_T for hadron collisions. In order to show that no collinear divergencies can appear with this isolation prescription let us consider in the e^+e^- case a quark emitted inside the isolation cone. Since a quark emission cannot produce a soft singularity, the leading behaviour of the cross section is $1/(k_q^T)^2 \sim 1/(1 - \cos\delta)$, therefore including the phase space integration we have

$$\sigma \sim \int_0 E_q dE_q \int_0^{\delta_0} \frac{d\cos\delta}{1 - \cos\delta} \theta(\mathcal{H}(\delta) - E_q) = \tag{3.2.12}$$

$$= \frac{E_\gamma^2 \epsilon_\gamma^2}{4n}. \tag{3.2.13}$$

Now we have eliminated the purely collinear region from the quark phase space the fragmentation component is identically zero because it comes precisely from the region we have excluded. In other words, the fragmentation is concentrated on the $z = 1$ (soft) region which is a set of zero measure.

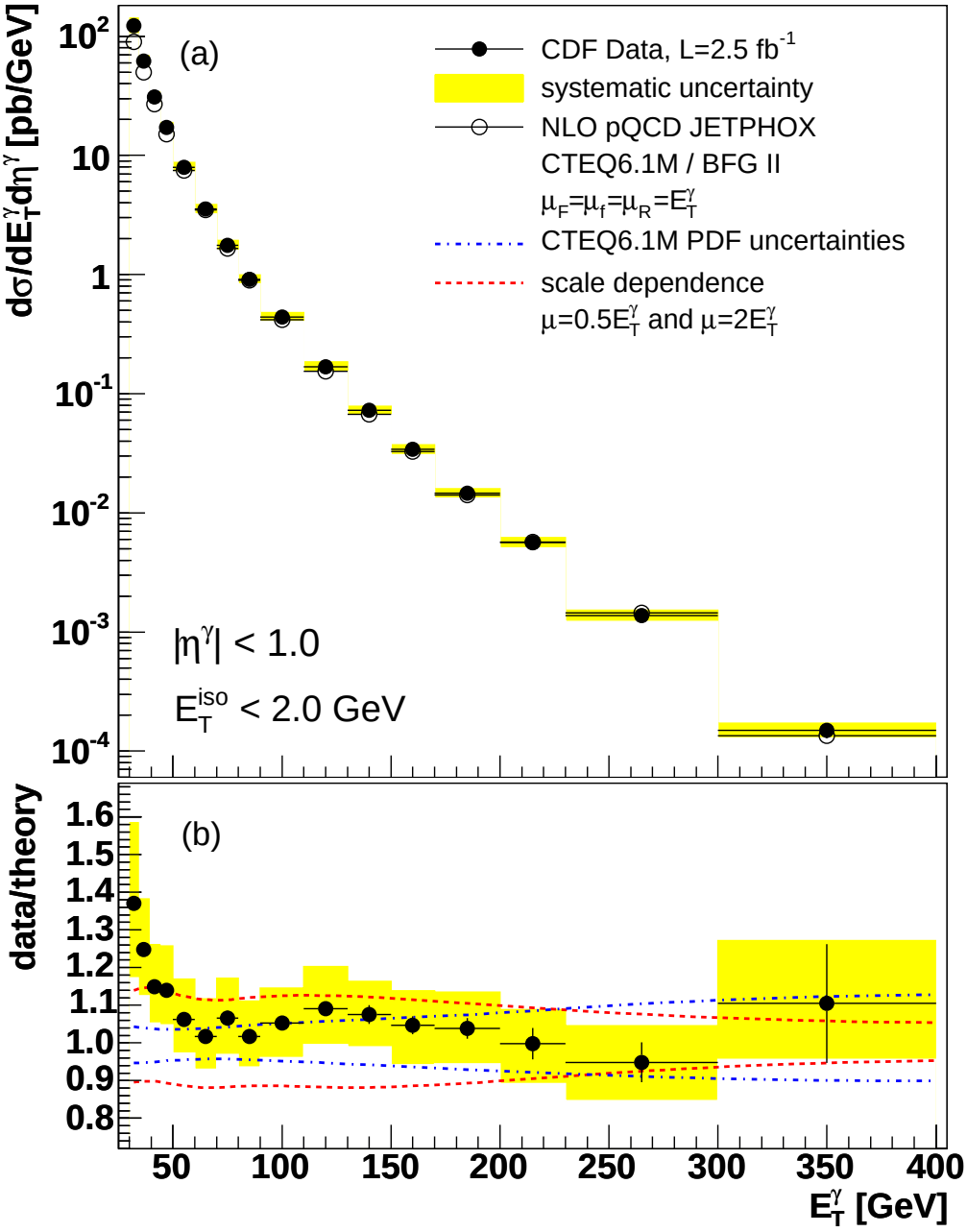

Figure 3.2: (a) Measured inclusive cross section at CDF runII compared to NLO prediction. (b) Ratio data/theory: the shaded bands show scale (red) and PDFs (blue) uncertainties.

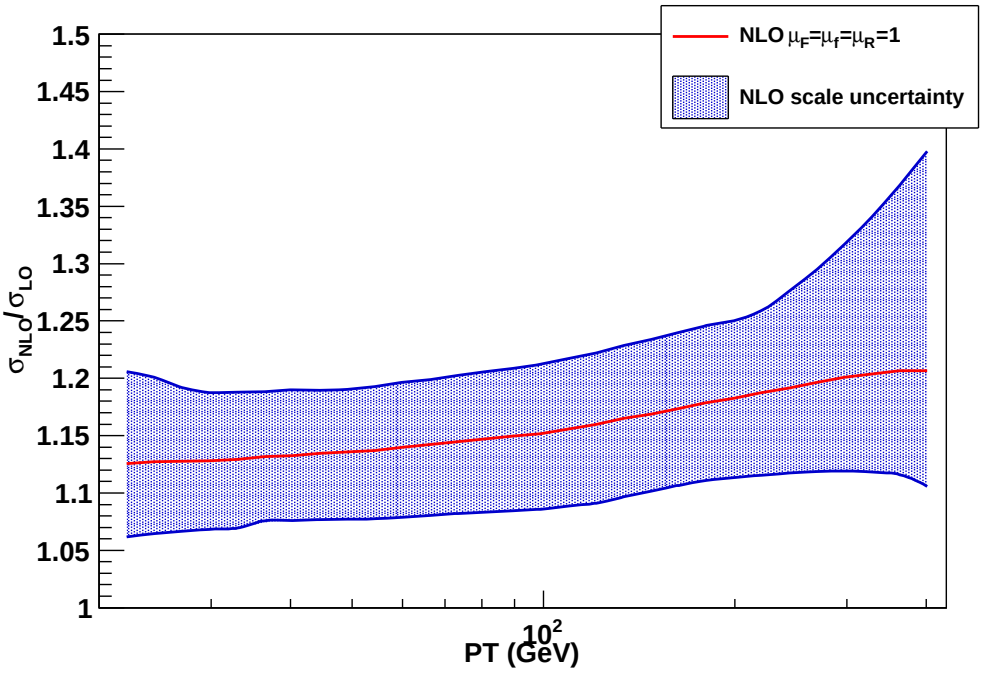

Figure 3.3: Ratio between NLO and LO unisolated cross section with scale uncertainty. The central line (solid, red) corresponds to the scale choice $\mu_F = \mu_R = \mu_f = 1$ while the blue band has been obtained vay varying independently the three subtraction scales between $2p_T$ and $p_T/2$ but excluding "large" scale ratios.

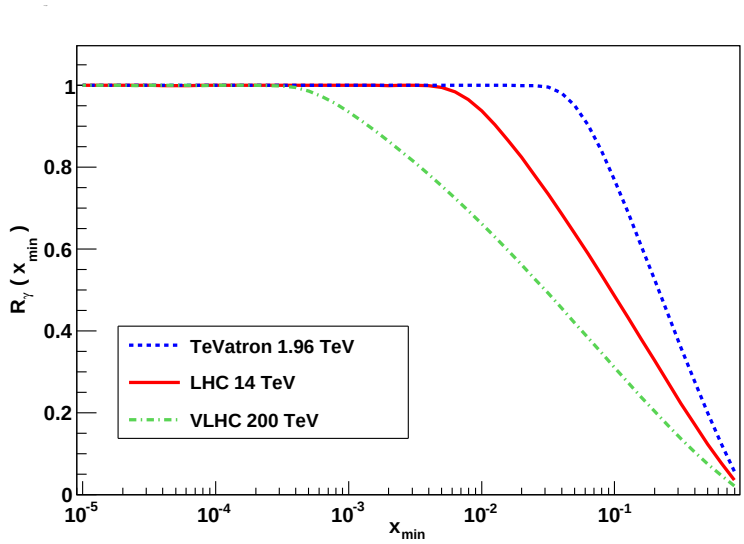

Figure 3.4: The function $R(x_{\min})$ at the LHC $\sqrt{S} = 14$ TeV (red solid line) and at Tevatron Run II $\sqrt{S} = 1.96$ TeV (blue dashed line) for the production of photon with $p_T = 20$ GeV. It is clear that the cross-section is dominated by the contribution of the coefficient function at medium and large-x, $x \gtrsim 5\,10^{-3}$ for LHC and $x \gtrsim 5\,10^{-2}$ for the Tevatron.

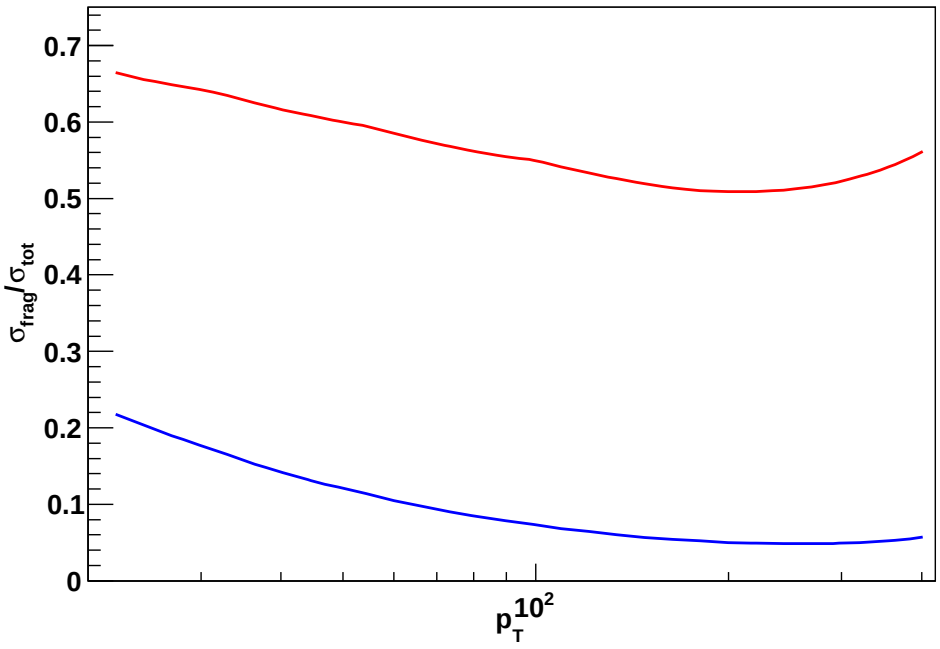

Figure 3.5: Ratio between The fragmentation contribution and the total cross section. Without any isolation, the fragmentation component (red) gives more than 50% of the cross section in a wide range of transverse momentum of the photon ($20 < p_T < 400$. Traditional cone isolation (blue) reduces the fragmentation to less than 20% and less than 10% for $p_T > 100$GeV. In both curves we used the CDF center-of-mass energy $\sqrt{s} = 1960$GeV.

Chapter 4

High Energy Resummation

Perturbative QCD provides accurate theoretical predictions for hard processes at high-energy colliders. Logarithmic corrections to the lowest-order cross-sections can be systematically computed in the region of large hard scale Q^2, $\Lambda^2 \ll Q^2 \sim S$, by a renormalization group approach which leads to the factorization theorem of mass singularities [29]. However, the TeV energy range opens up the two scale region $\Lambda^2 \ll Q^2 \ll S$, where the usual perturbative expansion receives large contributions characterized by logarithms of the ratio $x = Q^2/S$. In order to recover the accuracy of the perturbative results, logarithmically enhanced small-x contributions to the hard cross-sections, associated to multiple gluon emission, must be resummed to all orders.

The general procedure for the small-x leading-log (LLx) resummation of hard coefficient functions is well established in perturbative QCD within the framework of the k_t-factorization theorem [30, 31], and involves the computation of the leading amplitude of the process with off-shell incoming gluons. This technique has been used to obtain resummed cross-sections for heavy quarks photo- and hadro-production [30, 32, 33, 34], deep inelastic scattering [31, 35], Higgs production [36, 37, 38] and recently for the Drell-Yan process [39].

Other applications of the k_t-factorization theorem can be found in refs. [40, 41] for the NLO corrections to the jet vertex and the DIS impact factor. In this chapter we will discuss the high energy resummation in general, starting from the k_t-factorization theorem, which generalizes the well known collinear factorization to k_t-dependent parton distributions. We shall see that the high energy logarithms come from the BFKL kinematics and that the corresponding evolution equation is related to DGLAP by duality relations. The general technique which allows to resum all the small-x logarithms will be derived in the light of recent developments on the resummation of rapidity distributions. As application of this technique, we will focus on the processes

of heavy quark pair production and Drell-Yan.

4.1 A two-scale problem

4.1.1 Finding logarithms

As we anticipated, at high energy, physical observables are affected by large logarithms of the scaling variable x. At leading-log, gluon ladder diagrams are the only source of such logarithms[42, 43, 44, 45], let us consider the multiple gluon emission depicted in Fig. (4.1). In terms of light-cone variables, the

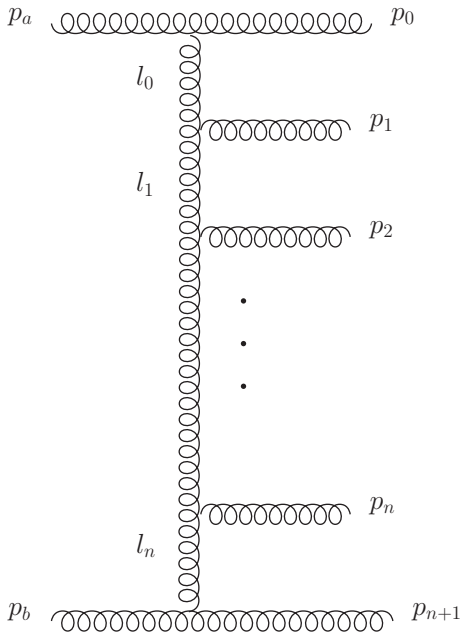

Figure 4.1: Multiple gluon emission.

phase space integration reads

$$d\Phi = \prod_{i=0}^{n+1} \left(d^2 p_i^{\perp} dp_i^{+} dp_i^{-} \delta(p_i^2) \right) \cdot \delta^4(p_a + p_b - P_{0,n+1}) \tag{4.1.1}$$

where we defined $P_{i,j} = \sum_{k=i}^{j} p_k$. Now if we express the integration in terms of the exchanged momenta in the propagators $l_i = p_b - P_{i+1,n+1}$, the on-shell constraint for outgoing momenta becomes

$$\begin{aligned} 0 = p_i^2 = (l_i - l_{i-1})^2 = l_i^2 - 2 l_i l_{i-1} + l_{i-1}^2 = \\ = 2(l_i^+ l_i^- - \bar{l}_i l_i) - 2(l_i^+ l_{i-1}^- + l_i^- l_{i-1}^+ + l_i \bar{l}_{i-1} + \bar{l}_i l_{i-1}) + l_{i-1}^2 \end{aligned} \tag{4.1.2}$$

we have

$$d\Phi = \prod_{i=0}^{n} \left(d^2 l_i^{\perp} \frac{dl_i^-}{2(l_i^- - l_{i-1}^-)} \right) \cdot \delta^4(p_a + l_0 - p_0) d^4 p_0. \tag{4.1.3}$$

with $l_{n+1} = p_b$. Notice that in the reference frame where

$$\begin{aligned} p_a &= (p_a^+, 0, 0, 0), \\ p_b &= (0, p_b^-, 0, 0), \end{aligned}$$

the "plus" component represents the longitudinal part, parallel to p_a, while the "minus" component is parallel to p_b. Now, in the region where the longitudinal components l_i^- are strong ordered

$$l_0^- \ll l_1^- \ll \cdots \ll l_{n-1}^- \ll l_n^-, \tag{4.1.4}$$

the phase space integration reduces to

$$d\Phi = \prod_{i=0}^{n} \left(d^2 l_i^{\perp} \frac{dl_i^-}{2l_i^-} \right) \tag{4.1.5}$$

which give rise to a large logarithm in the high energy limit. If we parametrize the light-cone components of outgoing momenta as

$$p_i = (p_i^{\perp} e^{y_i}, p_i^{\perp} e^{-y_i}; p_i, \bar{p}_i) \tag{4.1.6}$$

the constraint in eq. (4.1.4) becomes

$$p_1^{\perp} e^{-y_1} \ll p_2^{\perp} e^{-y_2} \ll \cdots \ll p_n^{\perp} e^{-y_n} \ll p_{n+1}^{\perp} e^{-y_{n+1}}. \tag{4.1.7}$$

The strong ordering of the "minus" components can be obtained in two ways. The first one is to impose the strong ordering of transverse momenta, which is the usual ordering for the factorization of collinear singularities. Another way to get the same hierarchy is to allow the strong ordering in rapidities y_i keeping the transverse momenta of the same order of magnitude, so we have

$$\begin{aligned} y_1 \gg y_2 \gg \cdots \gg y_n \gg y_{n+1} \\ p_1^{\perp} \sim p_2^{\perp} \sim \cdots \sim p_n^{\perp} \sim p_{n+1}^{\perp} \end{aligned} \tag{4.1.8}$$

which is known as the multi Regge kinematics.

4.1.2 Resummed coefficient function from k_t-factorization

In this section we will show how the properties of gluon ladders (from BFKL theory) can be used to obtain a resummed cross section. In the approach proposed in Ref. [30, 31], the collinear factorization of hard cross section and structure function is replaced with the corresponding high-energy factorization which is k_T-dependent

$$Q^2\sigma(x,Q^2/\mu^2)=\int\frac{d^2\mathbf{k}}{\mathbf{k}^2}\int_x^1\frac{dz}{z}\hat{\sigma}(x/z,\mathbf{k}^2/Q^2)\mathcal{F}(z,\mathbf{k}^2,\mu^2) \tag{4.1.9}$$

where $\mathcal{F}$ is the unintegrated gluon structure function and $\hat{\sigma}$ is the off-shell hard cross section, defined as the Born coefficient function with off shell incoming gluons.

This improved factorization reduces to the traditional form in the limit $S\gg Q^2\gg k_T^2$. In this limit, the hard cross section $\hat{\sigma}$ reduces to the on-shell Born cross section and the standard parton distribution function are obtained by integration in the transverse variables

$$G(z,\mu^2)=\int d^2\mathbf{k}\mathcal{F}(z,\mathbf{k},\mu^2) \tag{4.1.10}$$

but eq. (4.1.9) holds also for any value of the ratio k_T^2/Q^2. The k_T-factorization formula embodies all the high energy enhanced contributions which at leading-log level stem from ladder-type gluon exchanges. All the informations about the gluon ladder are included in the k_T-dependent structure function $\mathcal{F}$. Let us concentrate first on the properties of the gluon ladder. The structure function $\mathcal{F}$ satisfies the integral equation

$$\mathcal{F}(x,\mathbf{k}^2/Q_0^2)=\delta(1-x)\mathbf{k}^2\delta(\mathbf{k}^2-Q_0^2)+\bar{\alpha}_s\int\frac{\mathbf{k}^2d\mathbf{q}^2}{\mathbf{q}^2|\mathbf{q}^2-\mathbf{k}^2|_{reg}}\int_x^1\frac{dz}{z}\mathcal{F}(x/z,\mathbf{q}^2/Q_0^2) \tag{4.1.11}$$

where we used the regularized distribution

$$\frac{1}{|\mathbf{q}^2-\mathbf{k}^2|_{reg}}\equiv\frac{1}{|\mathbf{q}^2-\mathbf{k}^2|}-\delta(\mathbf{q}^2-\mathbf{k}^2)\int_0^{2\mathbf{k}^2}\frac{d\mathbf{q}'^2}{|\mathbf{q}'^2-\mathbf{k}^2|}. \tag{4.1.12}$$

The second piece in eq. (4.1.12) comes from the virtual correction to the multigluon ladder and regulates the singularity in $\mathbf{q}^2=\mathbf{k}^2$. If we take the Mellin moments in eq. (4.1.11) we obtain

$$\mathcal{F}_N(\mathbf{k}^2/Q_0^2)=\mathbf{k}^2\delta(\mathbf{k}^2-Q_0^2)+\frac{\bar{\alpha}_s}{N}\int\frac{\mathbf{k}^2d\mathbf{q}^2}{\mathbf{q}^2|\mathbf{q}^2-\mathbf{k}^2|_{reg}}\mathcal{F}_N(\mathbf{q}^2/Q_0^2). \tag{4.1.13}$$

with as usual

$$\mathcal{F}_N(\mathbf{k}^2/Q_0^2) \equiv \int_0^1 \frac{dx}{x} x^N \mathcal{F}(x, \mathbf{k}^2/Q_0^2). \tag{4.1.14}$$

Eq. (4.1.13) can be solved in terms of the double Mellin moments

$$\mathcal{F}_{NM} \equiv \int_0^\infty \frac{d\mathbf{k}^2}{\mathbf{k}^2} \left(\frac{\mathbf{k}^2}{Q_0^2}\right)^{-M} \mathcal{F}_N(\mathbf{k}^2/Q_0^2), \tag{4.1.15}$$

indeed we have

$$\begin{aligned}
\mathcal{F}_{NM} &= 1 + \frac{\bar{\alpha}_s}{N} \int_0^\infty \frac{d\mathbf{k}^2}{\mathbf{k}^2} \left(\frac{\mathbf{k}^2}{Q_0^2}\right)^{-M} \int_0^\infty \frac{\mathbf{k}^2 d\mathbf{q}^2}{\mathbf{q}^2|\mathbf{q}^2 - \mathbf{k}^2|_{reg}} \mathcal{F}_N(\mathbf{q}^2/Q_0^2) = \\
&= 1 + \frac{\bar{\alpha}_s}{N} \int_0^\infty \frac{d\mathbf{q}^2}{\mathbf{q}^2} \mathcal{F}_N(\mathbf{q}^2/Q_0^2) \left(\frac{\mathbf{q}^2}{Q_0^2}\right)^{-M} \int_0^\infty \frac{d\mathbf{k}^2}{\mathbf{q}^2|1 - \mathbf{k}^2/\mathbf{q}^2|_{reg}} \left(\frac{\mathbf{k}^2}{\mathbf{q}^2}\right)^{-M} = \\
&= 1 + \frac{\bar{\alpha}_s}{N} \mathcal{F}_{NM} f(M)
\end{aligned}$$

where

$$f(M) \equiv \int_0^\infty \frac{d\xi}{|1-\xi|_{reg}} \xi^{-M} = 2\psi(1) - \psi(M) - \psi(1-M), \tag{4.1.16}$$

therefore we have

$$\mathcal{F}_{NM} = \frac{1}{1 - \frac{\bar{\alpha}_s}{N} f(M)} \tag{4.1.17}$$

which in $\mathbf{k}$ space yields

$$\mathcal{F}_N(\mathbf{k}^2) = \frac{1}{2\pi i} \int_{\frac{1}{2}-i\infty}^{\frac{1}{2}+i\infty} \frac{dM}{1 - \frac{\bar{\alpha}_s}{N} f(M)} \left(\frac{\mathbf{k}^2}{Q_0^2}\right)^M. \tag{4.1.18}$$

Now we can rewrite the convolution in eq. (4.1.9) in Mellin space and using $\mathcal{F}$ in eq. (4.1.18) we have

$$\sigma_N(Q^2/Q_0^2) = \int_{\frac{1}{2}-i\infty}^{\frac{1}{2}+i\infty} \frac{dM}{2\pi i} \left(\frac{Q^2}{Q_0^2}\right)^M \frac{1}{1 - \frac{\bar{\alpha}_s}{N} f(M)} \frac{h(N,M)}{M} \tag{4.1.19}$$

where we introduced the impact factor

$$\frac{h(N,M)}{M} = \int_0^\infty \frac{d\mathbf{k}^2}{\mathbf{k}^2} \left(\frac{\mathbf{k}^2}{Q^2}\right)^M \hat{\sigma}_N(\mathbf{k}^2). \tag{4.1.20}$$

The integration in eq. (4.1.19) can be performed by closing the contour integral ($\mathrm{Re}(M) = 1/2$) at infinity as shown in fig. (4.4), therefore the result

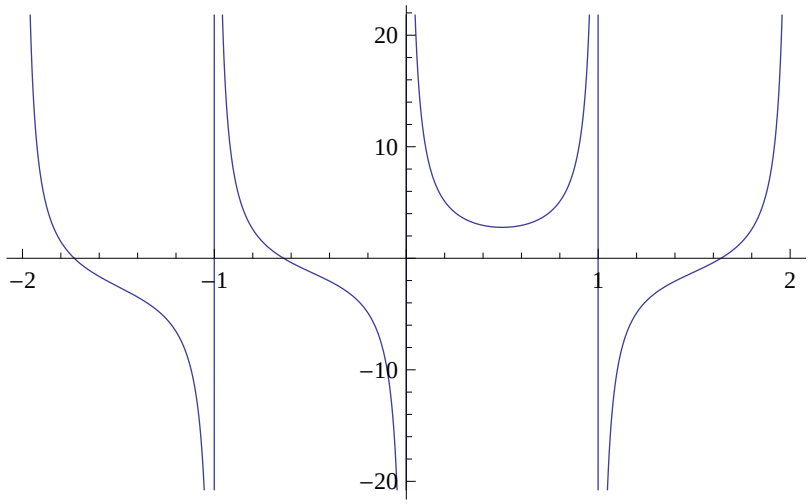

Figure 4.2: Plot of the function $f(M)$.

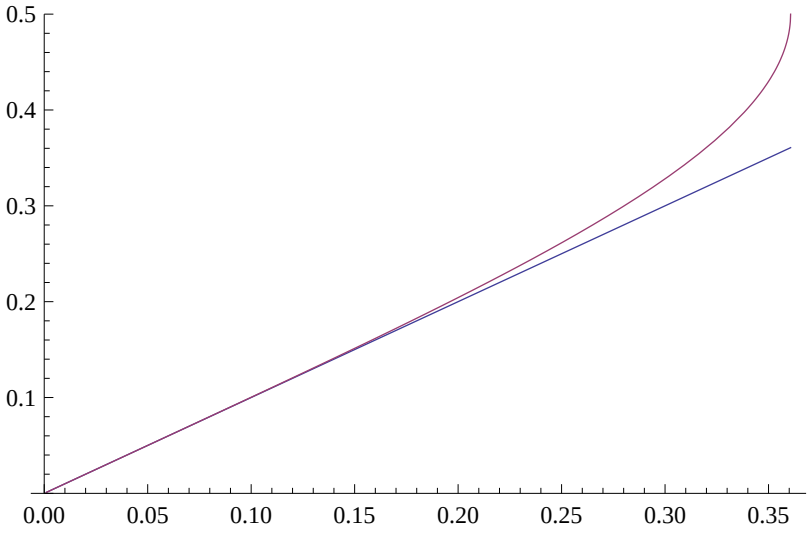

Figure 4.3: The perturbative branch γ_s.

is a sum of all residues of each pole of the integrand inside the contour. If the impact factor $h(M)$ is a holomorphic function everywhere, the poles are all the zeroes of the denominator $1 - \frac{\bar{\alpha}_s}{N} f(M)$. The contribution of a pole in the region $M < 0$ is suppressed by negative powers of Q^2/Q_0^2 which is the tipical behaviour of non perturbative effects. The perturbative branch can

be expressed as

$$M = \gamma_s(\bar{\alpha}_s/N) = \frac{\bar{\alpha}_s}{N} + 2\zeta(3)\left(\frac{\bar{\alpha}_s}{N}\right)^4 + \mathcal{O}\left(\left(\frac{\bar{\alpha}_s}{N}\right)^6\right). \tag{4.1.21}$$

As shown in fig. (4.3), in a wide range of the ratio $\bar{\alpha}_s/N$, γ_s can be approximated by $\bar{\alpha}_s/N$, while when $\bar{\alpha}_s/N$ approaches the minimum value of f, $(4\log 2)^{-1}$, γ_s is $1/2$. Thus the final result is

$$\sigma_N(Q^2/Q_0^2) = \left(\frac{Q^2}{Q_0^2}\right)^{\gamma_s}\left(-\gamma_s\frac{\bar{\alpha}_s}{N}f'(\gamma_s)\right)^{-1} h(N,\gamma_s). \tag{4.1.22}$$

where $h(N,\gamma_s)$ represents the resummed coefficient function.

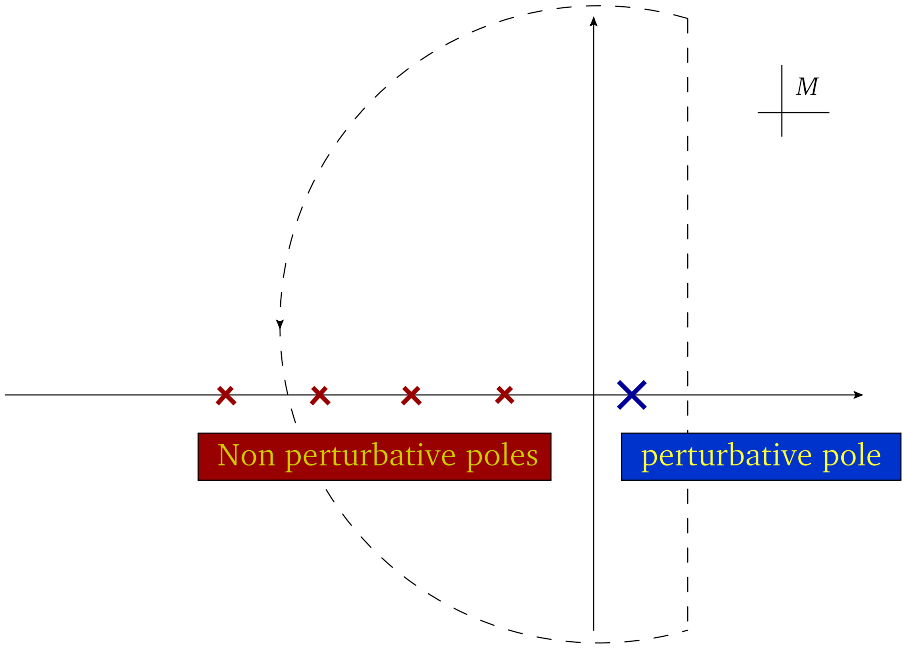

Figure 4.4: Pole structure of the cross section in MN-space. The contribution of poles in the region $M < 0$ is power suppressed. At high Q^2 the only contribution comes from the positive pole γ_s.

4.2 Resummation techniques

4.2.1 Inclusive cross section

In the previous section we focussed on the construction of a resummed coefficient function starting from the k_T-factorization theorem. We assumed to

be able to calculate the k_T-dependent hard cross section. In this section we show how to compute it in terms of ordinary Feynman diagrams. Consider the generic photo-production process

$$\gamma(n) + g(p) \to J + X \tag{4.2.1}$$

characterized by a hard scale Q^2. As we said, high energy enhanced contributions stem from multiple gluon emission. We can take advantage of this information by factorizing the generic cross section σ into a process-dependent part and an universal gluon ladder as shown in fig. (4.5). Thus

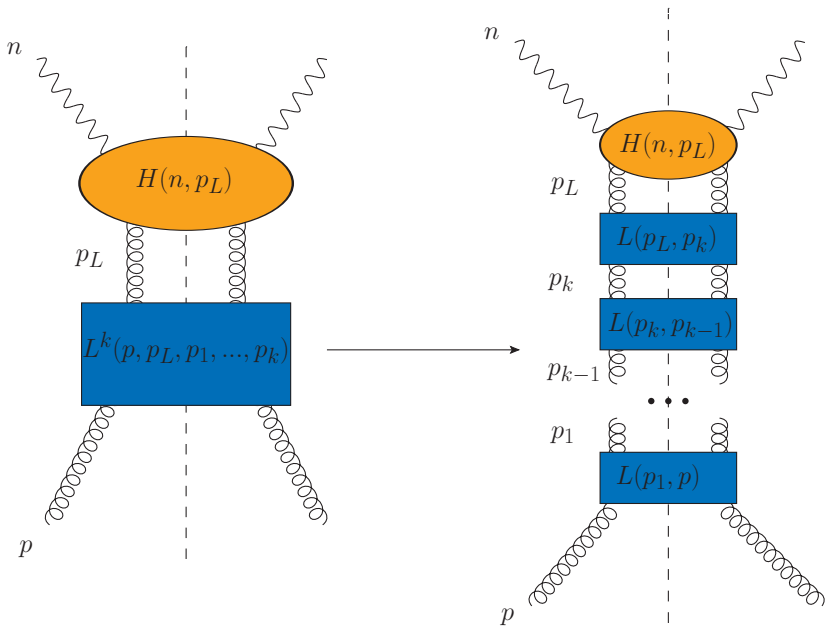

Figure 4.5: .

we write the differential cross section with k gluons in the final state as the Lorentz product

$$d\sigma \equiv \frac{Q^2}{2s} H^{\mu\nu}(n, p_L, Q^2) \cdot \left(L^k_{\mu\nu}(p_L, p, p_1, \cdots, p_k) \prod_{i=1}^{k} \frac{d^3 q_i}{2E_i} \right) \tag{4.2.2}$$

where H contains the phase space integration of the final state J as well as the momentum conservation delta function, q_i are the momenta of the outgoing gluons and p_i are the exchanged propagators through the ladder. Notice that the ladder part does not depend on the hard scale Q^2 of the

upper process. The hard part can be decomposed as

$$H^{\mu\nu} = \left(-g^{\mu\nu} + \frac{p_L^\mu p_L^\nu}{p_L^2}\right) H_\perp(p_L^2, n\cdot p_L, Q^2) + \\ + p_L^2 \left(\frac{p_l^\mu}{p_L^2} - \frac{n^\mu}{n\cdot p_L}\right)\left(\frac{p_l^\nu}{p_L^2} - \frac{n^\nu}{n\cdot p_L}\right) H_\parallel(p_L^2, n\cdot p_L, Q^2). \tag{4.2.3}$$

Now consider the one-gluon emission. The ladder part can also be decomposed as

$$L^{1,\mu\nu}(p, p_L) = \frac{1}{p_L^2}\left(-g^{\mu\nu} + \frac{p_L^\mu p_L^\nu}{p_L^2}\right) L_\perp^1(p_L^2, p\cdot p_L) + \\ + \left(\frac{p_l^\mu}{p_L^2} - \frac{n^\mu}{n\cdot p_L}\right)\left(\frac{p_l^\nu}{p_L^2} - \frac{n^\nu}{n\cdot p_L}\right) L_\parallel(p_L^2, n\cdot p_L). \tag{4.2.4}$$

with dimensionless tensor coefficients. In order to extract the high energy enhanced contribution to the cross section, we introduce the Sudakov parametrization for the emitted gluon

$$q = (1-z)p + k + \bar{z}n \tag{4.2.5}$$

where $k = (0, k_x, k_y, 0)$ with $k^2 = -\mathbf{k}^2$ and $p\cdot n = s/2$. The gluon phase space integration give

$$\frac{d^3q}{2E_q} = \frac{dz}{2(1-z)} d^2\mathbf{k} \tag{4.2.6}$$

with $\bar{z} = \frac{\mathbf{k}^2}{s(1-z)}$ fixed by the onshellness condition.

Tipically, the z integration is bounded from x to 1. The lower bound, in particular, is given by the kinematical constraint produced by the hard final state J and it depends on the process. The small-x limit is therefore associated with the small-z limit in the case of the one-gluon emission. Also the transverse momentum of the gluon is bounded by the hard scale Q^2, therefore the high energy limit $Q^2 \ll s$ can be replaced by $\mathbf{k}^2 \ll s$.

Now we assume that the functions $H_{\perp,\parallel}$ and $L^1_{\perp,\parallel}$ have the same small-x behaviour. Thus the leading behaviour is given by

$$d\sigma = \left[-\frac{Q^2}{2zs} H_\parallel\left(\frac{Q^2}{\mathbf{k}^2}, \frac{Q^2}{zs}, \theta\right)(1 + \mathcal{O}(z))\right](2\pi L_\parallel^1)\frac{dz}{z}\frac{d\mathbf{k}^2}{\mathbf{k}^2}. \tag{4.2.7}$$

A meaningfull way to extract the coefficient $H_\parallel$ is to apply the projector

$$\mathcal{P}^{\mu\nu} = \frac{k^\mu k^\nu}{\mathbf{k}^2} \tag{4.2.8}$$

to the full hard tensor $H^{\mu\nu}$. In the limit

$$\begin{aligned} z &\ll 1 \\ \mathbf{k}^2 &\ll s \end{aligned} \tag{4.2.9}$$

the combination in the squared brackets of eq. (4.2.7) can be interpreted as the partonic cross section of the process $\gamma + g^* \to J$ with an off-shell incoming gluon of momentum

$$q = zp + k, \qquad q^2 = -\mathbf{k}^2. \tag{4.2.10}$$

With this interpretation, the projector in eq. (4.2.8) can be thought asthe sum over the polarizations of the gluon. Now we discuss the ladder part. As we shall see, the high energy structure is completely determined by the collinear factorization. If we define the combination

$$C\left(\frac{Q^2}{zs}, \frac{Q^2}{\mathbf{k}^2}\right) = \frac{Q^2}{2zs}\mathcal{P}_{\mu\nu}H^{\mu\nu} \tag{4.2.11}$$

the cross section reads

$$\sigma(x, Q^2) = \int_x^1 \frac{dz}{z} \int \frac{d\mathbf{k}^2}{\mathbf{k}^2} C\left(\frac{x}{z}, \frac{Q^2}{\mathbf{k}^2}\right) (2\pi\alpha_s L_0^1) \tag{4.2.12}$$

where $L_{\|}^1 = \alpha_s L_0^1$. The z-integration can be done by taking the N-space mellin moments, thus we get

$$\sigma(N, Q^2) = \int \frac{d\mathbf{k}^2}{\mathbf{k}^2} C\left(N, \frac{Q^2}{\mathbf{k}^2}\right) \frac{2\pi\alpha_s L_0^1}{N} \tag{4.2.13}$$

The integration in the transverse momentum gives a collinear divergence which can be cured by doing the integration in $d = 4 - 2\epsilon$ dimensions then it can be subtracted in $\overline{\text{MS}}$ scheme. The d-dimensional form of eq. (4.2.13) is

$$\begin{aligned} & \sigma\left(N, Q^2, \alpha_s\left(\frac{\mu^2}{Q^2}\right)^{\epsilon}, \epsilon\right) = \\ = & \int_0^{\infty} \frac{d\mathbf{k}^2}{k_T^2}\left(\frac{Q^2}{\mathbf{k}^2}\right)^{\epsilon} C\left(N, \frac{Q^2}{\mathbf{k}^2}, \alpha_s\left(\frac{\mu^2}{Q^2}\right)^{\epsilon}, \epsilon\right) \alpha_s\left(\frac{\mu^2}{Q^2}\right)^{\epsilon} \frac{2\pi L_0^1\left(N^{\epsilon}, \epsilon\right)}{N} = \\ = & \int_0^{\infty} \frac{d\xi}{\xi^{1+\epsilon}} C\left(N, \xi, \alpha_s\left(\frac{\mu^2}{Q^2}\right)^{\epsilon}, \epsilon\right) \alpha_s\left(\frac{\mu^2}{Q^2}\right)^{\epsilon} \frac{2\pi L_0^1\left(N^{\epsilon}, \epsilon\right)}{N}, \end{aligned} \tag{4.2.14}$$

where we defined the ratio

$$\xi = \frac{\mathbf{k}^2}{Q^2}. \tag{4.2.15}$$

Now we take the collinear limit $\mathbf{k}^2 \ll Q^2$, thus eq. (4.2.14) becomes

$$\sigma\left(N, Q^2, \alpha_s\left(\frac{\mu^2}{Q^2}\right)^{\epsilon}, \epsilon\right) = \int_0^\infty \frac{d\xi}{\xi^{1+\epsilon}} C\left(N, \alpha_s\left(\frac{\mu^2}{Q^2}\right)^{\epsilon}, \epsilon\right)[1 + O(\xi)] \times$$
$$\times \alpha_s\left(\frac{\mu^2}{Q^2}\right)^{\epsilon} \frac{2\pi L_0^1\left(N^\epsilon, \epsilon\right)}{N} = -\frac{1}{\epsilon}\sigma\left(\gamma(n) + g(zp) \to \mathcal{V}\right)\frac{2\pi\alpha_s L_0^1}{N} + \text{finite}. \tag{4.2.16}$$

In the last step we see that the combination $2\pi\alpha_s L_0^1/N$ is an anomalous dimension since it is the residue of a collinear pole. In the one gluon case, it is precisely the small-N limit of the γ_{gg} anomalous dimension, namely

$$\frac{2\pi\alpha_s L_0^1}{N}\frac{\alpha_s N_C}{\pi}\gamma_0(N) = \bar{\alpha}_s\gamma_0 \tag{4.2.17}$$

where we have defined $\bar{\alpha}_s \equiv \alpha_s N_c/\pi$ and $\gamma_0 = 1/N$. If we iterate the single emission we obtain the standard exponentiation of collinear singularity. Furthermore, it can be shown[46] that the ladder part of the cross section is always an anomalous dimension, hence if we can consider the full kernel L instead of the single emission we obtain the formula

$$\sigma\left(N, Q^2, \alpha_s(Q^2)\right) =$$
$$L\left(\bar{\alpha}_s(Q^2), N\right)\int_0^\infty \frac{d\xi}{\xi}\xi^{L\left(\bar{\alpha}_s(Q^2), N\right)} C\left(N, \xi, \alpha_s(Q^2)\right) R\left(\alpha_s b(Q^2), N\right), \tag{4.2.18}$$

where the extra factor R comes from the interferences between $1/\epsilon$ poles and the ϵ-dependent part of the kernel L. In order to obtain the high energy limit, we can expand L as

$$L(\bar{\alpha}_s, N) = \gamma_s\left(\frac{\bar{\alpha}_s}{N}\right) + \bar{\alpha}_s\gamma_{ss}\left(\frac{\bar{\alpha}_s}{N}\right) + \cdots \tag{4.2.19}$$

and analogously for R. The coefficients of the expansion in eq. (4.2.19) can be obtained by the duality relation that we already anticipated in the previous section

$$f(\gamma_s) = \frac{\bar{\alpha}_s}{N} \tag{4.2.20}$$

where $f(\gamma)$ is the kernel of the BFKL at leading order in α_s defined in eq. (4.1.17).

4.2.2 Rapidity distributions

Differential distributions are in general much more sensitive to small-x effects than inclusive observables. As an example, in the case of Drell-Yan rapidity distribution, the slow convergence of the perturbative series in the large rapidity region shows that higher order corrections become more and more important. Thus, the impact of resummation effect should be more visible in this region. The rapidity in the partonic center-of-mass frame is defined as

$$y = \frac{1}{2}\ln\frac{E+p_z}{E-p_z} = \frac{1}{2}\ln\frac{p^+}{p^-}. \tag{4.2.21}$$

In this section we will give the recipe for the high energy resummation described in full detail in Ref. [46]. The derivation of this procedure is analogue to the inclusive case discussed in the previous section. The crucial difference is the introduction of a Mellin-Fourier transform

$$f(N,b) \equiv \int_0^1 dx x^{N-1} \int_0^\infty d\xi \xi^{M-1} \int_{-\infty}^\infty dy e^{iby} f(x,\xi,y) \tag{4.2.22}$$

in terms of which the resummation formulas have a factorized expression. Note that $f(N,M,0)$ is the inclusive cross section. The main steps in the derivation of Ref. [46] are the same of the inclusive case which can be summarized as follows

1. Separate the gluon ladder emissions from the hard part (*i.e.* withouth gluon emissions)
2. Perform the calculation of the n-gluon emission in the region of strong ordered transverse momenta.
3. Substitute the Altarelli-Parisi anomalous dimension with the small-x resummed γ_s.

In the inclusive case, we know that high energy enhanced contributions are given by poles of increasing order in $N = 0$. Now, these poles correspond to contributions of the form

$$\left(\frac{\alpha_s}{N + f(b)}\right)^k \tag{4.2.23}$$

with $f(0) = 0$, in the rapidity distribution because, in Mellin-Fourier space, setting $b = 0$ is equivalent to take the inclusive cross-section.

If we consider the gluon radiation coming from the lower leg only, the final form of the resummed rapidity distribution is

$$\frac{d\sigma}{dy}(N,b) = MC(N,M,b)|_{M\to\Gamma(N,b)} \tag{4.2.24}$$

where $C(N, M, b)$ is the Mellin-Fourier transform of the off-shell hard coefficient function and where we introduced the function $\Gamma_+(N, b)$ defined as

$$\Gamma(N, b) \equiv \gamma_s \left(\frac{\alpha_s}{N + \frac{ib}{2}} \right). \tag{4.2.25}$$

If we allow the gluon radiation from both initial legs we have the generalized version of eq. (4.2.25)

$$\frac{d\sigma}{dy}(N, b) = M_1 M_2 C(N, M_1, M_2, b) \tag{4.2.26}$$

with

$$M_1 = \Gamma(N, b), \qquad M_2 = \Gamma(N, -b) \tag{4.2.27}$$

4.2.3 Running coupling effects

So far, the formalism we developped both for the inclusive and the rapidity differential cross section does not account for running coupling effects. Indeed, as shown in Refs. [47, 48, 49, 32] the running of α_s produces a new series of relevant contributions in the high energy limit which modify the nature of the singularity of the anomalous dimension at small-x. Furthermore, the inclusion of these running coupling contributions is strongly required in order to obtain stable small-x limit because their leading singularities are of increasing higher order at higher orders in $\beta_0 \alpha_s$. The fixed coupling resummation, indeed, would produce a huge deviation from the NLO resuls, which is obviously not the case. This is the reason why the running coupling terms are required to make a precise prediction comparable with collider data.

At fixed α_s, the resummation procedure requires the identification of the Mellin variable M (conjugate of Q^2) with the sum of the leading singularities of the resummed anomalous dimension

$$M = \gamma_s \left(\alpha_s / N \right). \tag{4.2.28}$$

Now, if we include running effects, α_s becomes a function of Q^2 which corresponds to an operator in M-Mellin space, for example, at leading log level we have

$$\hat{\alpha_s} = \frac{\alpha_s}{1 - \beta_0 \alpha_s \frac{\partial}{\partial M}} \tag{4.2.29}$$

and Eq. (4.2.28) is understood as an equality between operators. At the running coupling level, the identification given by Eq. (4.2.28) produces a class of terms proportional to increasing derivatives of γ_s. In practice these are

most easily computed by using Eq. (4.2.28) to turn the expansion Eq. (6.2.1) in powers of $\bar{\alpha}_s/N$ into an expansion in powers of M: since powers of M correspond to derivatives with respect to $\ln Q^2$, this then gives the resummed coefficient function even when the coupling runs. For a thorough description of the inclusion of running coupling effects see Refs. [32, 35].

Chapter 5

High energy resummation in prompt photon production

As we discussed in the previous chapter, the inclusion of prompt photon data in a global next-to-leading order QCD fit can provide a strong constraint for medium-large values of x. However, large higher order corrections at small-x, would spoil the accuracy of the NLO cross section in the medium-x region. A thorough understanding of this process in the small-x limit is thus relevant to make predictions for the LHC.

Prompt photon cross-section contains two different contributions: the direct component, where the photon participates at leading order to the hard process, and a fragmentation component, which is needed to take account of the hadronic component of the photon. From a phenomenological point of view, at high-energy both terms are important [11]. This chapter is focused on the direct contribution. Future efforts on the fragmentation component will be discussed later on.

All the processes for which small-x resummation has been performed so far are free of collinear singularities in the final state since the corresponding cross-sections are totally inclusive; on the contrary such a divergence does appear in direct photon production because the process is exclusive with respect to the final state photon, which from this point of view must be viewed as another hadronic state [22]. In this work we perform the high-energy resummation of the direct photon coefficient function consistently with the $\overline{\text{MS}}$ scheme of subtraction of the final state singularity to all orders in perturbation theory.

5.1 Prompt photon production

5.1.1 Collinear factorization

As we discussed in detail, the prompt photon process is characterized by a hard event involving the production of a single photon. Let us consider the hadronic process

$$H_1(P_1) + H_2(P_2) \to \gamma(q) + X. \tag{5.1.1}$$

According to perturbative QCD, the direct and the fragmentation component of the inclusive cross-section at fixed transverse momentum $\mathbf{q}$ of the photon can be written as [9]

$$\begin{aligned}\mathbf{q}^3 \frac{d\sigma_\gamma(x_\perp, \mathbf{q}^2)}{d\mathbf{q}} &= \sum_{a,b} \int_{x_\perp}^1 dx_1 \; f_{a/H_1}(x_1, \mu_F^2) \int_{x_\perp/x_1}^1 dx_2 \; f_{b/H_2}(x_2, \mu_F^2) \times \\ &\times \int_0^1 dx \left\{ \delta\left(x - \frac{x_\perp}{x_1 x_2}\right) \mathcal{C}_{ab}^\gamma(x, \alpha_s(\mu^2); \mathbf{q}^2, \mu_F^2, \mu_f^2) + \right. \\ &\left. + \sum_c \int dz \; z^2 d_{c/\gamma}(z, \mu_f^2) \delta\left(x - \frac{x_\perp}{z x_1 x_2}\right) \mathcal{C}_{ab}^c(x, \alpha_s(\mu^2); \mathbf{q}^2, \mu_F^2, \mu_f^2) \right\},\end{aligned} \tag{5.1.2}$$

Let us recall that the customary scaling variable is defined as

$$x_\perp = \frac{4\mathbf{q}^2}{S}, \qquad 0 < x_\perp < 1. \tag{5.1.3}$$

in terms of the hadronic center-of-mass energy $S = (P_1 + P_2)^2$. In the factorization formula eq. (C.1.1) we have used the short-distance cross-sections

$$\mathcal{C}_{ab}^{\gamma(c)} \equiv \mathbf{q}^3 \frac{d\hat{\sigma}_{ab\to\gamma(c)}(x, \alpha_s(\mu^2); \mathbf{q}^2, \mu_F^2, \mu_f^2)}{d\mathbf{q}}, \tag{5.1.4}$$

where a, b and c are parton indices (q, $\bar{q}$, g) while $f_{i/H_j}(x_i, \mu_F^2)$ is the parton density at the factorization scale μ_F. The fragmentation component is given in terms of a convolution with the fragmentation function $d_{c/\gamma}(z, \mu_f^2)$.

If we define the Mellin moments

$$\begin{aligned}
\sigma^\gamma(N) &= \int_0^1 dx_\perp\, x_\perp^{N-1} \left(\mathbf{q}^3 \frac{d\sigma_\gamma(x_\perp, \mathbf{q})}{d\mathbf{q}}\right), \\
F_{i/H}(N, \mu_F^2) &= \int_0^1 dx\; x^{N-1}\; x f_{i/H}(x, \mu_F^2), \\
D_{c/\gamma}(N, \mu_f^2) &= \int_0^1 dx\; x^{N-1}\; x^3 d_{c/\gamma}(x, \mu_f^2), \\
\tilde{\mathcal{C}}_{ab}^{\gamma(c)}(N) &= \int_0^1 dx\; x^{N-1}\, \mathcal{C}_{ab}^{\gamma(c)}(x)
\end{aligned}$$

the collinear factorization theorem in N-space becomes

$$\sigma^\gamma(N) = \sum_{a,b} F_{a/H_1}(N) F_{b/H_2}(N) \left(\tilde{\mathcal{C}}_{ab}^{\gamma}(N) + \sum_c D_{c/\gamma}(N) \tilde{\mathcal{C}}_{ab}^{c}(N)\right). \quad (5.1.5)$$

5.1.2 Leading-order coefficient functions and beyond

At leading order the processes that contribute to the direct component of the prompt photon cross-section are

$$q\bar{q} \to \gamma g, \qquad q(\bar{q})g \to \gamma q(\bar{q}). \quad (5.1.6)$$

The corresponding leading-order hard coefficient functions are given by [6, 22]

$$\begin{aligned}
\mathcal{C}_{q\bar{q}}^{\gamma,LO}(x) &= \frac{\mathbf{q}^3 d\hat{\sigma}_{q\bar{q}\to\gamma g}}{d\mathbf{q}} = \alpha\alpha_s Q_q^2 \pi \frac{C_F}{C_A} \frac{x}{\sqrt{1-x}}(2-x), & (5.1.7)\\
\mathcal{C}_{q(\bar{q})g}^{\gamma,LO}(x) &= \frac{\mathbf{q}^3 d\hat{\sigma}_{q(\bar{q})g\to\gamma q(\bar{q})}}{d\mathbf{q}} = \alpha\alpha_s Q_q^2 \pi \frac{1}{2C_A} \frac{x}{\sqrt{1-x}}(1+\frac{x}{4}) & (5.1.8)
\end{aligned}$$

in terms of the partonic variable $x = 4\mathbf{q}^2/\hat{s}$, where $\hat{s}$ is the partonic center-of-mass energy. QCD corrections to the Born coefficient functions eqs. (5.1.7) and (5.1.8) have been computed in ref. [8] up NLO accuracy.

In the high-energy limit, the leading coefficient function is logarithmically enhanced by contributions of the form

$$\mathcal{C}_{qg}^{\gamma}(x) = \mathcal{C}_{qg}^{\gamma,LO}(x) + \alpha\alpha_s^2 \sum_{k=0}^{\infty} c_{qg}^{(k)} (\alpha_s \log x)^k + \mathcal{O}\left(\alpha\alpha_s^3 (\alpha_s \log x)^n\right) \quad (5.1.9)$$

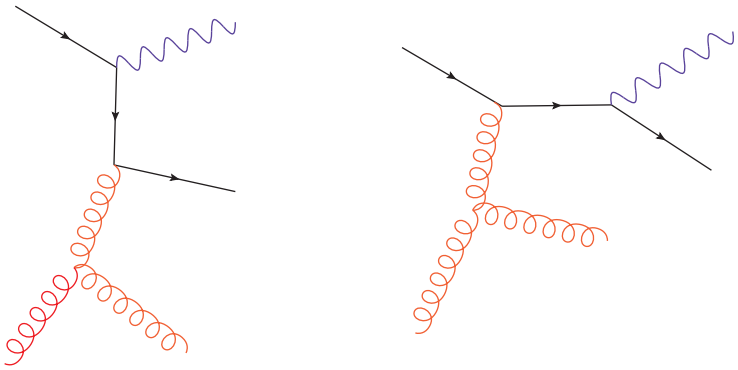

Figure 5.1: In this picture are shown the dominant Feynman graphs in the high-energy limit. Both of the two diagram determine the constant behaviour of the hard coefficient function $\mathcal{C}^{\gamma}_{q\bar{g}}$ at small-x.

which, in N-Mellin space, becomes a sum of poles at $N = 0$ of increasing order:

$$\tilde{\mathcal{C}}^{\gamma}_{qg}(N) = \tilde{\mathcal{C}}^{\gamma,LO}_{qg}(N) + \alpha\alpha_s \sum_{k=1}^{\infty} \tilde{c}^{(k)}_{qg} \left(\frac{\alpha_s}{N}\right)^k + \mathcal{O}\left(\alpha\alpha_s^2 \left(\frac{\alpha_s}{N}\right)^n\right), \quad n \geq 1. \tag{5.1.10}$$

As in the case of heavy quark production (HQ) and of the Drell-Yan processes (DY), the Born coefficients $\tilde{\mathcal{C}}^{\gamma,LO}_{ab}$ are regular as $N \to 0$: indeed, eqs. (5.1.7,5.1.8) vanish when x approaches zero. The first singular term in eq. (5.1.10) is a simple pole in $N = 0$ given by the NLO contribution to the perturbative series; in x-space, this pole corresponds to a constant value, while the small-x logarithms arise from the poles of increasingly higher order.

The NLO contribution to the expansion given in eq. (5.1.9) $\alpha\alpha_s^2 c^{(0)}_{qg}$ has been computed for various processes in ref. [50], in particular for direct photon production, by considering the Feynman diagrams in fig. (5.1) where an extra gluon is radiated from the initial state. This is a general feature of the high-energy limit to all orders in perturbation thory: dominant contributions at high-energy (LLx) are given by the exchange of spin-1 particles in the t-channel therefore all the relevant Feynman diagrams in the small-x limit are given by the BFKL ladders in fig. (5.2).

From the NLO onwards, the direct photon cross-section acquires a final state divergence when the photon becomes collinear to the outgoing parton; this collinear divergence cannot be removed by adding the virtual corrections, rather it must be absorbed in the fragmentation component of eq. (C.1.1) as it happens for the initial state collinear divergences which are properly absorbed in the definition of the parton densities [22]. In the next sections we will show how to remove this divergence in the $\overline{\text{MS}}$ scheme consistently

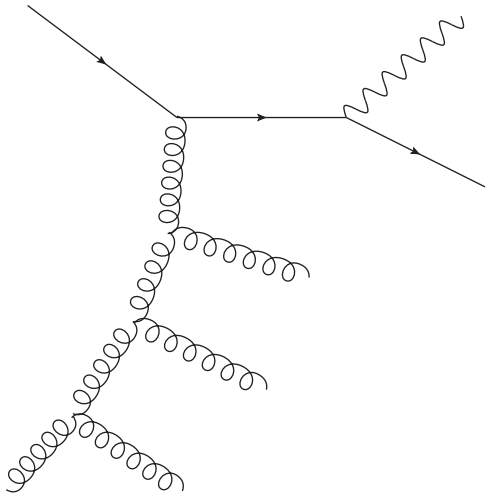

Figure 5.2: Multiple gluon emission (BFKL ladder) from the initial state in direct photon production.

with the resummation procedure of the gluon ladder and we will give the analytic expression for the resummed hard coefficient function $\mathcal{C}^{\gamma}_{q\bar{q}}$ and $\mathcal{C}^{\gamma}_{q\bar{g}}$.

5.2 High-energy resummation

In this section we compute the leading logarithmic corrections to the direct photon cross-section at high-energy. The high-energy resummation of gluon ladders arises from the general formalism of the k_t-factorization theorem [30, 31] and can be performed by following the computational procedure outlined in ref. [37] which allows us to compute the coefficient of the dominant $\log x$ to all orders in perturbation theory. This procedure requires the calculation of the Born cross-section with off-shell (transverse) incoming gluons and off-shellness fixed in terms of their transverse momenta $\mathbf{k}_i$ (impact factor).

For a single off-shell gluon, we can parametrize the dependence on the virtuality $\mathbf{k}^2$ through the dimensionless variable

$$\xi = \frac{\mathbf{k}^2}{Q^2}, \tag{5.2.1}$$

where Q^2 is the hard scale of the process which determines the argument of the running coupling $\alpha(Q^2)$. In direct photon production Q^2 is the magnitude of the transverse momentum of the photon $\mathbf{q}^2$. The LLx resummation is performed by taking a Mellin transform of the off-shell cross-section

$$h(N, M) \equiv \int_0^\infty d\xi \; \xi^{M-1} \int_0^1 dx \; x^{N-1} \hat{\sigma}(x, \xi), \tag{5.2.2}$$

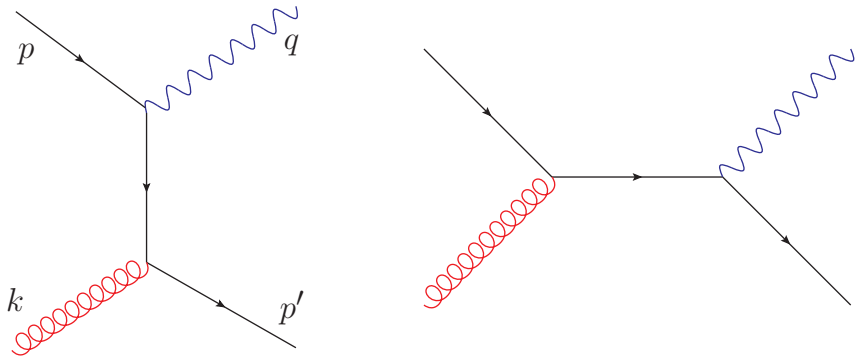

Figure 5.3: Diagrams for direct photon production.

and by identifying M as the sum of leading singularities of the largest eigenvalue of the singlet anomalous dimension matrix [51] (BFKL anomalous dimension)

$$M = \gamma_s\left(\frac{\alpha_s}{N}\right) + \mathcal{O}\left(\frac{\alpha_s^2}{N}\right) \tag{5.2.3}$$

$$\gamma_s\left(\frac{\alpha_s}{N}\right) = \sum_{n=1}^{\infty} c_n \left(\frac{C_A \alpha_s}{\pi N}\right)^n, \qquad c_n = 1, 0, 0, 2\zeta(3), \ldots \tag{5.2.4}$$

This corresponds to the sum of the high energy contributions coming from all diagrams of fig. (5.2). Finally, the $\mathrm{N^kLO}$ coefficient of the maximum power of $\log x$ is given by expanding the impact factor in powers of α_s.

5.2.1 The off-shell cross-section

Let us consider the process

$$g^\star(k) + q(p) \to \gamma(q) + q(p'), \tag{5.2.5}$$

with an off-shell incoming gluon. We use a Sudakov parametrization for both incoming and outgoing momenta of the diagrams in fig. 5.3, thus we have

$$p = z_2 p_2, \tag{5.2.6}$$

$$k = z_1 p_1 + k_\perp, \tag{5.2.7}$$

$$q = x_1 z_1 p_1 + (1 - x_2) z_2 p_2 + q_\perp, \tag{5.2.8}$$

$$p' = (1 - x_1) z_1 p_1 + x_2 z_2 p_2 + k_\perp - q_\perp, \tag{5.2.9}$$

where

$$\begin{aligned} k_\perp^2 &= -|\vec{k}_\perp|^2 = -\mathbf{k}^2, \\ q_\perp^2 &= -|\vec{q}_\perp|^2 = -\mathbf{q}^2, \end{aligned}$$

with light-like vectors p_1 and p_2 such that $p_1 \cdot p_2 = S/2$ where S is the energy in the center-of-mass frame. The relevant scalar products are

$$\begin{aligned} p \cdot k &= s/2, \\ p \cdot q &= x_1 s/2, \\ k \cdot q &= (1-x_2)s/2 - \vec{k}_\perp \cdot \vec{q}_\perp = \frac{\mathbf{q}^2}{2x_1} - \vec{k}_\perp \cdot \vec{q}_\perp, \end{aligned}$$

where we introduced the longitudinal energy $s = z_1 z_2 S$. The d-dimensional phase space

$$\begin{aligned} d\Phi^{(d)} &= \frac{1}{(2\pi)^{d-2}} d^d q d^d p' \; \delta(p'^2)\delta(q^2)\delta^{(d)}(k+p-q-p') = \\ &= \frac{1}{(2\pi)^{d-2}} d^d q \; \delta((p+k-q)^2)\,\delta(q^2) \end{aligned} \tag{5.2.10}$$

can be rewritten in terms of the Sudakov parameters since $d^d q = \frac{s}{2} d^{d-2}\mathbf{q} dx_1 dx_2$. We obtain

$$\begin{aligned} d\Phi^{(d)} &= \frac{1}{(2\pi)^2}\frac{s}{2} d^{d-2}\mathbf{q} dx_1 dx_2 \delta(-\mathbf{k}^2 + s - x_1 s - (1-x_2)s + 2\mathbf{k}\cdot\mathbf{q}) \cdot \\ &\qquad \cdot\delta(-\mathbf{q}^2 + x_1(1-x_2)s) = \\ &= \frac{(4\pi)^{-\epsilon}\sqrt{\pi}}{(2\pi)^2}\frac{(\sin\theta)^{2\epsilon}}{\Gamma(1/2+\epsilon)}\frac{dx_1}{x_1}\,\mathbf{q}^{1+2\epsilon} d\mathbf{q}\,\delta(-\mathbf{k}^2 + s(1-x_1) - \frac{\mathbf{q}^2}{x_1} + 2\mathbf{k}\cdot\mathbf{q}) \end{aligned} \tag{5.2.11}$$

where θ is the angle between $\mathbf{q}$ and $\mathbf{k}$ and we used the last δ-function to perform the integration in x_2, now fixed to $x_2 = 1 - \frac{\mathbf{q}^2}{x_1 s}$, which implies $x < 4x_1$.

Since we are interested in the differential cross-section $\hat{\sigma}(x,\xi) = \mathbf{q}^3 \frac{d\sigma}{d\mathbf{q}}$, our phase space in four dimension reduces to

$$\mathbf{q}^3 \frac{d\Phi^{(4)}}{d\mathbf{q}} = d\phi^{(4)} = \frac{1}{(2\pi)^2}\frac{dx_1}{2x_1}\,\mathbf{q}^4 d\theta\;\delta\left(-\mathbf{k}^2 + s(1-x_1) - \frac{\mathbf{q}^2}{x_1} + 2\mathbf{k}\cdot\mathbf{q}\right)\Theta(s-\mathbf{k}^2), \tag{5.2.12}$$

which in terms of the dimensionless partonic variables $x = 4\mathbf{q}^2/s$ and $\xi = \mathbf{k}^2/\mathbf{q}^2$ reads

$$\begin{aligned} d\phi^{(4)} &= \frac{1}{(2\pi)^2}\frac{xs dx_1}{8x_1}\,d\theta\;\delta\left(\frac{4}{x}(1-x_1) - \xi - \frac{1}{x_1} + 2\sqrt{\xi}\cos\theta\right)\Theta(\frac{4}{x}-\xi)\Theta(4x_1 - x) = \\ &= \frac{1}{(2\pi)^2}\frac{sx dx_1}{32x_1(1-x_1)}\,d\theta\;\delta\left(\frac{1}{x} - \frac{\xi + \frac{1}{x_1} - 2\sqrt{\xi}\cos\theta}{4(1-x_1)}\right)\Theta(\frac{4}{x}-\xi)\Theta(4x_1 - x). \end{aligned}$$

In the resummation procedure of refs. [30, 31, 37] the computation of Feynman diagrams is performed by using the eikonal rule for the gluon polarization sum

$$\sum_\lambda \epsilon_\mu^\lambda(k)\epsilon_\nu^\lambda(k) = \frac{\mathbf{k}_\mu \mathbf{k}_\nu}{\mathbf{k}^2}, \qquad \mathbf{k}_\mu \equiv (0, \mathbf{k}, 0), \tag{5.2.13}$$

understood as the projector $\mathcal{P}$ over the high-energy singularities, analogously to the approach of refs. [52], which factorizes the gluon ladder from the Born coefficient. The channels s and t lead to the simple result for the amplitude in $d = 4 + 2\epsilon$ dimensions

$$\begin{aligned} \mathcal{A}^{(d)}(x, x_1, \xi) &= \overline{\sum}\mathcal{M}^2 = \frac{4e^2 g_s^2}{2 \cdot 2C_A}\left[\frac{(\mathbf{q}^2 - s x_1)^2 + s^2 x_1^2 + \epsilon \mathbf{q}^4}{s x_1^3 (s - \mathbf{k}^2)}\right] \\ &= \frac{16 e^2 g_s^2}{2 \cdot 2C_A}\left[\frac{1 + \left(1 - \frac{x}{4x_1}\right)^2 + \frac{x^2}{16 x_1^2}\epsilon}{x x_1 \left(\frac{4}{x} - \xi\right)}\right] \end{aligned} \tag{5.2.14}$$

averaged over color and helicity (of the quark) and summed over the final states. This off-shell amplitude has been used in ref. [53] to evaluate numerically the cross section, however we will show that both Mellin and phase space integrals can be performed in closed form.

As shown in eq. (5.1.10), the high-energy enhancement appears as a series of poles in $N = 0$, therefore we are interested in the most singular term in the small-N limit.

Since the off-shell cross-section is well behaved at $N = 0$, all the singular terms come from the substitution shown in eq. (5.2.3), hence at this level we can reduce the computation to the $N = 0$ moment of the impact factor in the (N, M) space

$$\begin{aligned} h(0, M) &= \frac{1}{(2\pi)^2}\frac{1}{2s}\int_0^{2\pi} \mathrm{d}\theta \int_0^1 \frac{s\, \mathrm{d}x_1}{32 x_1 (1 - x_1)} \int_0^{4x_1} \mathrm{d}x \cdot \\ &\quad \cdot \int_0^{4/x} \mathrm{d}\xi\, \xi^{M-1} \mathcal{A}^{(4)}(x, x_1, \xi)\delta\left(\frac{1}{x} - \frac{\xi + \frac{1}{x_1} - 2\sqrt{\xi}\cos\theta}{4(1 - x_1)}\right) = \\ &= \frac{1}{(2\pi)^2}\frac{1}{2}\int_0^{2\pi} \mathrm{d}\theta \int_0^1 \frac{\mathrm{d}x_1}{32 x_1 (1 - x_1)} \int_0^{\infty} \mathrm{d}\xi\, \xi^{M-1} \cdot \\ &\quad \cdot \int_{\max(\frac{1}{4x_1}, \frac{\xi}{4})}^{+\infty} \frac{\mathrm{d}\rho}{\rho^2} \mathcal{A}^{(4)}(1/\rho, x_1, \xi)\delta\left(\rho - \frac{\xi + \frac{1}{x_1} - 2\sqrt{\xi}\cos\theta}{4(1 - x_1)}\right) \end{aligned} \tag{5.2.15}$$

where we introduced the variable $\rho = 1/x$ and we exchanged the order of

integration of ξ and ρ. By using the delta function we obtain:

$$h(0,M) = \frac{1}{(2\pi)^2}\frac{1}{2}\int_0^{2\pi}\mathrm{d}\theta\int_0^1\frac{\mathrm{d}x_1}{32x_1(1-x_1)}\int_0^\infty \mathrm{d}\xi\,\xi^{M-1}\cdot \cdot\frac{1}{\bar{\rho}^2}\mathcal{A}^{(4)}(1/\bar{\rho},x_1,\xi)\Theta\left(\bar{\rho}-\max(\frac{1}{4x_1},\frac{\xi}{4})\right), \quad (5.2.16)$$

where we have defined

$$\bar{\rho}=\frac{\xi+\frac{1}{x_1}-2\sqrt{\xi}\cos\theta}{4(1-x_1)}. \quad (5.2.17)$$

The argument of the Heaviside Θ-function in eq. (5.2.16) is always positive since

$$\bar{\rho}-\frac{1}{4x_1}=\frac{\xi x_1+1-2x_1\sqrt{\xi}\cos\theta-1+x_1}{4x_1(1-x_1)}=\frac{\xi-2\sqrt{\xi}\cos\theta+1}{4x_1(1-x_1)}>\frac{(\sqrt{\xi}-1)^2}{4x_1(1-x_1)}>0$$

when $1/x_1>\xi$, and

$$\bar{\rho}-\frac{\xi}{4}=\frac{\xi+\frac{1}{x_1}-2\sqrt{\xi}\cos\theta-\xi(1-x_1)}{4(1-x_1)}=\frac{\frac{1}{x_1}-2\sqrt{\xi}\cos\theta+\xi x_1}{4(1-x_1)}>\frac{(\frac{1}{\sqrt{x_1}}-\sqrt{\xi x_1})^2}{4(1-x_1)}>0$$

in the opposite case. Therefore we have

$$h(0,M) = \frac{1}{(2\pi)^2}\frac{1}{2}\int_0^\infty \mathrm{d}\xi\,\xi^{M-1}\int_0^{2\pi}\mathrm{d}\theta\int_0^1\frac{\mathrm{d}x_1}{32x_1(1-x_1)}\frac{1}{\bar{\rho}^2}\mathcal{A}^{(4)}(1/\bar{\rho},x_1,\xi). \quad (5.2.18)$$

The integration over the region $0<\theta<2\pi$, $0<x_1<1$ in eq. (5.2.18) is always divergent when $\xi>1$, *i.e.* $|\mathbf{k}|>|\mathbf{q}|$; indeed the latter condition defines the kinematical region where the photon can be radiated collinearly to the quark in the final state. In the collinear limit, the amplitude in eq. (5.2.14) is singular and the divergence is given by the fermionic propagator in the s-channel. In the collinear limit we have:

$$4\bar{\rho}-\xi=\frac{\xi x_1^2-2\sqrt{\xi}x_1\cos\theta+1}{x_1-x_1^2}=0, \quad (5.2.19)$$

which happens when

$$\begin{cases}\theta=0\\ x_1=\frac{1}{\sqrt{\xi}}\end{cases}. \quad (5.2.20)$$

5.2.2 Subtraction of the collinear singularity in $\overline{\rm MS}$ scheme

In order to cancel the collinear divergence in the $\overline{\rm MS}$ scheme, first, we regularize the integrations of eq. (5.2.18) by subtracting the collinear limit of the four dimensional amplitude before doing any integration, second we recover the pole in $\epsilon = 0$ and the remaining finite parts by adding back the same quantity computed in d dimensions.

We can do this by writing the impact factor in $4 + 2\epsilon$ dimensions as

$$h^{(d)}(x,\xi) \;=\; \int d\phi^{(d)}\, \mathcal{A}^{(d)}. \tag{5.2.21}$$

We then remove the singularity of the integrand by introducing a function $\mathcal{D}^{(d)}$ which has the same singular behaviour of the squared amplitute $\mathcal{A}^{(d)}$ in the collinear limit eq. (5.2.20). In four dimension we have

$$\mathcal{D}^{(4)} = \frac{e^2 g_s^2}{C_A} P_{q\gamma}(1/\sqrt{\xi}) \frac{\sqrt{\xi}-1}{(1-\sqrt{\xi}x_1)^2+\theta^2} \Theta(\xi-1), \tag{5.2.22}$$

where

$$P(z) = \frac{1+(1-z)^2}{z}. \tag{5.2.23}$$

By adding and subtracting the phase space integral of the function $\mathcal{D}^{(d)}$ to the d-dimensional impact factor we obtain

$$\begin{aligned} h^{(d)} \;&=\; \lim_{\epsilon\to 0}\left(\int d\phi^{(d)}\mathcal{A}^{(d)} - \int d\phi^{(d)}\,\mathcal{D}^{(d)}\right) + \int d\phi^{(d)}\,\mathcal{D}^{(d)} + \mathcal{O}(\epsilon) = \\ &=\; \int d\phi^{(4)}\left(\mathcal{A}^{(4)} - \mathcal{D}^{(4)}\right) + f_{\mathcal{A}} + \int d\phi^{(d)}\mathcal{D}^{(d)} + \mathcal{O}(\epsilon) \end{aligned} \tag{5.2.24}$$

where the first integral is finite in four dimensions and the finite part $f_{\mathcal{A}}$ comes from the linear term in ϵ in the d-dimensional amplitude eq. (5.2.14).

By using the d-dimensional phase space, the last term in eq. (5.2.24) is

$$d\phi^{(d)}\mathcal{D}^{(d)} = \frac{\alpha\alpha_s}{2C_A}\frac{\sqrt{\pi}(4\pi)^{-\epsilon}}{\Gamma(1/2+\epsilon)}\left(\frac{\mu^2}{\mathbf{q}^2}\right)^{-\epsilon}\frac{1}{\xi}P_{q\gamma}(1/\sqrt{\xi})\frac{\Theta(\xi-1)\delta\left(\frac{1}{x}-4x_1^2\right)}{\left[(1-\sqrt{\xi}x_1)^2+\theta^2\right]}\,\theta^{2\epsilon}\,dx_1 d\theta, \tag{5.2.25}$$

where the dimensional scale μ^2 (introduced by dimensional regularization) from now on will be identified with $\mathbf{q}^2$. By using this result in eq. (5.2.24) and performing the Mellin integrations with $N = 0$ we have

$$\begin{aligned} h^{(d)}(0,\xi) \;&=\; \frac{1}{(2\pi)^2}\frac{1}{2}\int_0^1 \mathrm{d}x_1\left(\int_{-\pi}^{\pi}\mathrm{d}\theta\frac{1}{\bar{\rho}^2}\frac{\mathcal{A}^{(4)}(\bar{\rho},x_1,\xi)}{32x_1(1-x_1)} - \int_{-\infty}^{\infty}\mathrm{d}\theta\frac{1}{2\xi}\mathcal{D}^{(4)}\right) + f_{\mathcal{A}} + \\ &\quad + \frac{\alpha\alpha_s}{2C_A}\frac{\sqrt{\pi}(4\pi)^{-\epsilon}}{\Gamma(1/2+\epsilon)}\frac{1}{\xi}\int_0^1 dx_1\int_{-\infty}^{+\infty}d\theta\frac{\theta^{2\epsilon}\,P_{q\gamma}(1/\sqrt{\xi})\Theta(\xi-1)}{\left[(1-\sqrt{\xi}x_1)^2+\theta^2\right]} \end{aligned} \tag{5.2.26}$$

where we have extended the limits of the angular integration of the function $\mathcal{D}$ in order to simplify the results of the integration while the finite part $f_{\mathcal{A}}$ is

$$\begin{aligned} f_{\mathcal{A}} &= \lim_{\epsilon\to 0}\frac{\alpha\alpha_s\epsilon}{C_A}\int \mathrm{d}\xi\, \xi^{M-1}\int_0^1 \mathrm{d}x_1\sqrt{\xi}\left(\int_{-\infty}^{+\infty}\mathrm{d}\theta\frac{\xi^{-2}\,\theta^{2\epsilon}}{\left[(1-\sqrt{\xi}x_1)^2+\theta^2\right]}\right) = \\ &= \frac{\pi\alpha\alpha_s}{C_A}\frac{1}{2-M}. \end{aligned} \tag{5.2.27}$$

All the integrations in eq. (5.2.26) can be performed in closed form, thus by subtracting the pole in $\epsilon = 0$ with the usual combination $1/\epsilon+\gamma_E-\log 4\pi$ we obtain[1]

$$\begin{aligned} h(0,\xi) &= \frac{\pi\alpha\alpha_s}{C_A}\left\{\Theta(\xi-1)\left(-\frac{1}{\xi}+\frac{8}{\sqrt{\xi}}(1-\log 2)\right)+\right. \\ &\left.+\,\mathrm{sign}(\xi-1)\left(3-\left(1+\frac{1}{2\xi}\right)\log(1-\xi)^2-\frac{1}{\sqrt{\xi}}\log\left(\frac{\sqrt{\xi}+1}{1-\sqrt{\xi}}\right)^2\right)\right\} \end{aligned} \tag{5.2.28}$$

while the M-Mellin moments are

$$h(0,M) = \frac{\alpha\alpha_s\pi}{C_A}\left\{\frac{(7-7M+2M^2)}{(M-1)(M-2)(2M-3)}\left(\pi\cot(M\pi)+2H_{M-2}+\frac{2}{M-1}\right)+\frac{1}{2-M}\right\}, \tag{5.2.29}$$

where H_{M-2} is the harmonic number of argument $M-2$.

[1] In ref. [50] the impact factor $h_q(a)$ was only computed in the region $0<\xi<1$ where no collinear singularity is present. The result for h_q, given in eq. (3.7) of ref. [50], is seen to agree with our result recalling that in the region $0<\xi<1$ h_q is related to h eq. (5.2.28) by

$$\xi\frac{dh_q(\xi)}{d\xi} = h(\xi), \qquad (0<\xi<1).$$

Note however that the expression for the cross-section $\sigma_{qg}(\mathbf{q}>p_T)$ given in eq. (3.11) of ref. [50] is too large by a factor 2 [54].

5.3 Results

5.3.1 The resummed coefficient function

By expanding the impact factor obtained in the previous section around $M = 0$, we obtain

$$Mh(0,M;\alpha_s) = \frac{\pi\alpha\alpha_s}{C_A}\left\{\frac{7}{6} + \frac{67}{36}M + \frac{385M^2}{216} + \left(\frac{2323}{1296} + \frac{7\zeta(3)}{3}\right)M^3 + \right.$$
$$\left. + \left(\frac{14233}{7776} + \frac{49\zeta(3)}{18}\right)M^4 + \left(\frac{87307}{46656} + \frac{331\zeta(3)}{108} + \frac{7\zeta(5)}{3}\right)M^5 + O\left(M^6\right)\right\} \quad (5.3.1)$$

Notice that in this formalism the collinear divergence from the initial state appears as a simple pole in $M = 0$. The resummed coefficient function in the $\overline{\text{MS}}$ factorization scheme is given by the relation

$$\tilde{\mathcal{C}}^{\gamma}_{qg}(N,\alpha_s) = Mh(N,M;\alpha_s)R(M)\big|_{M=\gamma_s} \quad (5.3.2)$$

in terms of the impact factor eq. (5.2.29) and the function

$$R(M) = 1 + \frac{8}{3}\zeta_3 M^3 - \frac{3}{4}\zeta_4 M^4 + \mathcal{O}(M^5) \quad (5.3.3)$$

which takes into account finite parts coming from the $\overline{\text{MS}}$ subtraction of initial state collinear singularities and where M is identified as the BFKL anomalous dimension

$$\gamma_s\left(\frac{\bar{\alpha}_s}{N}\right) = \frac{\bar{\alpha}_s}{N} + 2\zeta_3\left(\frac{\bar{\alpha}_s}{N}\right)^4 + 2\zeta_5\left(\frac{\bar{\alpha}_s}{N}\right)^6 + \ldots, \qquad \bar{\alpha}_s = \frac{\alpha_s C_A}{\pi} \quad (5.3.4)$$

We have

$$\tilde{\mathcal{C}}^{\gamma}_{qg}(N,\alpha_s) = \frac{\pi\alpha\alpha_s}{C_A}\left\{\frac{7}{6} + \frac{67}{36}\left(\frac{\bar{\alpha}_s}{N}\right) + \frac{385}{216}\left(\frac{\bar{\alpha}_s}{N}\right)^2 + \left(\frac{2323}{1296} + \frac{49\zeta(3)}{9}\right)\left(\frac{\bar{\alpha}_s}{N}\right)^3 + \right.$$
$$\left. + \left(\frac{14233}{7776} - \frac{7\pi^4}{720} + \frac{308\zeta(3)}{27}\right)\left(\frac{\bar{\alpha}_s}{N}\right)^4 + O\left(\left(\frac{\bar{\alpha}_s}{N}\right)^5\right)\right\}. \quad (5.3.5)$$

The NLO term in eq. (6.2.4) gives, in the x-space, the constant value $67/36\ \alpha\alpha_s^2$ which is in agreement with the fixed order calculation of refs. [8, 50]. By using the high-energy color charge relation between the hard coefficient functions

$$\tilde{\mathcal{C}}^{\gamma}_{q\bar{q}(q)}(N,\alpha_s) = \frac{C_F}{C_A}\left(\tilde{\mathcal{C}}^{\gamma}_{qg}(N,\alpha_s) - \tilde{\mathcal{C}}^{\gamma,LO}_{qg}(0,\alpha_s)\right) \quad (5.3.6)$$

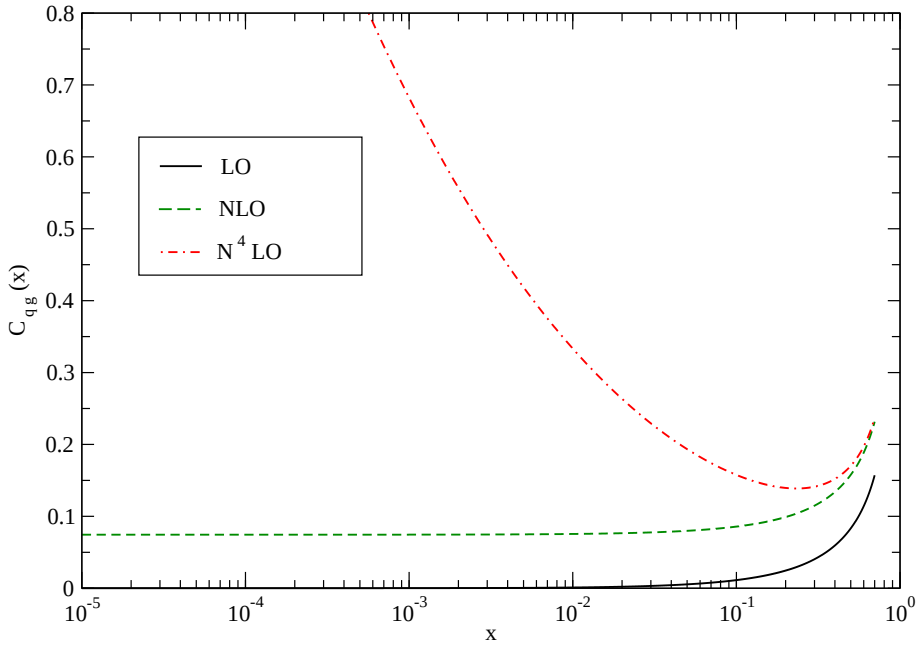

Figure 5.4: The picture shows a comparison between the leading order direct photon coefficient function (black solid) and the relative small-x corrections up to NLO (green dashed) and N^{4}LO (red dashed).

we can also obtain the LLx contributions coming from the process $q\bar{q} \to \gamma g$

$$\tilde{\mathcal{C}}^{\gamma}_{q\bar{q}(q)}(N,\alpha_s) = \alpha \frac{\alpha_s^2}{N}\frac{C_F}{C_A}\left\{\frac{67}{36} + \frac{385}{216}\left(\frac{\bar{\alpha}_s}{N}\right) + \left(\frac{2323}{1296} + \frac{49\zeta(3)}{9}\right)\left(\frac{\bar{\alpha}_s}{N}\right)^2 + \right.$$
$$\left. + \left(\frac{14233}{7776} - \frac{7\pi^4}{720} + \frac{308\zeta(3)}{27}\right)\left(\frac{\bar{\alpha}_s}{N}\right)^3 + O\left(\left(\frac{\bar{\alpha}_s}{N}\right)^4\right)\right\}. \quad (5.3.7)$$

5.3.2 Phenomenology

In fig. 5.4 we compare in x-space the coefficient function $\mathcal{C}_{qg}(x,\alpha_s)$ at LO, NLO and N^{4}LO in the high-energy limit. The large contributions at small-x spoil the perturbative expansion and must be resummed in order to recover accurate results. The resummation of these logarithmic terms in the hadronic cross-section can be performed to all orders [35, 49] including running coupling. A full phenomenological study could be performed by combining the resummed hard cross section computed here with the resummation

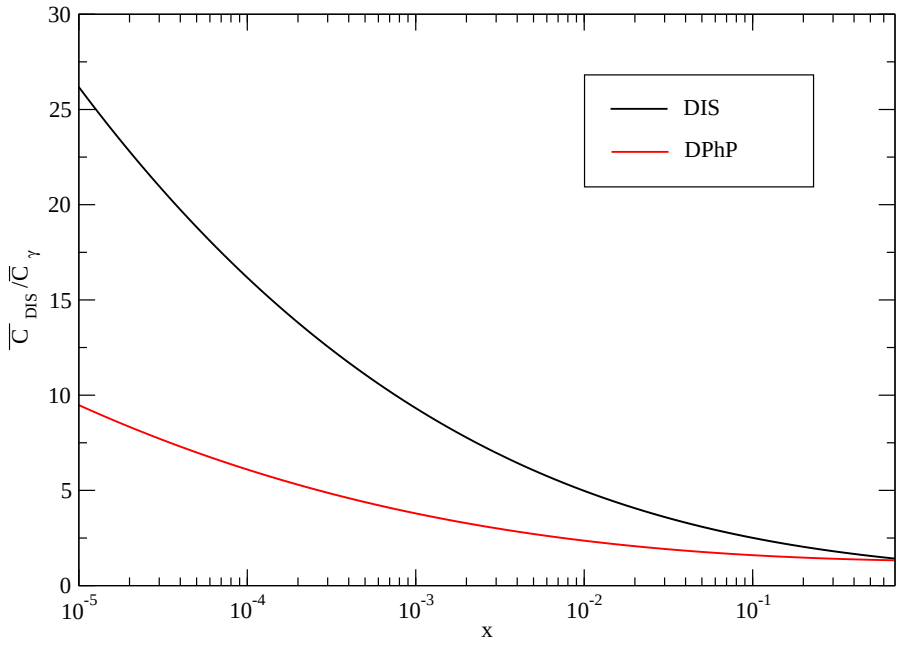

Figure 5.5: Ratio between F_2 ($\bar{\mathcal{C}}_{DIS}$ and direct photon (DPhP) ($\bar{\mathcal{C}}_{\gamma}$) coefficient functions, both of them normalized to their LO values

of DGLAP evolution equations, following the formalism of refs [35, 49] (see also ref. [47] for an alternative approach). However, we can get a feeling for the size of resummation effects by comparing the result in eq. (6.2.4) with the DIS coefficient function $C_2^g(N)$. As shown in fig. 5.5 the ratio between C_2^g and $\mathcal{C}_{qg}^{\gamma}$ (both of them normalized to the respective LO values) is of order 1, therefore we expect that, at low-x, resummation effects may be as important as those obtained in the DIS case.

Chapter 6

Resummation phenomenology at hadron collider

6.1 Prompt photon at high energy: introduction

The high–energy regime of QCD is the kinematical regime in which hard scattering processes happen at a center-of-mass energy $\sqrt{S}$ which is much larger than the characteristic hard scale of the process Q. An understanding of strong interactions in this region is therefore necessary in order to perform precision physics at high–energy colliders. The high–energy regime is also known as the small-x regime, since it is the regime in which the scaling variable $x = Q^2/S \ll 1$. In this sense, HERA was the first small x machine, while at LHC the small x regime will be even more important.

As is well known, deep–inelastic partonic cross sections and parton splitting functions receive large corrections in the small x limit due to the presence of powers of $\alpha_s \log x$ to all orders in the perturbative expansion [30, 31]. This suggests dramatic effects from yet higher orders, so the success of NLO perturbation theory at HERA was for a long time very hard to explain. In the last several years this situation has been clarified [55, 49, 32, 35, 47, 56, 48], showing that, once the full resummation procedure accounts for running coupling effects, gluon exchange symmetry and other physical constraints, the effect of the resummation of terms which are enhanced at small x is perceptible but moderate — comparable in size to typical NNLO fixed order corrections in the HERA region.

A major development for high–energy resummation was presented in Ref. [35] where the full small x resummation of deep-inelastic scattering (DIS) anomalous dimensions and coefficient functions was obtained includ-

ing quarks, which allowed for the first time a consistent small-x resummation of DIS structure functions. Furthermore, the resummation of hard partonic cross sections has been performed for several LHC processes such as heavy quark production [33], Higgs production [37, 36], Drell-Yan [39, 57] and prompt photon production [58]. Hints of the presence of small-x resummation have also recently found in inclusive HERA data [59]. Small–x resummation should also be very important at a high–energy DIS collider like the Large Hadron Electron Collider [60, 61]. A more detailed summary of recent theoretical developements in high–energy resummation may be found in Ref.[62]. These results mean that a detailed analysis of the impact of high–energy resummation on precision LHC physics is now possible.

As a part of such a program, in this letter we present a study of the phenomenological implications of the high–energy resummation of direct photon production at hadronic colliders. The production of direct photons [63] is a very important process at hadronic colliders, relevant both for fundamentals reasons (tests of perturbative QCD, measurement of the gluon PDF) and as background to new physics searches, the $H \to \gamma\gamma$ decay being the classical example. In the case of direct photon production, several works have studied in detail the comparison of theoretical QCD predictions with available experimental data from fixed target and collider experiments. Such comparisons have been performed using fixed order NLO computations [64, 28, 65], Monte Carlo event generators [66] and supplementing the fixed order result with threshold resummations [9, 67, 68, 21]. The latter aim to improve the accuracy of the perturbative prediction in the regime where the photon's p_T is large, close to the kinematic production threshold, where soft gluon emission enhances the cross section.

The present chapter is focused on the low p_T region, where terms of the type $\alpha_s^k \ln^p x$, enhanced by logarithms of the scaling variable $x_\perp \equiv 4p_T^2/S$, are important to all orders in perturbation theory. For this reason we do not consider fixed target data, which are characterized by moderate and large values of $x_\perp$ where high–energy resummation is certainly irrelevant, and concentrate instead on collider data for which the large center of mass $S \gg p_T^2$ available guarantees that the kinematical region sensitive to small-x effects is explored. As an illustration, if the small-p_T region is defined naively as the region in which the hadronic cross section becomes sensitive to PDFs and partonic coefficient functions for $x \lesssim 10^{-3}$, then at Tevatron this criterion corresponds to $p_T \lesssim 30$ GeV and at the LHC 14 TeV to $p_T \lesssim 200$ GeV.

The prompt photon process is characterized by a hard event involving the production of a single photon. Let us consider the hadronic process

$$H_1(P_1) + H_2(P_2) \to \gamma(q) + X. \tag{6.1.1}$$

According to perturbative QCD, the direct and the fragmentation component of the inclusive cross-section at fixed transverse momentum p_T of the photon can be written as [9]

$$p_T^3 \frac{d\sigma_\gamma(x_\perp, p_T^2)}{dp_T} = \sum_{a,b} \int_{x_\perp}^1 dx_1 \; f_{a/H_1}(x_1, \mu_{\rm F}^2) \int_{x_\perp/x_1}^1 dx_2 \; f_{b/H_2}(x_2, \mu_{\rm F}^2) \times$$
$$\times \int_0^1 dx \left\{ \delta\left(x - \frac{x_\perp}{x_1 x_2}\right) \mathcal{C}_{ab}^\gamma(x, \alpha_s(\mu^2); p_T^2, \mu_{\rm F}^2, \mu_{\rm f}^2) + \right.$$
$$\left. + \sum_c \int_0^1 dz \; z^2 d_{c/\gamma}(z, \mu_f^2) \delta\left(x - \frac{x_\perp}{z x_1 x_2}\right) \mathcal{C}_{ab}^c(x, \alpha_s(\mu^2); p_T^2, \mu_F^2, \mu_f^2) \right\} \quad (6.1.2)$$

where we have introduced the customary scaling variable in terms of the hadronic center-of-mass energy $S = (P_1 + P_2)^2$:

$$x_\perp = \frac{4p_T^2}{S}, \qquad 0 < x_\perp < 1 \; . \quad (6.1.3)$$

The fragmentation component is given in terms of a convolution with the fragmentation function $d_{c/\gamma}(z, \mu_f^2)$. In the factorization formula Eq. (C.1.1) we have used the short-distance cross-sections

$$\mathcal{C}_{ab}^{\gamma(c)} \equiv p_T^3 \frac{d\hat{\sigma}_{ab\to\gamma(c)}(x, \alpha_s(\mu^2); p_T^2, \mu_F^2, \mu_f^2)}{dp_T}, \quad (6.1.4)$$

where a, b and c are parton indices (q, $\bar{q}$, g) while $f_{i/H_j}(x_i, \mu_F^2)$ is the parton density at the factorization scale μ_F. The leading order coefficient functions for the Compton scattering channel (qg) and for the quark annihilation channel ($q\bar{q}$) are given by

$$\mathcal{C}_{qg}^{\gamma,\rm LO}(x) = \frac{\alpha\alpha_s e_q^2 \pi}{2N_c} \frac{x}{\sqrt{1-x}} \left(1 + \frac{x}{4}\right) \; ,$$
$$\mathcal{C}_{q\bar{q}}^{\gamma,\rm LO}(x) = \frac{\alpha\alpha_s e_q^2 C_F \pi}{N_c} \frac{x}{\sqrt{1-x}} (2 - x) \; . \quad (6.1.5)$$

In Fig. 6.1 we show the associated LO Feynman diagrams for these two channels. NLO corrections to the direct partonic cross section in Eq. (C.1.1) were computed in Refs. [69, 70, 8], while for the fragmentation component they were evaluated in Refs. [71, 72].

6.2 Kinematics and resummed coefficient function

The kinematics of direct photon production at hadronic colliders are summarized in Fig. 6.2, where the minimum value of x, $x_\perp$, probed in the pro-

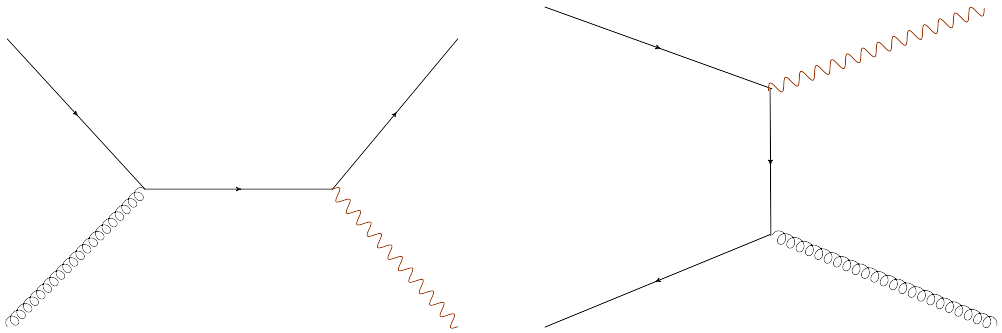

Figure 6.1: The Feynman diagrams for the direct production of a photon in hadronic collisions at leading order: the gq channel, also known as Compton scattering channel (left) and the $q\bar{q}$ channel, also known as quark annihilation channel (right).

duction of a photon with a given p_T is shown. For illustrative purposes, the corresponding kinematics for a notional VLHC with $\sqrt{S} = 200$ TeV are also shown. From Fig. 6.2 follows that collider experiments have the potential reach down to very small values of x, for example, at LHC 14 TeV PDFs and coefficient functions are probed down to $x \sim 10^{-5}$ for a $p_T \sim 20$ GeV photon. This implies that one should worry about those terms in the perturbative expansion which are formally subleading but which are logarithmically enhanced to all orders at small-x, both in the PDF evolution and in the partonic cross-sections.

Due to multiple gluon emissions, the perturbative expansion of the partonic cross sections, Eq. (6.1.4), is logarithmically enhanced at small-x starting from NNLO. While at NLO the single gluon emission produces the constant behaviour at low-x of the coefficient function Eq. (6.1.4), the NNLO behaves like a single logarithm and, in general, at N^{k}LO, the dominant contribution is given by $\alpha_s(\alpha_s \log x)^{k-1}$.

The high–energy resummed coefficient function of the direct component in Eq. (C.1.1) has been obtained in Ref. [58] in the framework of the k_T-factorization theorem, which allows one to perform the leading log resummation in terms of the off shell impact factor, which is the leading order cross section computed with off-shell incoming gluons. Following the resummation procedure one obtains the sum of the leading contributions at high–energy and, by re-expanding in powers of α_s, we have the coefficients of each power of $\log x$ to all orders in perturbation theory.

The high-energy enhanced terms in the direct photon partonic cross sec-

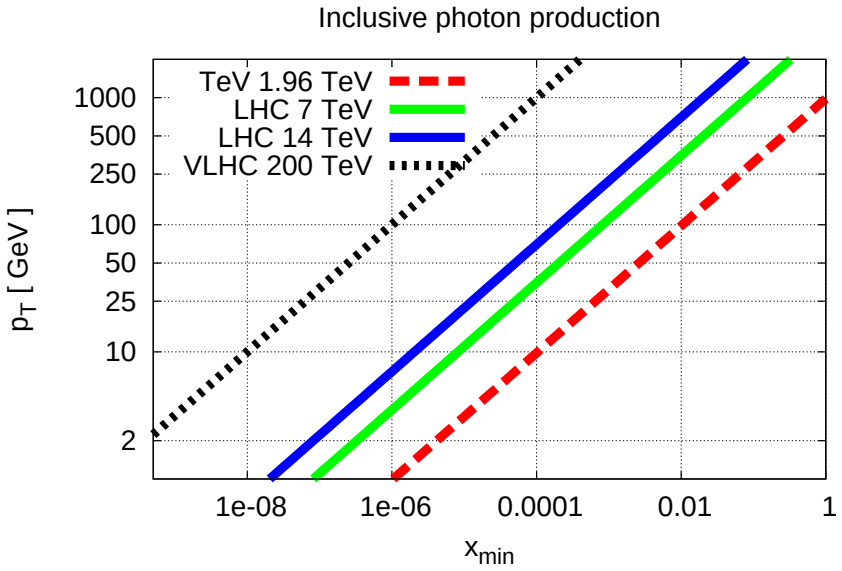

Figure 6.2: The minimum values of x, $x_{\rm min} = x_\perp = 4p_T^2/S$ which are probed in the production of a direct photon with transverse momentum p_T at hadronic colliders: Tevatron Run II ($\sqrt{S}$=1.96 TeV), LHC 7 TeV and LHC 14 TeV and VLHC 200 TeV. As can be seen from the plot, for the production of a $p_T \sim 20$ GeV photon, PDFs and coefficient functions are probed down to $x \sim 5\,10^{-4}$ at the Tevatron and $x \sim 10^{-5}$ at the LHC 14 TeV. Note that no cuts in rapidity are assumed in the definition of the kinematical ranges, experimentally realistic cuts reduce the reach in x for a given p_T.

tion, as discussed in Ref. [58], in N space are given in the qg channel by

$$\tilde{\mathcal{C}}^{\gamma}_{qg}(N,\bar{\alpha}_s,\kappa_r) = \frac{\alpha\alpha_s^2}{N}\sum_{k=0}^{\infty} c_{qg}^{(k)}(\kappa_r)\left(\frac{\bar{\alpha}_s}{N}\right)^{k-1} \tag{6.2.1}$$

where the renormalization scale has been set to proportional to the transverse momentum of the photon $\mu_{\rm r} = \kappa_r p_T$ and where $\bar{\alpha}_s \equiv \alpha_s C_A/\pi$ with α_s is the fixed strong coupling and $\alpha = 1/137$ the electromagnetic coupling constant. The first few coefficients in Eq. (6.2.1) read

$$\begin{aligned}
c_{qg}^{(0)} &= \tfrac{7}{6} \\
c_{qg}^{(1)} &= \tfrac{67}{36} - \tfrac{7}{3}\log\kappa_r \\
c_{qg}^{(2)} &= \tfrac{7}{4}\log^2\kappa_r - \tfrac{29}{9}\log\kappa_r + \tfrac{385}{216} \\
c_{qg}^{(3)} &= -\tfrac{7}{9}\ln^3\kappa_r - \tfrac{55}{26}\ln^2\kappa_r - \tfrac{179}{54}\ln\kappa_r + \tfrac{49}{9}\zeta(3) + \tfrac{2323}{1296}
\end{aligned} \tag{6.2.2}$$

The NLO term in Eqs. (6.2.1-6.2.2) gives, in the x-space, the constant value $\alpha\alpha_s^2 67/36$ for $\kappa_r = 1$, in agreement with the fixed order calculation of Refs. [8, 50]. By using the high-energy color charge relation between the hard coefficient functions

$$\tilde{\mathcal{C}}^{\gamma}_{q\bar{q}(q)}(N,\alpha_s,\kappa_r) = \frac{C_F}{C_A}\left(\tilde{\mathcal{C}}^{\gamma}_{qg}(N,\alpha_s,\kappa_r) - \tilde{\mathcal{C}}^{\gamma,\mathrm{LO}}_{qg}(0,\alpha_s,\kappa_r)\right) \tag{6.2.3}$$

we can obtain the high–energy coefficient function in the $q\bar{q}(q)$ channel.

In the rest of this work we will set $\kappa_r = 1$. In this case, the resummed coefficient function Eq. (6.2.1) in $x-$space reads

$$\begin{aligned}\mathcal{C}^{\gamma}_{qg}(x,\bar{\alpha}_s) &= \alpha\alpha_s^2\Big\{\tfrac{67}{36} + \tfrac{385}{216}\bar{\alpha}_s \ln\tfrac{1}{x} + \tfrac{1}{2}(\tfrac{2323}{1296} + \tfrac{49}{9}\zeta(3))\bar{\alpha}_s^2 \ln^2\tfrac{1}{x} \\ &+ \tfrac{1}{6}(\tfrac{14233}{7776} - \tfrac{7}{720}\pi^3 + \tfrac{308}{27}\zeta(3))\bar{\alpha}_s^3 \ln^3\tfrac{1}{x} + O(\bar{\alpha}_s^4 \ln^4\tfrac{1}{x})\Big\}\end{aligned} \tag{6.2.4}$$

Note that the logarithms of x (high–energy enhanced terms) which lead to the rise of the partonic cross section at small-x appear only from NNLO onwards.

However, this formalism is incomplete as we already discussed in the previous chapter because it does not account for running coupling effects. The running of α_s produces a new series of relevant contributions in the high energy limit which modify the nature of the singularity of the anomalous dimension at small-x and stabilize the small-x limit of the resummed coefficient function. For a thorough description of the inclusion of running coupling effects see Refs. [32, 35].

In this way a fully resummed coefficient function in the $\overline{\mathrm{MS}}$ scheme, which can be consistently matched to standard $\bar{\mathrm{M}}\mathrm{S}$ fixed order computations, can be obtained. This resummed coefficient function $\mathcal{C}^{\gamma,\mathrm{res}}_{ab}$ can be matched to the fixed order NLO coefficient function to obtain a resummed coefficient functions which reproduces at large-x the fixed order result,

$$\mathcal{C}^{\gamma,\mathrm{NLOres}}_{ab} = \mathcal{C}^{\gamma,\mathrm{NLO}}_{ab} + \mathcal{C}^{\gamma,\mathrm{res}}_{ab} - \mathcal{C}^{\gamma,\mathrm{dc}}_{ab}\ . \tag{6.2.5}$$

In Eq. (6.2.5) the matching between the fixed order NLO result and the resummed one has been performed being careful of avoiding double counting. Therefore, the double counting contribution $\mathcal{C}^{\gamma,\mathrm{dc}}_{ab}$, that is, the terms in Eq. (6.2.4) up to $\mathcal{O}\left(\alpha\alpha_s^2\right)$ is removed from the NLO coefficient functions. The fixed order NLO coefficient functions are taken from Ref. [8].

Note that Eq. (6.2.5) accounts for the high–energy resummation of the direct part of the photon production cross section without photon isolation effects. At the resummed level, the effects of the photon isolation in the coefficient function Eq. (6.2.1) can be computed in the small cone approximation. It can be shown that isolation leads an effect analogous to the variation of

the renormalization scale, that is, using the usual isolation with a cone of radius R implies a modifications of the renormalization scale $\kappa_r \to \kappa_r R$. Note also that we do not attempt a resummation of the fragmentation component of the photon production cross section, which in any case is very much suppressed by the photon isolation.

In Fig. 6.3 we show the LO, NLO and resummed coefficient functions for the two relevant channels: Compton scattering, qg, and quark annihilation, $q\bar{q}$. On top of these, we also show the NLO coefficient functions supplemented by the NNLO high–energy contribution (the $\mathcal{O}\left(\alpha\alpha_s^3\right)$ term in Eq. (6.2.4), and similarly for NLO plus NNNLO high–energy contributions (the $\mathcal{O}\left(\alpha\alpha_3^3\right)$ and $\mathcal{O}\left(\alpha\alpha_s^4\right)$ terms in Eq. (6.2.4). These two latter cases are shown for illustration, with the well know caveat that subleading corrections at a fixed α_s might sizably reduce the effect of the leading high–energy contributions. Fig. 6.3 shows the important result that the steep rise at small-x of the fixed order coefficient function due to the increasing powers of $\log x$ is stabilized after the including the running coupling effects, as happens for DIS [35].

Now that the resummed partonic cross-section, suitably matched to the fixed-order NLO result, has been obtained, we can use it to estimate the impact of high–energy resummation on the hadronic cross–section, Eq. (C.1.1), at the Tevatron and at the LHC. The fixed order NLO computation of isolated photon production has been obtained using the code of Ref. [8]. The small cone approximation for the isolation criterion has been used, which is shown to be an excellent approximation [27] to the exact result for typical isolation parameters. The photon fragmentation functions are the BFG set [73], although the choice is irrelevant since the fragmentation component is severely suppressed by the isolation criterion.

Note that in the following the same PDF set will be used used both in the NLO and in the resummed computations. The motivation for this is that we are interested only in the impact of the resummation of the partonic cross-section. A consistent high–energy resummed cross section would require PDFs obtained from a global analysis based on small-x resummation, which are not available yet.

6.3 Phenomenology at Tevatron and LHC

In order to assess the impact of high–energy resummation at the Tevatron, we consider recent Run II data on isolated photon production from the CDF collaboration [19]. CDF data is provided in the range $30\ \text{GeV} \leq \text{p}_\text{T} \leq 350\ \text{GeV}$, integrated in the photon's rapidity range $|\eta^\gamma| \leq 1.0$. The parameters of the photon isolation criterion in the theoretical calculation match those of

the experimental analysis, namely $R = 0.4$ and $E_T^{\rm had} \leq 2$ GeV. The parton distribution set used for the comparison with experimental data is the recent NNPDF2.0 global analysis [74]. As compared to previous NNPDF sets [75, 76, 77], NNPDF2.0 has a more precise gluon both at small-x from the combined HERA-I dataset and at large-x from the Tevatron inclusive jet data, which translate into very accurate predictions for direct photon production.

In Fig. 6.4 we present the results of this comparison between the fixed order NLO and the resummed predictions with the recent direct photon measurements from the CDF Collaboration at Run II. We show as well the PDF uncertainties and the theoretical uncertainties from missing higher orders estimated as usual varying the scales of the NLO expressions. Good agreement between NLO QCD and experimental data within the experimental uncertainties is found through most of the p_T range, except for a systematic discrepancy at small p_T. This discrepancy is present also for other PDF sets [65] as well as for the D0 data [78].

Since the high–energy resummed coefficient functions, Fig. 6.3 are integrated in the photon's rapidity η^γ, we will assume that the effects of the resummation are constant in η^γ. This means that the resummed result in Fig. 6.4 has been obtained as follows

$$\frac{d\sigma_\gamma^{\rm res}\left(x_\perp, p_T^2, |\eta^\gamma| \leq \eta_{\rm cut}\right)}{dp_T} = \frac{d\sigma_\gamma^{\rm NLO}\left(x_\perp, p_T^2, |\eta^\gamma| \leq \eta_{\rm cut}\right)}{dp_T} \frac{d\sigma_\gamma^{\rm res}\left(x_\perp, p_T^2\right)}{d\sigma_\gamma^{\rm NLO}\left(x_\perp, p_T^2\right)} \tag{6.3.1}$$

This approximation could be improved by computing the high–energy resummation of the photon rapidity distribution, for which qualitative arguments suggest that the impact of resummation is more important towards forward rapidities.

To estimate the theoretical uncertainty due to missing higher orders terms in the NLO computation the common scale $\kappa_r = \kappa_F = \kappa_f$ has been varied within a reasonable range. In particular we have computed the cross section for $\kappa_r = 0.5$, 1 and 2. The scale variation uncertainty is defined as the envelope of the most extreme results obtained this way for any given p_T. As seen in Fig. 6.4, PDF uncertainties for isolated photon production at the Tevatron are below 5% in all the p_T range, and $\mathcal{O}\left(2\%\right)$ in the small $p_T \lesssim 100$ GeV region. Scale variation uncertainties are $\mathcal{O}\left(5\%\right)$ approximately constant in p_T.

We do not attempt here to estimate the combined PDF and α_s uncertainty [79, 80, 81], which could be important in direct photon production since the cross section starts at $\mathcal{O}\left(\alpha\alpha_s\right)$. Moreover, in this work we do not address the important issue of the compatibility of predictions obtained

from different modern PDF sets, which has already been presented in detail in Ref. [65].

From Fig. 6.4 it is clear that at the Tevatron the prediction from high–energy resummation is essentially identical to that of the fixed order NLO computation. This might seem unintuitive, since we have shown in Fig. 6.3 that the respective coefficient functions are rather different in the small x region within the kinematical reach of experimental data (Fig. 6.2). In order to explain this result, let us define the contribution to the total cross section for $x \geq x_\perp^{\min}$ as follows

$$\mathbf{q}^3 \frac{d\sigma_\gamma(x_\perp, x_\perp^{\min}, p_T^2)}{d\mathbf{q}} \equiv \sum_{a,b} \int_{x_\perp^{\min}}^1 dx_1 \; f_{a/H_1}(x_1, \mu_{\rm F}^2) \int_{x_\perp^{\min}/x_1}^1 dx_2 \; f_{b/H_2}(x_2, \mu_{\rm F}^2) \times$$
$$\times \int_0^1 dx \left\{ \delta\left(x - \frac{x_\perp}{x_1 x_2}\right) \mathcal{C}_{ab}^\gamma(x, \alpha_s(\mu^2); p_T^2, \mu_{\rm F}^2, \mu_{\rm f}^2) + \text{fragmentation} \right\} \quad (6.3.2)$$

and then we can construct the ratio

$$R_\gamma\left(x_\perp, x_\perp^{\min}, p_T^2\right) \equiv \frac{d\sigma_\gamma(x_\perp, x_\perp^{\min}, p_T^2)/dp_T}{d\sigma_\gamma(x_\perp, x_\perp, p_T^2)/dp_T} \quad (6.3.3)$$

which measures the fraction of the cross–section for which PDFs and coefficient functions with $x \geq x_\perp^{\min}$ are probed.

In Fig. 6.5 we show this ratio at the Tevatron, the LHC and the notional VLHC for the production of a photon with $p_T = 20$ GeV. We observe that the direct photon cross section at the Tevatron is completely dominated by the region $x \gtrsim 5\,10^{-2}$. In this region, the resummed coefficient functions are almost identical to the fixed order NLO ones. Therefore, despite the fact that the values of x probed in small-p_T photon production are such that the resummed coefficient functions, Fig. 6.3, differ sizably from their fixed order NLO counterparts, this difference is restricted to a region with very little weight in the total cross–section. This feature of direct photon production (shared also by Higgs production [37, 36]) explains the smallness of high–energy resummation at the Tevatron. Note that this applies to the rapidity integrated cross–section, it is conceivable that more important effects are observed if one is restricted to forwards rapidities.

Note that Fig. 6.5 implies also that direct photon production is sensitive to the large-x PDFs, especially the gluon, but not to the small-x ones: the inclusion of collider direct photon data into a global PDF analysis might improve the precision of the gluon at large-x, but not at small-x.

Let us finish the discussion on the impact of high-energy resummation at the Tevatron by noting that the origin of the discrepancy between NLO QCD and experimental data at small p_T is still not completely understood, in

particular, it is not caused by unresummed terms in the high-energy regime. However, as we have discussed, since the direct photon cross section is much more sensitive to large-x effects, this discrepancy could be partially cured by soft resummation [21].

Now we turn to discuss the phenomenological impact of the resummation at LHC. At the LHC, the production cross section of isolated photons is much larger than at the Tevatron, which will make possible a high-statistics measurement. The ALICE, ATLAS, CMS and LHCb experiments at the LHC have photon reconstruction capabilities with the electromagnetic calorimetry in various rapidity ranges [65]. The two main LHC experiments can measure photons in the central rapidity region $|\eta^\gamma| \lesssim 3$ down to $p_T = 10$ GeV, ALICE can do measurements in the central region $|\eta^\gamma| \lesssim 0.7$ down to $p_T = 5$ GeV, while LHCb can measure forwards photons, $2 \leq |\eta^\gamma| \leq 5$ in the low $p_T \leq 20$ GeV region as well. The LHCb measurements are specially interesting since small-x resummation effects, which are only important at low p_T, should be enhanced at forward rapidities.

From the discussion in the case of the Tevatron, we expect the impact of high–energy resummation to be also small at the LHC. To illustrate such impact, in Fig. 6.6 we show the ratio between the resummed and NLO direct photon production cross section at LHC, for $\sqrt{S} = 14$ TeV. We show for simplicity the direct part of the photon production cross section only. No cuts in the photon's rapidity are imposed. We have used again the NNPDF2.0 set for the theoretical prediction, and scale variation uncertainty is estimated as discussed above.

From Fig. 6.6 we observe that the effect of high–energy resummation is very small above $p_T \sim 10$ GeV, and it is only for photon transverse momenta in the range 2 GeV $\lesssim$ $\mathrm{p_T}$ $\lesssim$ 10 GeV that it becomes of the order of a few percent. The origin of the smallness of the high–energy resummation can be traced back, as in the case of the Tevatron to Fig. 6.5: the direct photon cross section for the production of a photon with $p_T = 20$ GeV is completely dominated by the region $x \gtrsim 5\,10^{-3}$. In this region, the resummed coefficient functions are almost identical to the fixed order NLO ones. It is only for smaller values of p_T that the difference between NLO and resummed coefficient functions at small-x, evident from Fig. 6.3, begin to contribute to the total cross section. At very small-p_T the effects of high–energy resummation are much smaller than the PDF uncertainties. This implies that the small-p_T region can be used to constrain accurately the gluon PDF, provided that systematic experimental uncertainties in this region can be kept under control.

Let us emphasize however that the smallness of the high–energy resummation with respect to fixed order NLO does not imply that resumming

high–energy enhanced terms is not relevant at hadronic colliders. Indeed, the crucial role of high–energy resummation is to cure the instability of the cross section which appears in any fixed order calculation at high–energy starting from NNLO. To illustrate this point, in Fig. 6.6 we also show the results for direct photon production if the dominant NNLO contribution at small-x (the term proportional to $\mathcal{O}\left(\alpha_s^3\right)$ in Eq. (6.2.4) is added to the fixed order NLO result, as an approximation to the full fixed order NNLO result. We see that here the difference with respect NLO is more important, being $\sim$10% at $p_T \sim 20$ GeV and much larger at even smaller p_T. The corresponding effect would be even larger for the dominant NNNLO corrections. Thus the full high-energy resummation is required in order to obtain stable predictions for future higher order calculations of direct photon production (starting from NNLO accuracy) at small p_T at hadronic colliders.

Finally, in Fig. 6.7 we show the impact of the resummation of the high–energy coefficient function for photon production at a notional VLHC with $\sqrt{S} = 200$ TeV. From Fig. 6.5 we see that for a 20 GeV photon the cross section is sensitive to the coefficient functions with $x \geq 5\,10^{-4}$, so one expected the effects of the resummation to be more important that at lower CM energies. However, even at this huge energy, the effect is of a few percent at most at the smallest p_T.

To summarize, in this chapter results for the high energy resummation of direct photon production have been matched to NLO computations and predictions for hadronic colliders have been obtained. We have shown that main impact of the full high–energy resummation procedure is to stabilize the logarithmic enhancement of the cross section at high energies which is present at any fixed order in the perturbative expansion starting at NNLO. At the Tevatron the effects of the resummation are completely negligible, while at the LHC high–energy resummation of the partonic cross section enhances the hadronic cross section be a few percent at small p_T, $p_T \lesssim 10$ GeV. One important implication of our results is that the small p_T discrepancy between NLO QCD and Tevatron data cannot be described by unresummed higher order contributions enhanced in the high–energy regime. We have also shown that at the LHC the full resummation of the inclusive direct photo cross-section is very close to the fixed order NLO QCD result, becoming significant only at very low p_T, and that even at a VLHC resummation effects are rather small in this channel.

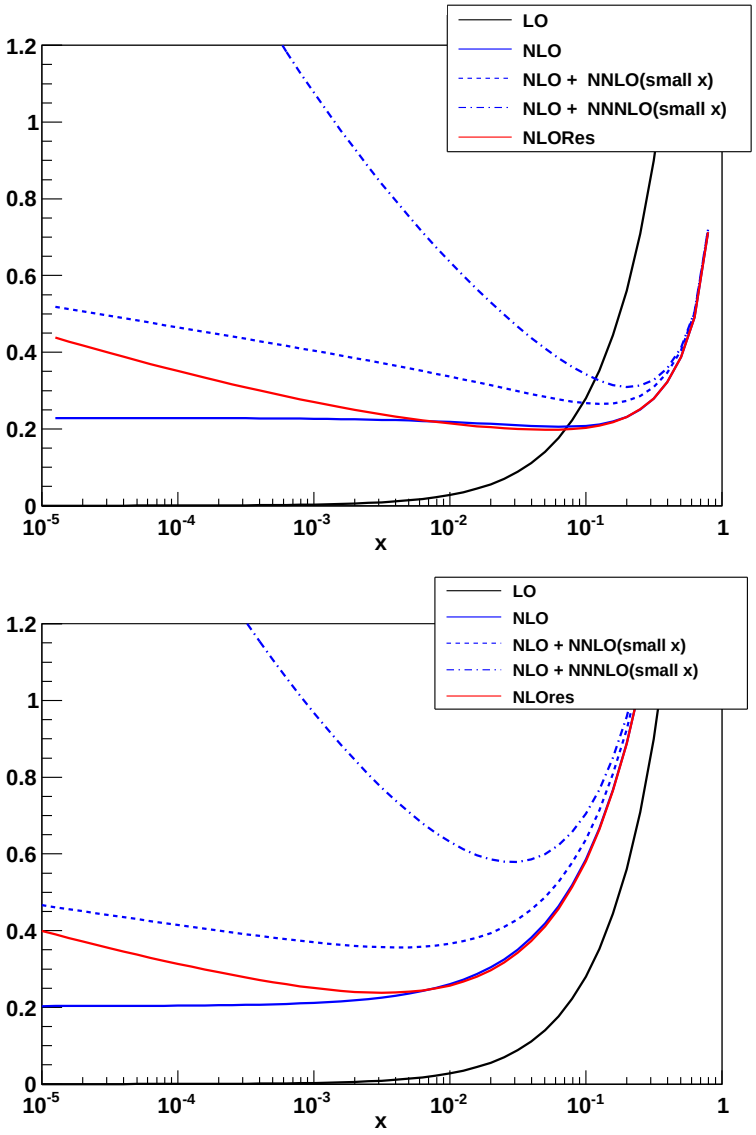

Figure 6.3: Upper plot: the coefficient functions (partonic cross sections) for direct photon production in the qg (Compton) channel. The following approximations to the partonic cross section are shown: LO (black, solid), NLO (blue, solid), NLO with the addition of the dominant small-x NNLO terms (blue, dashed), NLO with the addition of the dominant small-x NNNLO terms (blue, dot-dashed), and finally the high–energy resummed coefficient function, suitably matched of the fixed order NLO Eq. (6.2.5) (red, solid). Lower plot: the same comparison for the coefficient functions in the $q\bar{q}$ (quark annihilation) channel. Note that the coefficient functions rise at small-x begins at NNLO only.

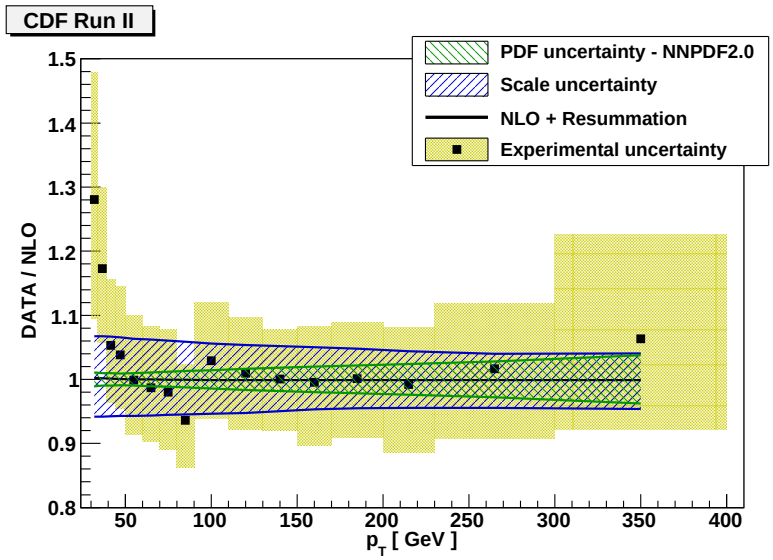

Figure 6.4: Comparison between the NLO cross section and the recent CDF data using the NNPDF2.0 PDF set. The solid black line is the ratio between the high–energy resummed result and the NLO prediction, as can be seen, the two results are essentially identical. The scale variation uncertainty corresponds to the NLO calculation.

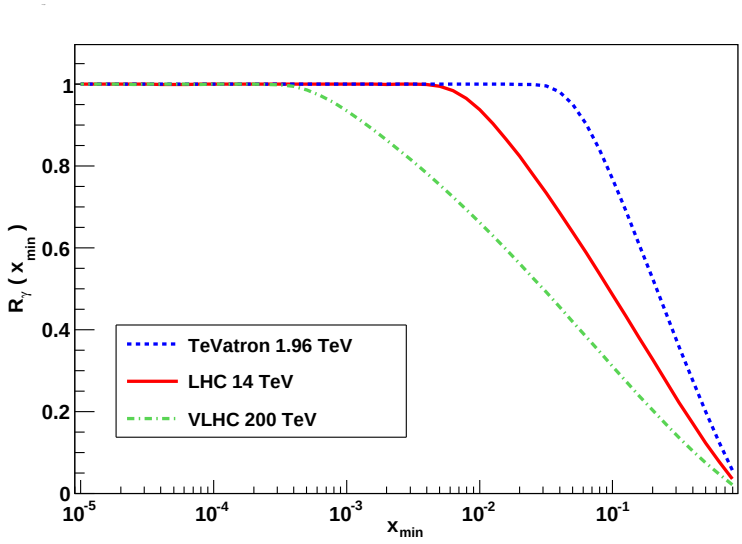

Figure 6.5: The ratio R_γ, Eq. (6.3.2), as a function of $x_\perp^{\min}$ at the LHC $\sqrt{S} = 14$ TeV (red solid line) and at Tevatron Run II $\sqrt{S} = 1.96$ TeV (blue dashed line) for the production of photon with $p_T = 20$ GeV. It is clear that the cross-section is dominated by the contribution of the coefficient function at medium and large-x, $x \gtrsim 5\,10^{-3}$ for LHC and $x \gtrsim 5\,10^{-2}$ for the Tevatron. The fact that the total cross section is insensitive to the partonic cross-sections at small-x explains the reduced impact of the high–energy resummation at hadronic colliders.

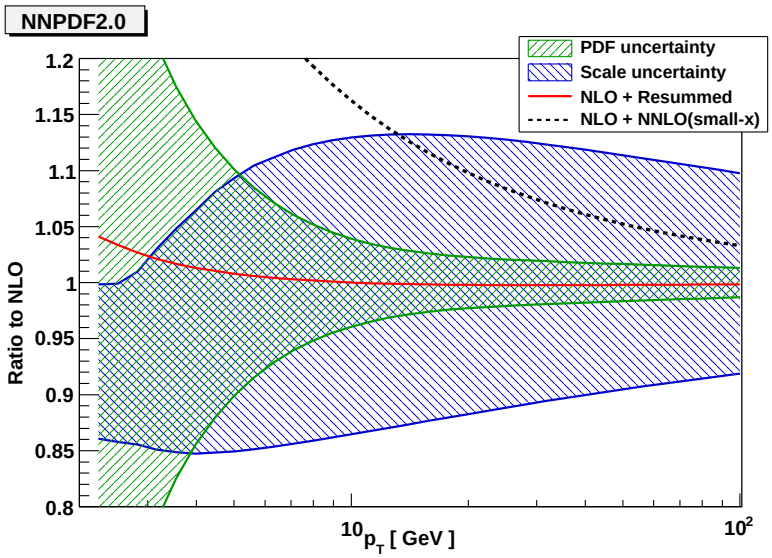

Figure 6.6: Ratio between resummed and NLO prediction (solid red line) for the inclusive cross section at LHC, for a center of mass energy of $\sqrt{S} = 14$ TeV. The NNPDF2.0 set has been used to compute the theoretical prediction. PDF and scale variation uncertainties are also shown. We also show the ratio to NLO of the approximated NNLO result, where the dominant NNLO contributions at small x have been added to the fixed order NLO result (black dashed line) .

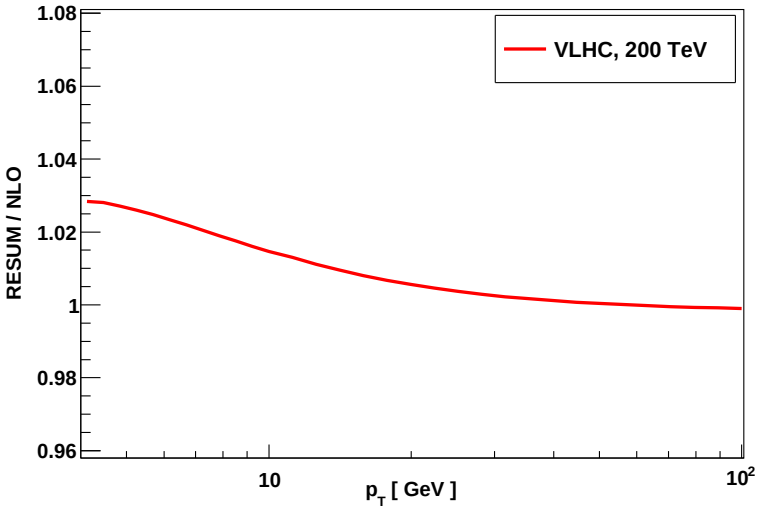

Figure 6.7: Ratio between resummed and NLO prediction (solid red line) for the cross section for photon production, integrated in rapidity, at a notional VLHC with a center of mass energy of $\sqrt{S} = 200$ TeV. The NNPDF2.0 set has been used to compute the theoretical prediction. Note that the very large PDF and scale variation uncertainties are not shown for simplicity.

Chapter 7

Conclusion and Outlook

7.1 Renormalization group and resummation at high energy

As we have seen, in the high energy limit the dominant contribution to the cross section is given by logarithms of increasing powers of the scaling variable x, defined as the ratio between the characteristic scale of our process and the center-of-mass energy. When x approaches to zero, terms of the form

$$(\alpha_s \log x)^k \sim \mathcal{O}(1) \tag{7.1.1}$$

are present to all orders in the perturbative expansion and are all equally relevant in the ordinary expansion in powers of the coupling α_s.

It is a very known fact that large logarithms can appear in the perturbative expansion in quantum field theory. Tipically the key ingredient in solving this problem is the renormalization group. This method allow to resum all the large contributions to all order in terms of running couplings. This is precisely what we have shown in Chapter 2 when we discussed the DGLAP equations.

The renormalization group provide a very simple resummation recipe when the perturbative expansion involves a single energy scale, say Q^2. However, in the small-x limit we have two scales, in particular at the LHC energy range, the phase space opens up the high energy region

$$\Lambda_{QCD} \ll Q^2 \ll S \tag{7.1.2}$$

where the renormalization group is not sufficient to solve the problems of perturbation theory.

The resummation of the large logarithms of x can be performed both in the inclusive cross section and the rapidity distributions by summing all the

BFKL ladder-type diagrams which are multiple gluon emission in the Regge kinematics. In Chapter 4 we discussed how the resummation recipe can be obtained by summing up the n-gluon emissions (strong ordered in the transverse momenta) and substituting the DGLAP anomalous dimension with the BFKL anomalous dimension γ_s which contains all the leading singularities at small-x.

7.2 Prompt photon and resummation

In Chapter 3 we focussed our attention to the prompt photon process. The motivations to study the production of photons in hadronic collisions are many, among them we mentioned the well known fact that photons can be used as 'probes' of the gluon density of the proton. Furthermore, the prompt photon process is the most important reducible background for the signal $H \to \gamma\gamma$ signal in the light Higgs scenario.

Unlike the most of the benchmark QCD processes, the prompt photon cross section contains two different contributions. In the direct component, the photon participates to the hard process while in the fragmentation component it is produced during the jet fragmentation and require the introduction of the fragmentation function that cannot be calculated from perturbative QCD and it is poorly known so far. From the theoretical point of view, the separation of these two contribution to the cross section is not trivial. Without any restriction to the phase space of the photon only the sum of the two coponent is meaningful, however, thanks to the careful analysis of Frixione[12], it can be shown that a isolation criterion for the direct component can be defined properly in such a way that the fragmentation part, vanishes identically.

In Chapters 5 and 6 we have discussed the application of the inclusive high energy resummation to the direct photon production cross section and its phenomenological impact at Tevatron and LHC. The effect of the leading log resummation to the NLO prediction is less than 1% even at the LHC energy range. This result has been obtained by considering all the logarithmic enhancement at small-x as well as the running coupling effects. In particular we noticed that the reason of this small effect to the hadronic cross section is the shape of the resummed coefficient function, which starts to deviate from the NLO result only for $x < 10^{-2}$. Since the resummation impact is so small, our conclusion is that the resummation procedure stabilize the perturbative expansion in the high energy limit. This is a remarkable information which is related to higher order calculations from the NNLO towards; indeed, as we have shown in Chapter 6, the cross section is much more sensitive to the

inclusion of the next powers of $\log x$ thus the resummation will be needed in order to stabilize the behaviour at low x.

7.3 Outlooks

In this work we have discussed only the direct component of the prompt photon cross section. We justified this choice because in the small isolation cone approximation we have control on the extra contributions coming from an isolation criterion which in general reduces the effect of the fragmentation component. We can mention here that a resummed result for the fragmentation contribution would require the resummation of the two-jet cross section. In particular, this calculation cannot be performed in terms of the simple recipe given by the k_T-factorization theorem, instead it requires the new approach developped in Ref. [46] where the sum of the leading contribution is performed by direct calculation of the Feynman diagrams.

Even though the resummation of the inclusive cross section is small, it is possible that the rapidity distribution of the prompt photon is the right observable to see the resummation effect, indeed while the inclusive result spread the resummation to the whole rapidity range, by looking to the rapidity distribution we can focus on the large rapidity region which is much more sensitive to the small-x contributions.

As we mentioned many times, the prompt photon data can provide important constraints to the gluon density since it appears at leading order in perturbation theory. Moreover the discrepancies between the fixed target set of data and the NLO prediction are still not completely understood. However, it could be easy and interesting to evaluate the impact of different data sets on the actual global fit of parton distribution. This could be done by means of a Bayesian reweighting.

Appendix A

Light-cone coordinates

Given a four dimensional vector $p^\mu = (E, p_x, p_y, p_z)$, the following variables

$$p^\pm = \frac{E \pm p_z}{\sqrt{2}} \tag{A.0.1}$$

$$k = \frac{p_x + ip_y}{\sqrt{2}} \tag{A.0.2}$$

$$\bar{k} = \frac{p_x - ip_y}{\sqrt{2}} \tag{A.0.3}$$

define the light-cone parametrization

$$p_{LC} = (p^+, p^-, k, \bar{k}). \tag{A.0.4}$$

The matrix form of this transformation is

$$M = \frac{1}{\sqrt{2}} \begin{pmatrix} 1 & 0 & 0 & 1 \\ 1 & 0 & 0 & -1 \\ 0 & 1 & i & 0 \\ 0 & 1 & -i & 0 \end{pmatrix} \tag{A.0.5}$$

Since the matrix M is not real, the complex conjugate of a complex vector transforms with the matrix $M\star$, *i.e.* with p and $\bar{p}$ exchanged. In terms of these variables, Lorentz scalars become

$$p^\mu q_\mu = p^+ q^- + p^- q^+ - p\bar{q} - \bar{p}q \tag{A.0.6}$$

$$(p^\star)^\mu q_\mu = (p^+)^\star q^- + (p^-)^\star q^+ - (p^\star)q - (\bar{p})^\star \bar{q} \tag{A.0.7}$$

For a massless particle, the relation $p^2 = 0$ takes the form

$$p^+ p^- = \bar{p}p \tag{A.0.8}$$

Polarization vectors for a particle with momentum $\vec{k}$ are given by eigenvectors of the operator associated to eigenvalues +1 and -1.

$$J(k) = k_x J_x + k_y J_y + k_z J_z \tag{A.0.9}$$

that is

$$\epsilon^-(\vec{k}) = N\left(-\frac{k_z E + ik_x k_y}{k_x E - ik_y k_z}, \frac{i\,(k_x^2 + k_z^2)}{k_x E - ik_y k_z}, 1\right) \tag{A.0.10}$$

$$\epsilon^+(\vec{k}) = N\left(-\frac{k_z E - ik_x k_y}{k_x E + ik_y k_z}, -\frac{i\,(k_x^2 + k_z^2)}{k_x E + ik_y k_z}, 1\right) \tag{A.0.11}$$

where N is the normalization factor. For $\epsilon^-(\vec{k})$ we obtain

$$\epsilon^-(\vec{k}) = N\left(-\frac{(p^+)^2 - (p^-)^2 - \bar{k}^2 + k^2}{2kp^- + 2\bar{k}p^+}, \frac{i((p^+)^2 + (p^-)^2 + \bar{k}^2 + k^2}{2kp^- + 2\bar{k}p^+}, 1\right)$$

which in light-cone coordinates becomes

$$\begin{aligned}\epsilon^-(\vec{k}) &= \frac{N}{\sqrt{2}}\left(1, -1, \frac{-(p^+)^2 - k^2}{kp^- + \bar{k}p^+}, \frac{(p^-)^2 + \bar{k}^2}{kp^- + \bar{k}p^+}\right) \\ &= \frac{N}{\sqrt{2}}\left(1, -1, -\frac{p^+}{\bar{k}}, \frac{\bar{k}}{p^+}\right)\end{aligned} \tag{A.0.12}$$

The constant N can be obtained by the condition $\epsilon \cdot \bar{\epsilon} = -1$

$$\frac{N^2}{2}\left(-2 - \frac{(p^+)^2}{k\bar{k}} - \frac{k\bar{k}}{(p^+)^2}\right) = -1 \tag{A.0.13}$$

$$N^2 = \frac{2}{\left|\frac{p^+}{k} + \frac{\bar{k}}{p^+}\right|^2} = \frac{k_T^2}{(p^+ + p^-)^2} \tag{A.0.14}$$

The polarization vector $\epsilon^+(\vec{k})$ can be derived by the complex conjugate of $\epsilon^-(\vec{k})$ by exchanging the third component with the fourth one (complex conjugate vector are mapped in the light-cone representation with the matrix $M^\star$). Therefore we obtain

$$\epsilon^+(\vec{k}) = \frac{k_T}{\sqrt{2}(p^+ + p^-)}\left(1, -1, \frac{k}{p^+}, -\frac{p^+}{k}\right) \tag{A.0.15}$$

Appendix B

Helicity formalism

In this appendix we recall the notation of the helicity formalism. The two dimensional spinors λ and $\tilde{\lambda}$ for a massless fermion with momentum p are defined through the Dirac equation

$$\not{P}\lambda(p) = 0, \qquad \bar{\not{P}}\tilde{\lambda}(p) = 0, \tag{B.0.1}$$

with

$$\not{P} \equiv p_\mu \sigma^\mu, \quad \bar{\not{P}} \equiv p_\mu \bar{\sigma}^\mu, \quad \sigma^\mu = (\mathbf{1}, \vec{\sigma}), \quad \bar{\sigma}^\mu = (\mathbf{1}, -\vec{\sigma}) \tag{B.0.2}$$

$$\sigma_1 = \begin{pmatrix} 0 & 1 \\ 1 & 0 \end{pmatrix}, \quad \sigma_2 = \begin{pmatrix} 0 & i \\ -i & 0 \end{pmatrix}, \quad \sigma_3 = \begin{pmatrix} 1 & 0 \\ 0 & -1 \end{pmatrix}. \tag{B.0.3}$$

Now we define

$$[u_+(k_i)]_\alpha = [v_-(k_i)]_\alpha \equiv |i\rangle \equiv (\lambda(k_i))_\alpha \tag{B.0.4}$$

$$[u_-(k_i)]^{\dot{\alpha}} = [v_+(k_i)]^{\dot{\alpha}} \equiv |i] \equiv (\tilde{\lambda}(k_i))^{\dot{\alpha}} \tag{B.0.5}$$

conjugate spinors are obtained by lowering (raising) the dotted (undotted) indices by the antisymmetric tensors ϵ^{ab} and $\epsilon_{\dot{a}\dot{b}}$:

$$[\bar{u}_+(k_i)]_{\dot{\alpha}} = [\bar{v}_-(k_i)]_{\dot{\alpha}} \equiv [i| \equiv (\tilde{\lambda}(k_i))_{\dot{\alpha}} \equiv \epsilon_{\dot{\alpha}\dot{\beta}}(\tilde{\lambda}(k_i))^{\dot{\beta}} \tag{B.0.6}$$

$$[\bar{u}_-(k_i)]^{\alpha} = [\bar{v}_+(k_i)]^{\alpha} \equiv \langle i| \equiv (\lambda(k_i))^{\alpha} \equiv \epsilon^{\alpha\beta}(\lambda(k_i))_{\beta} \tag{B.0.7}$$

Scalar spinor products are defined as

$$\langle ij\rangle \equiv \bar{u}_-(k_i)u_+(k_j) = (\lambda(k_i))^\alpha(\lambda(k_j))_\alpha, \tag{B.0.8}$$

$$[ij] \equiv \bar{u}_+(k_i)u_-(k_j) = (\tilde{\lambda}(k_i))^{\dot{\alpha}}(\tilde{\lambda}(k_j))_{\dot{\alpha}}. \tag{B.0.9}$$

Because $\phi_a k^a = \epsilon_{ab}\phi^a k^b$, both the products above $[\spadesuit|\clubsuit]$ and $\langle\spadesuit|\clubsuit\rangle$ are antisymmetric, hence $\langle ii\rangle = [jj] = 0$.

From the condition in eq. (B.0.1) we can write

$$(\not{P})^{\dot{a}a} = \tilde{\lambda}^{\dot{a}}\lambda^{a} = |\lambda]\langle\lambda| \tag{B.0.10}$$

$$(\not{P})_{\dot{a}a} = \tilde{\lambda}_{\dot{a}}\lambda_{a} = |\lambda\rangle[\lambda| \tag{B.0.11}$$

thus Lorentz vector products can be written in terms of spinor products since we have

$$\langle i|j\rangle\,[ij] = (\not{k}_i)^{\dot{a}a}(\not{k}_j)_{\dot{a}a} = k_i^{\mu}k_j^{\nu}\mathrm{Tr}(\sigma_\mu\bar{\sigma}_\nu) \tag{B.0.12}$$

but we have also $\mathrm{Tr}(\sigma_\mu\bar{\sigma}_\nu) = 2g_{\mu\nu}$, therefore we have

$$\langle i|j\rangle\,[ij] = 2k_ik_j. \tag{B.0.13}$$

In this formalism polarization vectors of gauge bosons can be expressed in terms of spinor products

$$\epsilon_\mu^{\pm}(k;q) = \pm\frac{\langle q|\gamma_\mu|k]}{\sqrt{2}\langle qk\rangle} \tag{B.0.14}$$

where q is a reference Lorentz vector. Since the amplitude do not depend on q's, the recerence vectors can be choosen properly to reduce the number of Feynman diagrams.

Let us consider an n-gluon amplitude with two gluons of negative helicity and $(n-2)$ gluons with positive helicity. This amplitude is known as Maximal-Helicity-Violating (MHV) and it can be shown that

$$\begin{aligned}\mathcal{A}_n^{\text{tree MHV},\,(jk)} &\equiv \mathcal{A}_n(1^+,\ldots,j^-,\ldots,k^-,\ldots,n^+) = \\ &= i\frac{\langle jk\rangle}{\langle 12\rangle\langle 23\rangle\cdots\langle n1\rangle}.\end{aligned} \tag{B.0.15}$$

A similar expression holds in the opposite case of two positive helicities and $(n-2)$ negative helicities:

$$\begin{aligned}\mathcal{A}_n^{\text{tree MHV},\,(jk)} &\equiv \mathcal{A}_n(1^-,\ldots,j^+,\ldots,k^+,\ldots,n^-) = \\ &= -i\frac{[jk]}{[12]\,[23]\cdots[n1]}.\end{aligned} \tag{B.0.16}$$

Appendix C

Inclusive cross section and rapidity distribution

C.1 Factorization

In this Appendix we discuss some tecnical details which involve the rapidity integration. In the litterature, the rapidity distributions are written in terms of two variables v and w related to the momentum fractions x_1 and x_2 of the parton distribution. With these variables, the distributions which appear in the NLO coefficient function are simple "plus" prescriptions and δ-functions. Here we show how to derive the inclusive factorization formula from the rapidity distribution in (v, w) variables. The differential cross section for the prompt photon production can be written in the following form:

$$E_\gamma \frac{d^3\sigma^{AB}}{d^3p_\gamma} = \frac{1}{\pi p_T^4} \sum_{a,b} \int_{\frac{\sqrt{x}}{2}e^{\eta}}^{1-\frac{\sqrt{x}}{2}e^{-\eta}} dv \int_{\frac{\sqrt{x}}{2v}e^{\eta}}^{1} dw \; x_1 f_a^A(x_1) \; x_2 f_b^B(x_2) \cdot$$
$$\cdot v(1-v) w \hat{s} \frac{d\hat{\sigma}^{ab}}{dvdw} \qquad \text{(C.1.1)}$$

where the momentum fractions x_1 and x_2 are given in terms of the variables v and w:

$$x_1 = \frac{\sqrt{x}e^{\eta}}{2vw}, \qquad x_2 = \frac{\sqrt{x}e^{-\eta}}{2(1-v)}, \qquad \text{(C.1.2)}$$

and $x = 4p_T^2/S$. We parametrize the photon momentum p_γ in terms of the transverse momentum and pseudorapidity

$$p_\gamma = (p_T \cosh\eta, \vec{p}_T, p_T \sinh\eta). \qquad \text{(C.1.3)}$$

In the center-of-mass frame, the momenta of hadrons A and B are

$$P_A = \frac{\sqrt{S}}{2}(1,0,0,1), \qquad P_B = \frac{\sqrt{S}}{2}(1,0,0,-1) \qquad \text{(C.1.4)}$$

therefore, from the condition $(P_A + P_B - p_\gamma)^2 > 0$ we have

$$S - 2\sqrt{S}E_\gamma > 0 \to \cosh\eta < \frac{1}{x}. \tag{C.1.5}$$

which in terms of η becomes

$$\frac{1}{\sqrt{x}}(1 - \sqrt{1-x}) < e^\eta < \frac{1}{\sqrt{x}}(1 + \sqrt{1-x}) \tag{C.1.6}$$

Let us consider the rapidity integration. We have

$$d\sigma = \frac{1}{\pi p_T^4 E_\gamma} d^3p_\gamma(\cdots) = \frac{2}{p_T^3} dp_T d\eta(\cdots) = \frac{2}{p_T^3} dp_T \frac{dy}{y}(\cdots) \tag{C.1.7}$$

where we introduced the variable $y = e^\eta$. The cross section $p_T^3 \frac{d\sigma}{dp_T}$ is given by

$$p_T^3 \frac{d\sigma^{AB}}{dp_T} = \sum_{a,b} 2 \int_{\frac{1}{\sqrt{x}}(1-\sqrt{1-x})}^{\frac{1}{\sqrt{x}}(1+\sqrt{1-x})} \frac{dy}{y} \int_{\frac{\sqrt{x}}{2}e^\eta}^{1-\frac{\sqrt{x}}{2}e^{-\eta}} dv \int_{\frac{\sqrt{x}}{2v}e^\eta}^{1} dw\; x_1 f_a^A(x_1)\; x_2 f_b^B(x_2) \cdot$$
$$\cdot v(1-v) w \hat{s} \frac{d\hat{\sigma}^{ab}}{dvdw} \tag{C.1.8}$$

In order to obtain the partonic cross section $p_T^3 \frac{d\sigma}{dp_T}$, first we change the integration variables to x_1 and x_2, then we need to integrate Eq. (C.1.1) in rapidity and change the integration ordering from (η, x_2, x_1) to (x_2, x_1, η). If we express v and w from Eq. (C.1.2) we obtain

$$v = 1 - \frac{\sqrt{x}e^{-\eta}}{2x_2}, \qquad w = \frac{\sqrt{x}e^\eta}{2vx_1}. \tag{C.1.9}$$

From $v < 1 - \frac{\sqrt{x}}{2}e^{-\eta}$ and $w > \frac{\sqrt{x}}{2v}e^\eta$ we obtain $x_1, x_2 < 1$, furthermore we have

$$v > \frac{\sqrt{x}}{2}e^\eta \quad \to \quad x_2 > \frac{\sqrt{x}e^{-\eta}}{2 - \sqrt{x}e^\eta} \tag{C.1.10}$$

$$w < 1 \quad \to \quad x_1 > \frac{\sqrt{x}e^\eta}{2 - \sqrt{x}/x_2 e^{-\eta}} \tag{C.1.11}$$

By taking into account the jacobian we have

$$dvdw = dx_1 dx_2 \frac{x}{4v(x_1 x_2)^2}, \tag{C.1.12}$$

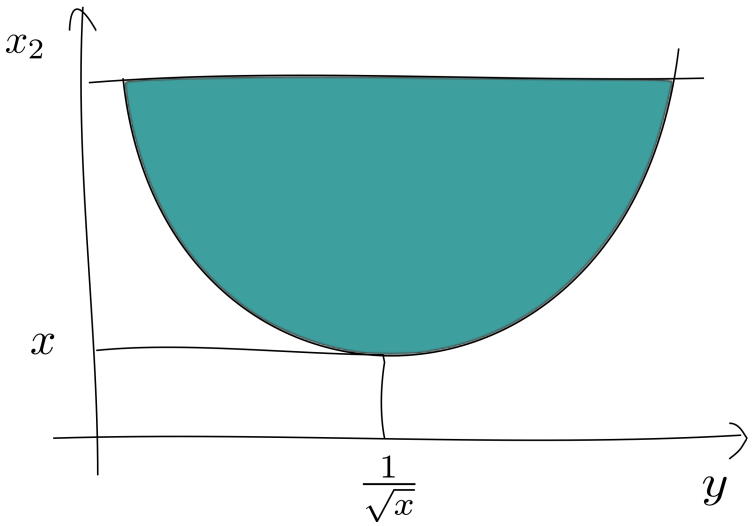

thus the integrations are

$$\int_{\frac{1}{\sqrt{x}}(1-\sqrt{1-x})}^{\frac{1}{\sqrt{x}}(1+\sqrt{1-x})} \frac{dy}{y} \int_{\frac{\sqrt{x}}{2}e^{\eta}}^{1-\frac{\sqrt{x}}{2}e^{-\eta}} dv \int_{\frac{\sqrt{x}}{2v}e^{\eta}}^{1} dw =$$
$$= \int_{\frac{1}{\sqrt{x}}(1-\sqrt{1-x})}^{\frac{1}{\sqrt{x}}(1+\sqrt{1-x})} \frac{dy}{y} \int_{\frac{\sqrt{x}}{2y-\sqrt{x}y^2}}^{1} dx_2 \int_{\frac{\sqrt{x}y^2}{2y-\sqrt{x}/x_2}}^{1} dx_1 \frac{x}{4v(x_1x_2)^2}. \quad \text{(C.1.13)}$$

Let us start by inverting the order of integration of y and x_2. The integration region is

$$\begin{cases} \frac{\sqrt{x}/y}{2-\sqrt{x}y} < x_2 < 1 \\ \frac{1}{\sqrt{x}}(1-\sqrt{1-x}) < y < \frac{1}{\sqrt{x}}(1+\sqrt{1-x}) \end{cases} \quad \text{(C.1.14)}$$

Note that the lower value of x_2 as a function of y is symmetric respect to $y = \frac{1}{\sqrt{x}}$ and for $y = \frac{1}{\sqrt{x}}(1 \pm \sqrt{1-x})$, $x_2 = 1$. Thus by inverting Eq. (C.1.14) we have

$$\begin{cases} \frac{1}{\sqrt{x}}(1-\sqrt{1-x/x_2}) < y < \frac{1}{\sqrt{x}}(1+\sqrt{1-x/x_2}) \\ x < x_2 < 1 \end{cases} . \quad \text{(C.1.15)}$$

Now let us invert y and x_1. The integration region now is

$$\begin{cases} \frac{\sqrt{x}y^2}{2y-\sqrt{x}/x_2} < x_1 < 1 \\ \frac{1}{\sqrt{x}}(1-\sqrt{1-x/x_2}) < y < \frac{1}{\sqrt{x}}(1+\sqrt{1-x/x_2}) \end{cases} . \quad \text{(C.1.16)}$$

and analogously to x_2 we have

$$\begin{cases} \frac{x}{x_2} < x_1 < 1 \\ \frac{x_1}{\sqrt{x}}(1-\sqrt{1-\frac{x}{x_1x_2}}) < y < \frac{x_1}{\sqrt{x}}(1+\sqrt{1-\frac{x}{x_1x_2}}) \end{cases} . \quad \text{(C.1.17)}$$

Thus, the reordered integrations are

$$\int_{\frac{1}{\sqrt{x}}(1-\sqrt{1-x})}^{\frac{1}{\sqrt{x}}(1+\sqrt{1-x})} \frac{dy}{y} \int_{\frac{\sqrt{x}}{2y-\sqrt{x}y^2}}^{1} dx_2 \int_{\frac{\sqrt{x}y^2}{2y-\sqrt{x}/x_2}}^{1} dx_1 \frac{x}{4v(x_1x_2)^2} =$$
$$\int_x^1 dx_2 \int_{x/x_2}^1 dx_1 \int_{\frac{x_1}{\sqrt{x}}(1-\sqrt{1-\frac{x}{x_1x_2}})}^{\frac{x_1}{\sqrt{x}}(1-\sqrt{1+\frac{x}{x_1x_2}})} \frac{dy}{y} \frac{x}{4v(x_1x_2)^2} \tag{C.1.18}$$

Now we introduce the partonic variable $\hat{y} = \sqrt{\frac{x_2}{x_1}}y$ and change the inner integration variable, so we obtain

$$\int_x^1 dx_2 \int_{x/x_2}^1 dx_1 \int_{\frac{1}{\sqrt{\hat{x}}}(1-\sqrt{1-\hat{x}})}^{\frac{1}{\sqrt{\hat{x}}}(1-\sqrt{1-\hat{x}})} \frac{dy}{y} \frac{\hat{x}}{4vx_1x_2} \tag{C.1.19}$$

where we introduced the partonic variable $\hat{x} = \frac{x}{x_1x_2}$. Note that v and w can be written in terms of partonic variables

$$v = 1 - \frac{\sqrt{\hat{x}}}{2\hat{y}}, \qquad w = \frac{\sqrt{\hat{x}}\hat{y}}{2v}. \tag{C.1.20}$$

Therefore, the final factorized expression is

$$p_T^3 \frac{d\sigma^{AB}}{dp_T} = \sum_{a,b} \int_x^1 dx_2 \int_{x/x_2}^1 dx_1 \int_{\frac{1}{\sqrt{\hat{x}}}(1-\sqrt{1-\hat{x}})}^{\frac{1}{\sqrt{\hat{x}}}(1-\sqrt{1-\hat{x}})} \frac{dy}{y} \frac{\hat{x}}{2v} f_a^A(x_1)\, f_b^B(x_2) \cdot \mathcal{C}(v,w) \tag{C.1.21}$$

where

$$\mathcal{C}(v,w) = v(1-v)w\hat{s}\frac{d\hat{\sigma}^{ab}}{dvdw} \tag{C.1.22}$$

now, we can use w as integration variable since

$$y = f(w) \equiv \frac{w}{\sqrt{\hat{x}}}\left(1 \pm \sqrt{1-\hat{x}/w}\right) \tag{C.1.23}$$

and the measure is

$$\frac{dy}{y} = \begin{cases} \frac{dw}{2w} J_-(w) & y < \frac{w}{\sqrt{x}} \\ \frac{dw}{2w} J_+(w) & y > \frac{w}{\sqrt{x}} \end{cases},$$
$$J_\pm(w) = 1 \pm \frac{1}{\sqrt{1-\hat{x}/w}} \tag{C.1.24}$$

We can also express v in terms of w

$$v_\pm = g_\pm(w) \equiv \frac{1}{2}(1 \pm \sqrt{1-\hat{x}/w}) \tag{C.1.25}$$

So we obtain

$$\sum_{a,b}\int_x^1 dx_2 f_a^A(x_2)\int_{x/x_2}^1 dx_1 f_b^B(x_1)\int_{\hat{x}}^1 \frac{dw}{4w}\hat{x}\left[J_+\frac{\mathcal{C}(v_+,w)}{v_+}-J_-\frac{\mathcal{C}(v_-,w)}{v_-}\right] \tag{C.1.26}$$

C.2 δ and "+" distributions

The formula we derived above is meaninful only for contributions to the coefficient $\frac{d\hat{\sigma}^{ab}}{dvdw}$ which do not contain plus or delta-function distributions because they modify the argument of the parton density.

Let us start with the simplest case of the delta-distribution $\delta(1-w)$ which appears in the NLO computation. We have

$$\begin{aligned} p_T^3\frac{d\sigma}{dp_T} &= 2\sum_{a,b}\int_x^1 dx_2 f_a^A(x_2)\int_{y_-}^{y_+}\frac{dy}{y}\frac{x'}{4v(y)}\int_{\frac{\sqrt{x'}y}{2v(y)}}^1\frac{dw}{w}f_b^B\left(\frac{\sqrt{x'}y}{2v(y)}\right)\cdot k(v)\delta(1-w) = \\ &= 2\sum_{a,b}\int_x^1 dx_2 f_a^A(x_2)\int_{y_-}^{y_+}\frac{dy}{y}\frac{x'}{4v(y)}f_b^B\left(\frac{\sqrt{x'}y}{2v(y)}\right)\cdot k(v) \end{aligned}$$

with $x'=x/x_2$, by changing the inner integration variable to $x_1=\frac{\sqrt{x'}y}{2-\sqrt{x'}/y}$ (which is not the same x_1 as before!) $y=\frac{x_1}{\sqrt{x'}}(1\pm\sqrt{1-x'/x_1})$ thus

$$\begin{aligned} &= \sum_{a,b}\int_x^1 dx_2 f_a^A(x_2)\int_{x'}^1\frac{dx_1}{4}f_b^B(x_1)\,\hat{x}\left(\frac{J_+(1)}{g_+(1)}k(g_+(1))-\frac{\tilde{J}_-}{g_-(1)}k(g_-(1))\right) = \\ &= \sum_{a,b}\int_x^1 dx_2 f_a^A(x_2)\int_{x/x_2}^1 dx_1 f_b^B(x_1)\int_{\hat{x}}^1\frac{dw}{4w}\hat{x}\left[J_+\frac{k(v_+)}{v_+}-J_-\frac{k(v_-)}{v_-}\right]\delta(1-w). \end{aligned} \tag{C.2.1}$$

Now consider contributions to $v(1-v)w\hat{s}\frac{d\hat{\sigma}^{ab}}{dvdw}$ of the form

$$\frac{c(v,w)}{(1-w)_+}, \tag{C.2.2}$$

where

$$\begin{aligned} \frac{1}{(1-w)_+} &= \frac{1}{(1-w)_A}+\log(1-A)\delta(1-w), \\ \int_A^1\frac{f(w)}{(1-w)_A}dw &\equiv \int_A^1\frac{f(w)-f(1)}{1-w}dw. \end{aligned} \tag{C.2.3}$$

From Eq. (C.1.8) we have

$$p_T^3 \frac{d\sigma^{AB}}{dp_T} = \sum_{a,b} 2 \int_{\frac{1}{\sqrt{x}}(1-\sqrt{1-x})}^{\frac{1}{\sqrt{x}}(1+\sqrt{1-x})} \frac{dy}{y} \int_{\frac{\sqrt{x}}{2}y}^{1-\frac{\sqrt{x}}{2y}} dv \int_{\frac{\sqrt{x}}{2v}y}^{1} dw \; x_1 f_a^A(x_1) \; x_2 f_b^B(x_2) \cdot \frac{c(v)}{(1-w)_+} \tag{C.2.4}$$

Bibliography

[1] C. J.

[2] M.L. Mangano and S.J. Parke, Phys. Rept. 200 (1991) 301, hep-th/0509223.

[3] V. Del Duca and E.W.N. Glover, JHEP 05 (2008) 056, 0802.4445.

[4] Z. Bern, L.J. Dixon and D.A. Kosower, Annals Phys. 322 (2007) 1587, 0704.2798.

[5] E. Witten, Commun. Math. Phys. 252 (2004) 189, hep-th/0312171.

[6] H. Fritzsch and P. Minkowski, Phys. Lett. B69 (1977) 316.

[7] The ATLAS, G. Aad et al., (2009), 0901.0512.

[8] L.E. Gordon and W. Vogelsang, Phys. Rev. D48 (1993) 3136.

[9] S. Catani et al., JHEP 03 (1999) 025, hep-ph/9903436.

[10] P. Aurenche et al., Phys. Rev. D39 (1989) 3275.

[11] M. Gluck et al., Phys. Rev. Lett. 73 (1994) 388.

[12] S. Frixione, Phys. Lett. B429 (1998) 369, hep-ph/9801442.

[13] WA70, M. Bonesini et al., Z. Phys. C37 (1988) 535.

[14] UA6, G. Ballocchi et al., Phys. Lett. B436 (1998) 222.

[15] Fermilab E706, L. Apanasevich et al., Phys. Rev. Lett. 81 (1998) 2642, hep-ex/9711017.

[16] E. Anassontzis et al., Z. Phys. C13 (1982) 277.

[17] CMOR, A.L.S. Angelis et al., Nucl. Phys. B327 (1989) 541.

[18] Axial Field Spectrometer, T. Akesson et al., Sov. J. Nucl. Phys. 51 (1990) 836.

[19] The CDF, .T. Aaltonen, (2009), 0910.3623.

[20] P. Aurenche et al., Eur. Phys. J. C9 (1999) 107, hep-ph/9811382.

[21] T. Becher and M.D. Schwartz, (2009), 0911.0681.

[22] R.K. Ellis, W.J. Stirling and B.R. Webber, QCD and collider physics (Cambridge University Press, 1996).

[23] P. Aurenche et al., Nucl. Phys. B297 (1988) 661.

[24] P. Aurenche et al., Nucl. Phys. B399 (1993) 34.

[25] L.E. Gordon and W. Vogelsang, Phys. Rev. D50 (1994) 1901.

[26] S. Frixione and W. Vogelsang, Nucl. Phys. B568 (2000) 60, hep-ph/9908387.

[27] S. Catani et al., JHEP 05 (2002) 028, hep-ph/0204023.

[28] P. Aurenche et al., Phys. Rev. D73 (2006) 094007, hep-ph/0602133.

[29] G. Altarelli and G. Parisi, Nucl. Phys. B126 (1977) 298.

[30] S. Catani, M. Ciafaloni and F. Hautmann, Nucl. Phys. B366 (1991) 135.

[31] S. Catani and F. Hautmann, Nucl. Phys. B427 (1994) 475, hep-ph/9405388.

[32] R.D. Ball, Nucl. Phys. B796 (2008) 137, 0708.1277.

[33] R.D. Ball and R.K. Ellis, JHEP 05 (2001) 053, hep-ph/0101199.

[34] G. Camici and M. Ciafaloni, Nucl. Phys. B496 (1997) 305, hep-ph/9701303.

[35] G. Altarelli, R.D. Ball and S. Forte, Nucl. Phys. B799 (2008) 199, 0802.0032.

[36] S. Marzani et al., Nucl. Phys. Proc. Suppl. 186 (2009) 98, 0809.4934.

[37] S. Marzani et al., Nucl. Phys. B800 (2008) 127, 0801.2544.

[38] F. Hautmann, Phys. Lett. B535 (2002) 159, hep-ph/0203140.

[39] S. Marzani and R.D. Ball, Nucl. Phys. B814 (2009) 246, 0812.3602.

[40] J. Bartels, D. Colferai and G.P. Vacca, Eur. Phys. J. C24 (2002) 83, hep-ph/0112283.

[41] J. Bartels et al., Phys. Rev. D66 (2002) 094017, hep-ph/0208130.

[42] L.N. Lipatov, Sov. J. Nucl. Phys. 23 (1976) 338.

[43] E.A. Kuraev, L.N. Lipatov and V.S. Fadin, Sov. Phys. JETP 45 (1977) 199.

[44] I.I. Balitsky and L.N. Lipatov, Sov. J. Nucl. Phys. 28 (1978) 822.

[45] M. Ciafaloni, Nucl. Phys. B296 (1988) 49.

[46] F. Caola, S. Marzani and S. Forte, *in preparation* .

[47] M. Ciafaloni et al., Phys. Rev. D68 (2003) 114003, hep-ph/0307188.

[48] M. Ciafaloni et al., JHEP 08 (2007) 046, 0707.1453.

[49] G. Altarelli, R.D. Ball and S. Forte, Nucl. Phys. B742 (2006) 1, hep-ph/0512237.

[50] R.K. Ellis and D.A. Ross, Nucl. Phys. B345 (1990) 79.

[51] T. Jaroszewicz, Phys. Lett. B116 (1982) 291.

[52] G. Curci, W. Furmanski and R. Petronzio, Nucl. Phys. B175 (1980) 27.

[53] A.V. Lipatov and N.P. Zotov, Phys. Rev. D72 (2005) 054002, hep-ph/0506044.

[54] R.K. Ellis, *Private comunication* .

[55] G. Altarelli, R.D. Ball and S. Forte, Nucl. Phys. B674 (2003) 459, hep-ph/0306156.

[56] M. Ciafaloni et al., Phys. Lett. B587 (2004) 87, hep-ph/0311325.

[57] S. Marzani and R.D. Ball, (2009), 0906.4729.

[58] G. Diana, Nucl. Phys. B824 (2010) 154, 0906.4159.

[59] F. Caola, S. Forte and J. Rojo, Phys. Lett. B686 (2010) 127, 0910.3143.

[60] J. Rojo et al., (2009), 0907.0443.

[61] J. Rojo and F. Caola, (2009), 0906.2079.

[62] S. Forte, G. Altarelli and R.D. Ball, Nucl. Phys. Proc. Suppl. 191 (2009) 64, 0901.1294.

[63] J.F. Owens, Rev. Mod. Phys. 59 (1987) 465.

[64] J. Huston et al., Phys. Rev. D51 (1995) 6139, hep-ph/9501230.

[65] D. D'Enterria et al., in preparation, 2010.

[66] S. Hoeche, S. Schumann and F. Siegert, Phys. Rev. D81 (2010) 034026, 0912.3501.

[67] N. Kidonakis and J.F. Owens, Phys. Rev. D61 (2000) 094004, hep-ph/9912388.

[68] P. Bolzoni, S. Forte and G. Ridolfi, Nucl. Phys. B731 (2005) 85, hep-ph/0504115.

[69] P. Aurenche et al., Phys. Lett. B140 (1984) 87.

[70] P. Aurenche et al., Nucl. Phys.. B297 (1988) 661.

[71] F. Aversa et al., Nucl. Phys. B327 (1989) 105.

[72] P. Aurenche et al., Nucl. Phys. B399 (1993) 34.

[73] L. Bourhis, M. Fontannaz and J. Guillet, Eur. Phys. J. C2 (1998) 529.

[74] The NNPDF Collaboration, R.D. Ball et al., (2010), 1002.4407.

[75] The NNPDF Collaboration, L. Del Debbio et al., JHEP 03 (2007) 039, hep-ph/0701127.

[76] The NNPDF Collaboration, R.D. Ball et al., Nucl. Phys. B809 (2009) 1, 0808.1231.

[77] The NNPDF, R.D. Ball et al., Nucl. Phys. B823 (2009) 195, 0906.1958.

[78] D0, V.M. Abazov et al., Phys. Lett. B639 (2006) 151, hep-ex/0511054.

[79] F. Demartin et al., (2010), 1004.0962.

[80] A.D. Martin et al., Eur. Phys. J. C64 (2009) 653, 0905.3531.

[81] H.L. Lai et al., (2010), 1004.4624.

Ringraziamenti

Al seguito di questi tre anni di dottorato, in primo luogo vorrei ringraziare il mio relatore Stefano Forte, che mi ha guidato lungo questa mia prima esperienza nel mondo della ricerca scientifica.

La persona a cui devo i miei più sentiti ringraziamenti è Fabrizio, con cui ho condiviso tutta la mia esperienza a Milano. Il nostro continuo confronto di idee ha alimentato, in questi anni, una particolare attenzione verso la comprensione profonda della Fisica. Insostituibile amico e maestro, a lui devo tutta la mia gratitudine.

Un grazie particolare va a Keith, il cui intervento speciale mi ha fatto piangere di gioia per la prima volta nella mia vita.

Un ringraziamento speciale va a Salvatore, mio punto di riferimento costante per ogni difficoltà. La competitività "gomito a gomito" dei primi anni di università ha ceduto presto il passo alla comprensione, al calore di un abbraccio, alla gioia del rivedersi e raccontarsi storie di vita comune.

Ringrazio la mia famiglia, ogni singolo sorriso di mia madre e mio padre, delle mie sorelle. Porterò ovunque quel sorriso per non dimenticare l'azzurro da cui provengo.

Ringrazio tutti gli inquilini attuali e passati del corridoio al primo piano a destra della palazzina ex-solidi (a cui un giorno daranno un nome più aggiornato, spero), in particolare a Sara, Arianna, Kowalsky (rappresentativo dei vari nickname assegnatigli nell'ultimo anno), Davide e Marco.

Grazie ai miei amici, alla loro presenza. A chi ha già capito che per conoscermi non ha bisogno di ascoltare le mie spiegazioni fuorvianti. In particolare ringrazio Saul (inutile dire perchè), Samuele (qui dovrei aggiungere vari link audio alle telefonate-sveglia), Chiara ("Giò, vattene!"), Alessandro ("Amigo! Ciumbooooooo", "tienes el papel?", "massage?" ecc..), Elisa, Giulia, Daniele, Carlo, Antonio, Linda, Daniela.

Un grazie speciale a te. Non ti ho nominato appositamente per dedicarti una riga intera...

Grazie alla persona che più ho fatto soffrire. Grazie per sempre, grazie per tutto. Un "grazie" che non arriverà mai, lo so. Continuerò a parlare *di* te credendo di parlare *con* te, senza capire che non dovrei, che non potrei.